DTU Library

Design and development of electrochemical polymer-based lab-on-a-disc devices for biological applications

Sanger, Kuldeep

Publication date:
2017

Document Version
Publisher's PDF, also known as Version of record

[Link back to DTU Orbit](#)

Citation (APA):
Sanger, K. (2017). *Design and development of electrochemical polymer-based lab-on-a-disc devices for biological applications*. DTU Nanotech.

DTU

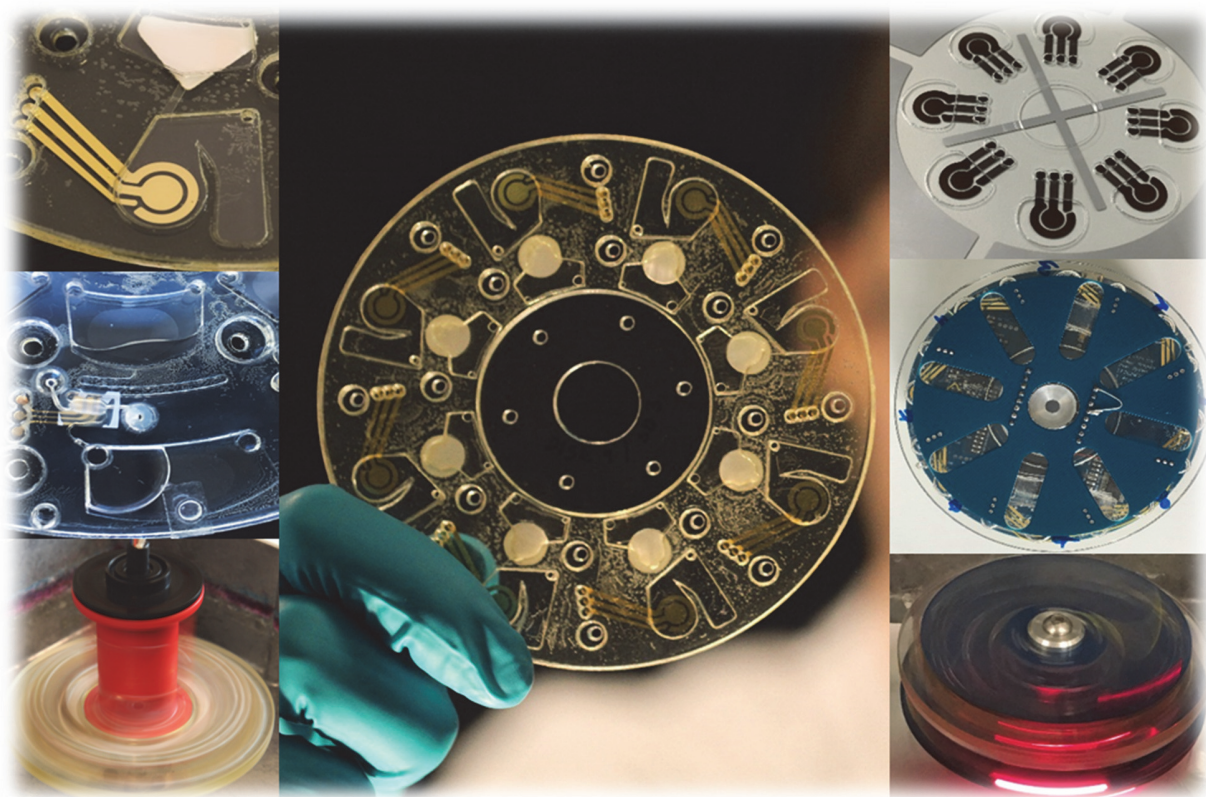# Design and Development of Electrochemical Polymer-Based Lab-on-a-Disc Devices for Biological Applications

Kuldeep Sanger
PhD Thesis August 2017

DTU Nanotech
Department of Micro- and Nanotechnology

Design and Development of Electrochemical Polymer-Based Lab-on-a-Disc Devices for Biological Applications

Ph.D. Thesis

Kuldeep Sanger

August 2017

DESIGN AND DEVELOPMENT OF ELECTROCHEMICAL POLYMER-BASED LAB-ON-A-DISC DEVICES FOR BIOLOGICAL APPLICATIONS

A thesis presented to the academic faculty

by

Kuldeep Sanger

In partial fulfillment of the requirements for the

Ph.D. Degree

in the Department of Micro- and Nanotechnology

Technical University of Denmark

August 2017

DESIGN AND DEVELOPMENT OF ELECTROCHEMICAL POLYMER-BASED LAB-ON-A-DISC DEVICES FOR BIOLOGICAL APPLICATIONS

Main Supervisor:

Professor Anja Boisen

Department of Micro- and Nanotechnology

Denmark Technical University

Co-Supervisors:

Researcher Kinga Zor

Department of Micro- and Nanotechnology

Denmark Technical University

Senior Researcher Arto Heiskanen

Department of Micro- and Nanotechnology

Denmark Technical University

PREFACE

The scientific work presented in this thesis was carried out at the Department of Micro- and Nanotechnology, Technical University of Denmark. The European Research Council financially supported the Ph.D. project under the European Union's Seventh Framework Programme (FP7/2007-2013) grant no. 320535-HERMES. The employment took place in DTU Nanotech, from 1st of September, 2014, until 31st of August, 2017.

ACKNOWLEDGEMENTS

The journey to the attainment of the ambition is full of ups and downs. During this roller coaster ride you may come across someone who will consistently guide you on the right path, you may discover some individuals who will help you in shaping up your skills, you may have some colleagues who will encourage you and help you in your difficult times and finally you may come across a bunch of indispensable friends who will play the pivotal role of your family members when you are away from the family. This work somewhere or at some stages of the whole journey reflects the contribution from all of the above-mentioned.

First and foremost, I am forever indebted to my Principal supervisor Professor Anja Boisen for offering me the opportunity to carry out this Ph.D. project. Throughout this work, she had unflagging faith on me and provided major moral support. Each time I slowed down due to exhaustion, she encouraged to push the boundary little more. She has provided the excellent example, not just as a successful Professor, also as a great leader. Hence I am very thankful to Anja and words would not be enough to express my gratitude towards her. I would especially like to thank my co-supervisor Dr. Kinga Zor who helped me in planning my experiments, devising the direction of research and suggesting invaluable additions to my research work. She made herself available for help whenever I asked for and rescued my sinking ship in difficult times. At the same time, I also would like to thank my co-supervisor Dr. Arto Heiskanen for his valuable guidance and fruitful discussions.

Secondly, every endeavor in life is a story about colleagues and collaborators. It has been my pleasure to work with people in Nanoprobes group, DTU Danchip, DTU Biosustain and Edwin's group in Taiwan. I am thankful to Onur, Sune, Kaiyu, Anil, Edwin, Alex and Christian for helping me in my experiments and collaborating with me on different research projects. Apart from professional collaborations, some of my colleagues such as Lukas, Onur, Rokon, Zarmeena, and Suhith made the work life quite stress-free through our chitchats and refreshments sessions of playing table foosball. So I thank all of the above people for the wonderful moments I shared with them; I will cherish these memories throughout my life.

ABSTRACT

The need for reliable, fast, easy to use, portable and cost effective analytical tools has led to several novel approaches in the development of miniaturized microfluidic platforms integrated with electrochemical sensors. This thesis presents the design and development of an electrochemical detection based centrifugal microfluidic platforms towards applications in bioprocess monitoring, medical diagnostics, food and environmental analysis, etc. Stencil based electrode fabrication approach was developed and optimized to pattern reliable and reproducible electrodes on a polymeric substrate. Also, a fast, easy to use and simplified approach was established for interfacing the electrodes integrated with the polymeric Lab-on-a-disc (LoD) devices. On-disc filtration and supported liquid membrane (SLM) extraction was adapted on LoD devices for sample pre-treatment (e.g., filtration, extraction, enrichment). The applicability of the developed microfluidic systems was demonstrated by monitoring a biological process, namely quantifying the amount of the bacterial metabolite *p*-Coumaric acid (pHCA) produced by genetically modified *E. coli* cells. The first generation LoD device (with integrated filtration) was used to quantify pHCA at the end of bacterial culture (24 hours) when the cell density is the highest. We demonstrated the efficiency of the centrifugal filtration, which enabled cell-free electrochemical detection eliminating the effect of high cell density on electrochemical quantification of pHCA. The second generation LoD device (with integrated SLM extraction) was more advanced and facilitated extraction, enrichment, as well as electrochemical detection of pHCA from the complex sample matrix, i.e., *E. coli* supernatant at different time points during the cell culture. Realizing the need for more advanced sensors that can be integrated with microfluidic devices, we developed dual functionality sensors facilitating surface-enhanced Raman spectroscopy (SERS) based sensing as well as electrochemical detection. Moreover, to eliminate the need for bulky peripheral instrumentation connected through slip rings for on-disc electrochemical measurements, we present a miniaturized smartphone controlled wireless potentiostat, which can be integrated on a rotating microfluidic platform.

DANSK RESUME

Behovet for analytiske redskaber som er pålidelige, hurtige, omkostningseffektive samt nemme at transportere og bruge har ført til flere nye metoder indenfor udviklingen af små mikrofluide platforme med integrerede elektrokemiske sensorer. Denne afhandling præsenterer design og udvikling af en centrifugal mikrofluid platform med elektrokemisk detektion til brug indenfor monitorering af biologiske processer, medicinsk diagnosticering, analyse af miljø og fødevarer osv. En stencil-baseret metode til elektrodefabrikation blev udviklet og optimeret til fremstilling af pålidelige og reproducerbare elektroder på et polymer-substrat. Herudover blev der udviklet en metode til integrering af elektroderne på en 'lab-on-a-disc'(LoD) enhed, der er hurtig, simpel og nem at håndtere. Til forbehandling af prøver (f.eks. filtrering, ekstraktion, op-koncentration) blev procedurer for filtrering og 'supported liquid membrane' (SLM) ekstraktion tilpasset LoD enheden. Anvendeligheden af det udviklede system blev demonstreret ved at overvåge mængden af metabolitten p-Coumaric acid (pHCA) produceret af genetisk modificerede *E.coli* bakterieceller. Første generation af LoD enheden (med integreret filtrering) blev brugt til at måle pHCA mængden efter 24 timers dyrkning af bakterierne hvor celledensiteten er højest. Vi demonstrerede effektiviteten af centrifugal filtrering der gjorde cellefri elektrokemisk detektion muligt og dermed eliminerede effekten af den høje celledensitet på den elektrokemiske måling af pHCA. Anden generation af LoD enheden (med integreret SLM ekstraktion) var mere avanceret og gjorde det muligt at ekstrahere, op-koncentrere og elektrokemisk detektere pHCA fra en kompleks prøve som for eksempel supernatant fra *E.coli* på forskellige tidspunkter af celledyrkningen. Da der er et behov for mere avancerede sensorer der kan integreres med mikrofluide enheder, udvikledes der også sensorer med dobbelt funktion baseret på 'surface-enhanced Raman spectroscopy' (SERS) og elektrokemi. Ydermere, for at undgå eksterne, uhåndterbare instrumenter, præsenteres der et samarbejdsprojekt med mål om at fremstille en miniature potentiostat der kan kontrolleres med en smartphone og integreres på en roterende mikrofluid platform.

CONTENTS

1. Introduction

The first miniaturized analytical system, a gas chromatograph, was reported in 1979 capable of separating gaseous hydrocarbon mixtures in less than 10 seconds and was three orders of magnitudes smaller than conventional instruments[1]. Almost a decade later, Manz et al. formally introduced the concept of the miniaturized total chemical analysis system, where they proposed the downscaling of well-established chemical analysis systems (based on chromatography, electrophoresis and flow injection analysis) onto a single platform[2]. Advancement in microfabrication techniques in silicon industries helped to evolve further the miniaturization concept towards design and fabrication of more advanced and integrated microfluidic systems to perform complete analysis, the now-called micro total analysis systems (µTAS). Over the time, the concept of µTAS was developed into lab-on-a-chip (LOC) technology, aimed to incorporate not only miniaturized chemical analysis but also other laboratory processes towards a fully automated miniaturized laboratory system[3]. These microfluidic systems offer several advantages (such as low sample and reagents requirement, short response time, portability, etc.) over conventional analysis systems, which are quite often time-consuming, labor intensive and require large and expensive instrumentation. These advantages assisted µTAS or LOC to gain enormous popularity for addressing various challenges in different sectors like drug discovery and development, disease biomarker detection, diagnostics, food quality analysis, bioprocess monitoring and environmental toxicity monitoring.

In early LOC devices, glass and silicon (Si) were the major options available as materials for microfabrication. However, different polymeric materials like PDMS, PMMA, PC, PS, etc. were investigated over time and became the preferred choice for the researchers[4,5]. The use of polymers drastically expanded the research in the field of LOC technologies and applications, given the multitude of fabrication processes that can be performed even outside the expensive cleanroom facilities. Moreover, polymers also allow the development of cheap and disposable analytical devices. Lab-on-a-disc (LoD) is a type of LOC device, which turned out to be an ideal option for adaptation and integration of bio(chemical) assays in microfluidic platforms. LOD devices, with intrinsic pumping and separation mechanisms based on centrifugal forces; enable miniaturization, automation, and parallelization of the assays. In the majority of cases, LOC and LoD refer to

particular step or process adapted to microscale devices but do not necessarily indicate a complete analytical process. However, to obtain sample-to-answer devices, it is mandatory to integrate the entire analytical process onto a single platform, which is often the case for point-of-care (POC) devices. So far, the LoD technology focused mainly on developing devices for biomedical analysis and POC diagnostics[6–8]. However, a few reports are also presenting the application of centrifugal devices for food analysis and environmental applications[9–11]. Recent reviews showed that LoD devices can incorporate several detection principles such as optical, mechanical, and electrochemical detection[12–14]. Among these detection principles, electrochemical detection has certain advantages when it comes to implementation and integration on LOD devices, such as the possibility of miniaturization using fabrication methods already developed for the microelectronics industry, low power requirements for operation and low production cost.

In this thesis, we have developed electrochemical detection based polymeric LoD platforms incorporated with eight sample pre-treatment (filtration / supported liquid membrane (SLM) extraction) units. The motivation was to perform the complete assay, from sample pre-treatment to quantitative analysis, on an automated, low-cost microfluidic disc with integrated electrodes fabricated on a polymer substrate. The simple, yet robust electrode fabrication process (lithography-free) has been optimized to fabricate electrodes on a polymer substrate. Finally, we have demonstrated the applicability of the LoD systems developed during this Ph.D. project by choosing bioprocess monitoring as a case study.

Application of the LoD devices in the field of bioprocess monitoring is not well represented. Therefore the work presented in Paper I and II, screening of genetically modified *Escherichia coli* (*E. coli*) cells, is a significant contribution to the LoD field. In Paper I, the screening was achieved by cell free (using filtration) electrochemical detection and quantification of the produced secondary metabolite, *p*-Coumaric acid (pHCA) from bacterial culture supernatant after 24 hours of cell culture. pHCA is a key analyte in pharmaceutical and food industry, synthetized in bacterial cell factories to obtain industrially relevant quantities. Quantification of the produced pHCA is of great significance to screen genetically modified *E. coli* cells to identify the best performing strain, which is performed commonly with although accurate and precise, but time-consuming and labor intensive techniques (such as HPLC, mass spectroscopy, etc.). For electrochemical measurements,

the LOD device was connected to a multichannel potentiostat, using magnetic clamping enabled PCB unit, facilitated robust connection as well as easy and quick assembly. The developed LoD platform was used to quantify the amount of pHCA produced by two different genetically modified *E. coli* strains (CBJ792 and CBJ800), and compared with results obtained from wild type strain (CBJ786).

In Paper II, we have further improved the LoD system to be able to measure pHCA at different time points in the production process. Time independent detection was not achievable with the first generation LoD system (Paper I), due to the presence of high amount of an interfering compound tyrosine (Tyr) in the initial phase of the bioprocess. A LoD system was designed to integrate on-disc supported liquid membrane (SLM) extraction followed by electrochemical detection. To the best of our knowledge, this was the first report demonstrating the combination of SLM with in-situ electrochemical detection, as well as the integration of SLM extraction on a LoD device. The compact LoD platform facilitates efficient extraction and simultaneous detection of the target analyte from a complex matrix even at low concentration, in the presence of interfering compounds at the early stage in the production. Consequently, the quantification of the pHCA produced by a genetically modified *E. coli* strain was achieved at different time points (6, 9 and 24h). The obtained results indicate the potential for high-throughput analysis and highlight the relevance of SLM extraction combined with in-situ electrochemical detection on the developed LoD device.

The data acquired through electrochemical detection in Paper I and Paper II, correlated well with data obtained from the high-performance liquid chromatography analysis. Thus, we believe that both the LoD platforms developed during this Ph.D. project have the potential to be used as an at-line bioprocess monitoring tool, enabling time and cost efficient analysis.

In last few years, reports showed the advantages of combining SERS and electrochemical detection for various applications[15–27]. There are some significant benefits when using the two techniques individually or simultaneously on the same substrate. SERS has been used for monitoring electrochemical reactions at ultra-low concentrations, and it has been shown that applied potential promotes adhesion of the target molecule to the Au layer on the SERS substrate and improves detection[28,29]. A more advanced technique involves using fluctuation of the applied electrode

potential to adsorb and desorb different sets of molecules while monitoring the Raman signature and thereby avoid spectral congestion. This is especially relevant with coadsorption of molecules in complex solutions, as is typically the case with biological solutions[30]. In paper III, we have worked on developing a dual functionality sensor for identification and quantification of an unknown electroactive molecule using two different detection techniques SERS and electrochemistry. For proof of concept, paracetamol was chosen as a model analyte, which was identified and quantified using SERS and electrochemistry, respectively.

1.1 Thesis outline

The thesis is divided into six chapters that guide the reader through the development process, describing in detail the fabrication procedures, design, and integration of sample pre-treatment methods and electrochemical sensors into the LoD devices. Also, certain chapters introduce the basic theory of the tools and techniques used in the Ph.D. project.

Chapter 2

This chapter gives a brief introduction to centrifugal microfluidics as an emerging field with several advantages over traditional microfluidic systems and covers different theoretical aspects that are important to understand the fluid dynamics in centrifugal microfluidic devices, also called as Lab-on-a-disc (LoD) devices. In addition, this chapter describes the need for sample pre-treatment prior to detection, when dealing with complex sample matrix and presents the on-disc integration of two sample pre-treatment approaches, i.e., filtration and SLM extraction.

Chapter 3

This chapter introduces the basic considerations for sensor development followed by in detailed description of miniaturization and integration of optical, mechanical and electrochemical sensors on LoD devices for various applications. As more emphasis has been given to electrochemical detection based applications, a brief introduction to general electrochemistry is also presented. A small section also focuses on the newly emerging concept of dual functionality sensors. Besides the sensor, miniaturization, and integration of peripheral devices for detection and data processing is also an important aspect to consider when developing a fully automated portable device for

decentralized analysis. In the last part of this chapter, the results of an ongoing collaborative project focused on the development of a smartphone controlled wireless potentiostat integrated with LoD device, are also presented.

Chapter 4

A basic introduction to electrochemical (cyclic voltammetry, amperometry, and square wave voltammetry) and optical detection techniques (surface enhanced Raman spectroscopy) used for sensor characterization and analyte (pHCA, paracetamol, dopamine) detection is presented in this chapter.

Chapter 5

Fabrication was a considerable part of this thesis. Thus this chapter introduces the reader to all the main fabrication procedures and steps optimized and followed to develop polymer based microfluidic devices and lithography-free electrochemical sensors (electrodes) on different substrates like PMMA, Si, and glass. The electrode integration into the microfluidic devices and further interfacing of the electrodes with the potentiostat via custom-made PCB are also discussed.

Chapter 6

A concluding chapter that summarizes the achieved results and discusses the future perspectives.

2. µTAS and centrifugal microfluidics

Hundreds of years ago, researchers' curiosity to extract information from body fluids led them to investigate the color and appearance of urine samples in examination flasks known as "matulas"[31]. Surprisingly, they managed to provide diagrams and pictures of "matulas" of colored urine that could be used as a diagnostic tool[32]. However, there was still a great need to study and understand the fluid behavior more precisely and accurately to make a reliable conclusion. Thankfully, the growth of the semiconductor industry and with it the fast-paced development of microfabrication techniques led to a new world of microscale structuring methods. This consequently helped researchers to confine fluids into micro- or nanochannels instead of "matulas" to predict and understand the fluid behavior more systematically. With the development of the first on-chip gas chromatograph[1] and the highly promoted research on inkjet printers by IBM[33], microfluidic technology gained the interest of more and more researchers, leading to the concept of miniaturized total chemical analysis system by Manz et al.[2], followed by several publications and patents on microfluidic structures and devices such as microvalves,[34–36] micropumps,[37–41] mixers,[42–44] and concentrators[45,46], etc. This development and progress in microfluidic technology led to the miniaturization and automation of laboratory processes, also called as micro total analysis systems (µTAS) and Lab-on-a-chip (LOC) devices.

The key purpose of µTAS is to replace the time consuming and labor intensive laboratory protocols with fully automated process steps (including sample preparation and pre-treatment) integrated on a single miniaturized chip. Thus, µTAS are expected to offer several advantages over sophisticated (bio-)chemical analysis, such as the use of low sample and reagents volumes, low-energy consumption, portability, high precision, fast response, and parallelization. With the miniaturization of the fluidic devices, the surface area-to-volume ratio increases and surface forces such as surface tension and shear stress start influencing the fluidic operations significantly[47,48]. Based on the predominant fluid propulsion forces, microfluidic devices can be classified into capillary, pressure driven, electrokinetic, acoustic and centrifugal microfluidic systems[49–51]. Although there are various possibilities available in microfluidics, every particular application needs a tailored analytical device, which meets the specific requirements of the respective application. Thus, for different applications, several microfluidic devices were designed, developed

and even commercialized over time. Volpatti et al. and Chin et al. have reviewed and presented a long list of companies engaged in the commercialization of microfluidic technologies for numerous applications[52,53].

Centrifugal microfluidic platforms also known as Lab-on-a-disc/CD (LoD) devices comply well with the concept of μTAS as all the necessary steps of a (bio-)chemical assay can be incorporated on a single compact disc. Unlike other microfluidic devices, centrifugal microfluidics does not require any active components such as pumps, actuators and active valves for successful fluid manipulation. Rather it requires a small rotational motor that can control the complex microfluidic workflows. Alternatively, we can also say that the spinning speed of the disc (rotational frequency of the motor) is the sole parameter that regulates the entire fluid propulsion mechanism, which makes centrifugal microfluidic devices simple and relatively cheap solution for implementing a variety of microfluidic operations. For instance, a dynamic range of flow rates can be easily achieved by controlling the rotational frequency and channel geometries. Also, by simply changing the rotational frequencies, the body forces such as centrifugal force can be adjusted to remove bubbles from the channels and chambers (a most common problem in traditional microfluidics) and to separate the suspensions (by sedimentation). Contrary to the pressure driven microfluidics where large liquid volumes are lost in channels and tubings, fluid loss on channel walls due to surface forces can be minimized efficiently by increasing the rotational frequency that facilitates the handling of nanoliter sample volumes. The fluid handling and pumping mechanism on a disc are independent of the physiochemical properties (e.g., ionic strength, pH, conductivity, etc.) of the sample. Therefore many samples can be used on the same disc[54]. Moreover, a same rotating motor can be programmed to handle different centrifugal discs with completely different fluidic designs. Consequently, due to the instrumentation simplicity, scalable and cost-efficient fabrication techniques, and several other advantages over traditional microfluidic platforms, centrifugal microfluidics has been a focus of intense research for many years now. As a result, many companies and startups are actively participating in the development of the technology for numerous applications and commercializing the centrifugal microfluidics based products (Table 1).

Table 1. Embodiments of centrifugal microfluidic platforms that are either currently commercially available, in a pre-commercial phase announcing the release date shortly, or showing promising developments (adapted from[55]).

Provider (Developer)	Identifier Cartridge/name of system	Applications	Commercialization status
Abaxis	Piccolo Xpress	Blood parameter analysis	Commercially available
Samsung	LABGEO IB10	Immunoassays	Commercially available
Focus Diagnostics (3M)	Universal Disc & Direct Amplification Disk/Integrated Cycler	Nucleic acid analysis	Commercially available
Roche (Panasonic)	Cobas 101b	Blood parameter analysis (HbA1c and lipid panel)	Commercially available
Capital Bio	RTisochip	Nucleic acid analysis (respiratory tract infections)	Commercially available
Gyros AB	Gyrolab Bioaffy CD	Immunoassays	Commercially available
LaMotte	Water Link Spin Lab	Water analysis	Commercially available
Skyla	VB 1 Veterinary Clinical Chemistry Analyzer	Blood chemistry testing for veterinary applications	Commercially available
Biosurfit	Spinit	Immunoassays/blood parameter analysis	Commercially available
Radisens Diagnostics	Unknown	Immunoassay, clinical chemistry, and hematology assays	Precom
GenePOCDiagnostics	Unknown	Nucleic acid analysis	Precom
SpinChip Diagnostics	Unknown	Blood analysis	Development
Espira Inc.	Unknown	Nucleic acid analysis	Development
Hahn-Schickard	LabTube	Various applications	Development
Hahn-Schickard	LabDisk	Various applications	Development
SpinDiag	SpinDiag One	Nucleic acid analysis	Development
Sandia National Labs	Spin DX	Various applications	Development
BluSense Diagnostics	Blubox	Blood analysis	Development

2.1 Microfluidics – brief introduction

In microfluidic devices, as we scale down the dimensions to the micro-scale range, the physical phenomena are governed by forces other than the forces responsible for microfluidic operations in macroscale devices. Inertial effects dominate fluid flow in the macroscale regime that introduce instabilities and turbulence to the macroscale system, making it chaotic and unpredictable. On the other hand, in microfluidic systems, capillary and viscous forces dominate and a laminar flow regime is developed, resulting in sliding layers of fluids rather than chaotic turbulence[56]. In this section, those effects that describe the behavior of the fluid in a microfluidic device are explained briefly.

Surface forces versus body/volume forces

In sub-millimeter sized channels of a microfluidic system, the surface area of the liquid increases drastically as compared to its volume. That means the surface area-to-volume ratio increases by several orders of magnitude[57]. Consequently, the surface forces such as surface tension and shear stress become prominent, whereas the volume forces such as gravity and inertia become insignificant[56]. In centrifugal microfluidics, this does not seem to be a major problem as the centrifugal force (body force) can overcome the effect of surface forces (capillary force) simply by increasing the rotational frequency. Moreover, the surface forces can be utilized to create valves.

Surface tension, contact angle

One of the main surface forces in microfluidics is surface tension. The cohesive forces between the liquid molecules at the liquid/gas interface give rise to surface tension. By nature, liquid tends to form in such a way that its surface area is minimized. At liquid/gas interface, the molecules at the front most surface of the liquid cannot form as many chemical bonds as the bulk molecules make with their neighbors. This is because there are fewer or almost no molecules in the gas. Therefore, surface molecules have a higher energy compared to the ones in bulk. Since this is not intrinsically favorable, the molecules reorganize themselves to acquire a surface area as small as possible. As a result, the liquid forms a hemispherically shaped meniscus at its front. The meniscus creates an inward force named surface tension. Gibbs free energy per area (referred to as surface free energy)

determines how much tension a liquid contains at an interface at constant pressure and temperature[56,57].

The contact angle is another important parameter, which is commonly used to define the behavior of fluids on a surface. Contact angle θ_c is the angle that the contact line of liquid/gas interface makes with the solid/liquid interface at the meeting point of the three phases as shown in the figure 1.
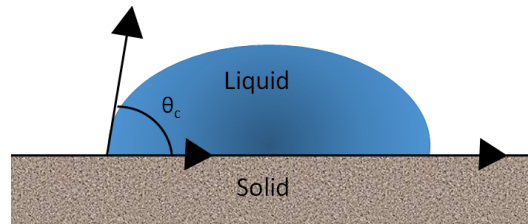

Figure 1. The contact angle between contact line of liquid/fluid (gas) interface and the solid/liquid interface.

Contact angle measured in a static condition (when the liquid is not moving on the solid), is different from the dynamic contact angle which is measured while the liquid is moving on the solid surface. The latter is a complex quantity that depends on the dynamical state of the advancing or receding liquid edge[56].

Static contact angle can be calculated from Young's equation,

$$cos\theta_c = \frac{\gamma_{sg} - \gamma_{sl}}{\gamma_{lg}} \tag{2.1}$$

where γ_{sg}, γ_{sl} and γ_{lg} are the surface tension of solid/gas, solid/liquid and liquid/gas interface respectively. Contact angle is in fact a measure of the wettability of a solid surface with a liquid. If the contact angle is smaller than 90°, the surface is hydrophilic and the liquid can spread on the surface. Contrary, if the contact angle is larger than 90°, the surface is hydrophobic and the liquid form droplets and shows poor spreading.

Surface tension and contact angle are two fundamental concepts that help to understand the passive fluid valving mechanism in centrifugal microfluidic systems. The bursting of capillary[58] and

hydrophobic valves[59] strongly depends on the surface tension and adjusting the rotational frequency of the disc accordingly[6].

Reynolds number and laminar flow regime

Reynolds number is a dimensionless number, which is defined as the ratio between the inertial and viscous forces[56],

$$Re = \frac{\rho dv}{\eta} \qquad (2.2)$$

where ρ is the density, d is the length scale, e.g. t,he capillary diameter, v is the linear flow velocity and η is the viscosity. For the limit of low Reynolds number, $Re \ll 1$, the viscous forces dominate the inertial forces. Due to its micro scale dimensions, a microfluidic system operates in the limit of low Reynolds number ($0.001 < Re < 10$)[60]. In this domain, the fluid behavior is laminar, steady and smooth rather than turbulent. The absence of turbulence have many positive effects, however it makes the mixing of fluids more challenging.

2.2 Centrifugal microfluidics – theory

An effective fluid manipulation on a centrifugal microfluidic platform is mainly achieved by controlling three different pseudo forces namely centrifugal force (F_c), Coriolis force (F_{Co}), and Euler force (F_E) present on the rotating platform (Figure 2),

$$F_c = -\rho\omega \times (\omega \times r) \qquad (2.3)$$

$$F_{Co} = -2\rho\omega \times \frac{d}{dt}r \qquad (2.4)$$

$$F_E = -\rho\frac{d}{dt}\omega \times r \qquad (2.5)$$

where ρ is the sample liquid density and ω is the angular frequency. Among the pseudo forces, the centrifugal force is the primary force that acts radially outwards and drags the fluid from the center

of the disc to the outer periphery. The Coriolis force acts in the direction perpendicular to the centrifugal force. At high spin frequencies, the Coriolis force becomes more dominant than the centrifugal force. Depending on the spin direction of the disc (clockwise or counter-clockwise), the Coriolis force tends to direct the flow to the opposite side of the rotational direction and helps in switching the direction of the flow[61]. The Euler force acts opposite to the rotational acceleration in the plane of the disc and facilitates the fluid mixing by creating lateral motion of the fluid during disc acceleration[62].
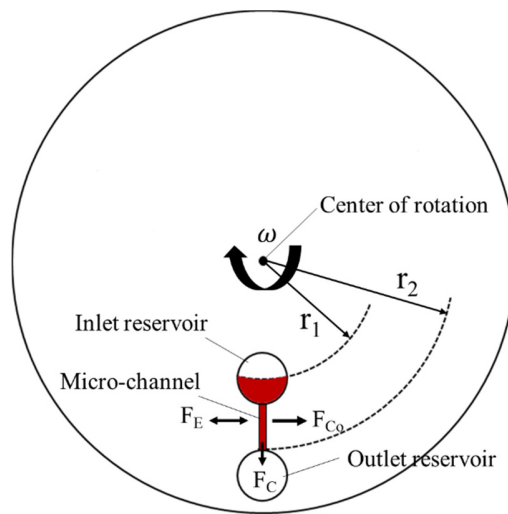
Figure 2. Schematic forces acting on a liquid plug on a rotating platform (adapted and modified from[12])

Centrifugal Pumping

Figure 2 shows the schematic illustration of a simple microfluidic disc with two reservoirs and an interconnecting micro-channel. A liquid plug is at rest in the inlet reservoir. As the disc spins, the centrifugal force induces a pressure which tends to drive the liquid radially outwards from the center towards the periphery of the disc. If the disc's surface is hydrophilic and the channel is narrow enough, the liquid flows into the channel until it reaches the junction of the channel and the outlet reservoir. This type of flow has been extensively reviewed and characterized[54,63–65].

The centrifugally induced pressure for a resting liquid plug is[66],

$$\Delta P_{centrifugal} = \rho \omega^2 r_m \Delta r \qquad (2.6)$$

12

where ρ is the sample liquid density, ω is the angular frequency, $\Delta r = r_2 - r_1$ is the radial extent of the liquid and $r_m = (r_2 + r_1)/2$ is the average radial distance of the liquid in the channel from the center of the disc. r_1 and r_2 are the radial distance from the center of rotation to the top and bottom of the liquid column respectively (Figure 2).

Operating in the limit of low Reynolds number regime, the moving liquid in the micro-channel has the features of a laminar, viscous and incompressible fluid. Thus, the Hagen-Poiseuille equation can be used to calculate the flow rate in the micro-channel[67],

$$Q = \frac{\Delta P}{R} \tag{2.7}$$

where ΔP is the pressure gradient between the two ends of the channel and R is the fluidic resistance of the channel, which depends on its cross-sectional geometry. For a long flat channel (with high aspect ratio i.e., $w \ll h$ or $h \ll w$) with rectangular cross-section, the fluidic resistance is given by[57],

$$R = \frac{12\mu L}{wh^3} \tag{2.8}$$

where L is the length of the channel, w and h are the width and height of the channel cross-section respectively and μ is the dynamic viscosity of the fluid (in Ns m-2). By placing equation 2.6 for the centrifugally induced pressure gradient across the channel and equation 2.8 for the fluidic resistance into Hagen-Poiseuille equation 2.7, the flow rate initiated by the centrifugal force in the rectangular channel can be calculated[67],

$$Q = \frac{\rho \omega^2 r_m \Delta r w h^3}{12\mu L} \tag{2.9}$$

This equation shows that the geometry and the location of the channel, the fluid properties (e.g., density & viscosity) and the spin speed affect the fluid propulsion on the disc. It is noteworthy that the channel does not necessarily need to be radially oriented and it can be inclined or varied in shape[65].

Centrifugal valving

As mentioned earlier, the flow stops at the junction of the narrow channel and the wide outlet reservoir, even though the disc continues to spin. This happens when the surface tension force (barrier pressure) is greater than that of the centrifugal force. The liquid will flow into the outlet reservoir only if the spin speed (angular frequency) of the disc exceeds a threshold value also called as burst frequency,

$$\Delta P_{centrifugal} \geq \Delta P_{burst} \tag{2.10}$$

In this way, the centrifugal pressure will overcome the barrier pressure, and the valve will burst. This is the basic principle of passive valving on centrifugal microfluidic platforms[68,69]. Valving is an important function for complex sample handling and fluid flow control on the disc. Several types of active and passive valves have been developed[6], among which the capillary, hydrophobic and siphon valves have been theoretically analyzed and described in literature[59,66]. A capillary valve can be formed when the cross-section of a hydrophilic micro-channel expands abruptly, or the wetting properties of the channel are changed suddenly. In both cases, the surface tension at the liquid meniscus induces an inward pressure to the liquid, which is known as capillary pressure. As the rotational frequency of the disc increases, the pressure induced by centrifugal force overcomes the capillary pressure and results in bursting of the valve.

Volume metering on a centrifugal microfluidic platform can be achieved through implementing an overflow channel connected to the main fluidic chamber[70,71]. Once the chamber has filled to the radial level of the overflow channel, additional fluid is routed to a waste chamber (Figure 3).
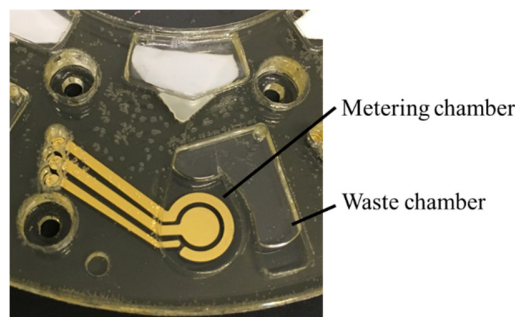

Figure 3. Photograph of a centrifugal microfluidic unit showing volume metering.

2.3 Sample pre-treatment

In past few years, tremendous progress has been made in developing detection techniques for analytical microsystems. However, in the majority of cases, direct analysis of real samples is still challenging to achieve using those techniques. Therefore, the pretreatment of a sample prior to analysis is a vital part of many analytical measurements, independently of whatever technique is subsequently applied for detection. Thus, only those µTAS or LOC devices, which integrate all the essential analytical steps for a complete assay (e.g., sample pretreatment steps and detection) on a single platform, can be considered as truly micro total analysis systems. Whereas, microfluidic systems that possess limited functionalities and require large peripheral equipment for a complete set of analysis are practically chip-in-a-lab, instead of lab-on-a-chip systems[52,72–74].

Analytical chemistry offers a vast number of sample preparation techniques that can be used efficiently to treat samples in laboratories and at large-scale industry processes. However, miniaturization and integration of all such analytical processes in µTAS is a complex task and represents one of the remaining hurdles towards achieving truly miniaturized systems. Thanks to the advancement in microfabrication techniques and the possibility of designing sophisticated microfluidic layouts, it has now been possible to integrate several of these analytical processes in µTAS devices. In general, when working with a real crude sample or a complex sample matrix, µTAS sample preparation methods are expected to achieve:

- Extraction of the analyte of interest: This means that the analytical processes should be selective enough to extract and isolate the analyte of interest from rest of the matrix. In addition, it should also ensure that the analyte is present in a form compatible with the detection method chosen for the final analysis.
- Sample preconcentration: Sometimes the sample contains the analyte of interest in such a low concentration that the detection method is not sensitive enough. In such cases, sample preconcentration or upconcentration methods are needed prior to analysis.

A large number of sample pretreatment procedures has already been integrated with microfluidic devices[75–78], however, it is far beyond the scope of this thesis to cover all of them. Moreover, there

is no universal approach to sample pretreatment, and the sample preparation always has to be adopted according to the sample under investigation as well as the analytical method chosen. Therefore, we decided to discuss only two types of sample preparation procedures that have been used in this work, i.e., filtration and supported liquid membrane (SLM) extraction, especially regarding integration on a LoD platform. The sample pretreatment procedures used here are based on two entirely different principles. Besides filtration, which is based on the physical properties (size) of the particles that have to be removed from the liquid phase, the SLM extraction is completely dependent on the chemical properties (ionized/charged state) of the analytes that have to be extracted and enriched from the sample.

In the frame of this Ph.D. project, we have been working with liquid samples from suspension culture of wild type (CBJ786) and genetically modified (CBJ792 and CBJ800) *E. coli* cells grown for up to 24 hours. The genetically modified strains were incorporated with a tyrosine ammonia lyase (TAL) gene with the variable efficiency of pHCA production. pHCA is a valuable phenolic compound with anti-oxidant properties, obtained via deamination of tyrosine (Tyr)[79] by TAL. Before the cell culture, cheaply available Tyr was added to the cell culture media as a substrate to get the commercially valuable compound, pHCA at the end of the cell culture (24 hours). In the absence of TAL gene, the wild type strain consumes the entire Tyr, whereas based on the efficiency of the incorporated TAL gene, the genetically modified strains partially metabolized the Tyr and converted the rest into pHCA.

To optimize the production of pHCA, the best performing strains need to be identified. However, Tyr and pHCA are structurally very similar with adjacent electrochemical oxidation potentials. Therefore, they are difficult to be identified when both analytes are present in the same sample. As mentioned earlier, and shown in supplement information of Paper I, after 24 hours of cell culture, almost the entire amount of Tyr was metabolized and/or converted into pHCA. Therefore, Tyr did not interfere with the electrochemical detection of pHCA in cell culture samples grown for at least 24 hours. However, it was found that the cell density in a cell culture increases prominently over time which in turn affects the electrochemical measurements due to sedimentation of cells onto the electrode, resulting in electrode fouling. Hence, it was decided to integrate the on-disc cell filtration

to determine the pHCA produced at the end of the bacterial culture (24 hours) as it is presented in Paper I.

2.3.1 Filtration

To avoid clogging of the microfluidic channels or to prevent the negative interference of the particulates in the sample with the analytical procedure, the particulates must be removed from the sample prior to analysis. The removal of particulates can be done off-device (before injecting the sample into the microfluidic device) leading to the chip-in-a-lab system, or it can also be done on-device leading to true LOC system. In many cases, the off-device filtration processes require a larger volume of samples than the volume needed for filtration directly on a microfluidic device. Off-device filtration is thus likely to result in longer and more expensive sample processing. The on-device particulate removal can be done by physical separation techniques such as filtration[67,80–84] or sedimentation[85–89]. However, sedimentation may not be capable of eliminating fine particulate matter that may not be significantly affected by the centrifugal force applied due to size and density. Incorporating on-device filtration, that is automated and need small sample volume has advantages associated with time, cost and analytical throughput. As discussed by Rios and Zougagh, two approaches have already been employed several times for on-chip sample filtration, i.e., structural-based filtration and diffusion based filtration[78]. However, these approaches require very sophisticated technology and are not very convenient to incorporate into centrifugal devices.

Inspired by a successful demonstration of achieving axial centrifugal filtration by incorporating physical filters into the centrifugal device by Karle et al. and Templeton et al., we also decided to adopt this hassle free, yet very effective approach[80,81]. The overall processing time of the on-disc filtration process depends on parameters like the type of filter, the composition of the sample matrix, rotational frequency and radial distance from the axis of rotation. Hence, other than the composition of the sample matrix, all the remaining parameters can be tuned as per requirements to obtain fast and efficient filtration. As described in Paper I, microporous cellulose acetate membranes (Tisch Scientific, North Bend, OH, USA) with 0.2 μm pore size were successfully incorporated into the custom made LoD system. Before analyzing a real sample, the functionality of the integrated filter membranes was first tested using a solution of magnetic beads as these beads

provide a strong contrast and agglomerates be easily visible to the naked eye. To make a translucent solution, 10 µl of 100 mg/ml magnetic beads (diameter = 1µm, Dynabeads MyOne Streptavidin beads, Invitrogen) were added to 2 ml of 100 mM cell culture PBS. The loading chamber was filled with 120 µl of this translucent solution as shown in Figure 4A. As the device was spun at 700 rpm, the liquid started moving from loading chamber to the collection chamber via the filter membrane and finally from the collection chamber to the detection chamber (Figure 4B). Within five minutes of rotation, clusters of bead start becoming evident at the bottom edge of the loading chamber and over the filter membrane, whereas the optically clear PBS was transferred to the detection chamber as shown is Figure 4C. To keep the sample volume constant for electrochemical measurements, the detection chamber was made in the form of a metering chamber able to accommodate 80 µl of liquid; thereby the extra liquid was over flown to the waste chamber during the filtration process. As can be seen in Figure 4C, even after five minutes of filtration, a little volume of magnetic bead solution was left unfiltered in the loading chamber. This was not the case while working on the *E. coli* cell culture suspension. The obvious reason for this could be the clogging of the filter membrane due to the high concentration of magnetic beads, whereas the cell density of *E. coli* cells in cell suspension was not sufficient to clog the membrane. Although clogging of filter membranes was not an issue for our experimental work, it can be easily prevented on centrifugal microfluidic platforms as described by Karle et al. Hence, the preliminary filtration test with magnetic bead solution confirmed the successful integration of the filter membrane into the LoD device for efficient and leak proof filtration. Thenceforth, the platform was used to filter out the *E. coli* cells from the cell culture grown for 24 hours, enabling electrochemical measurement of pHCA without any interference.
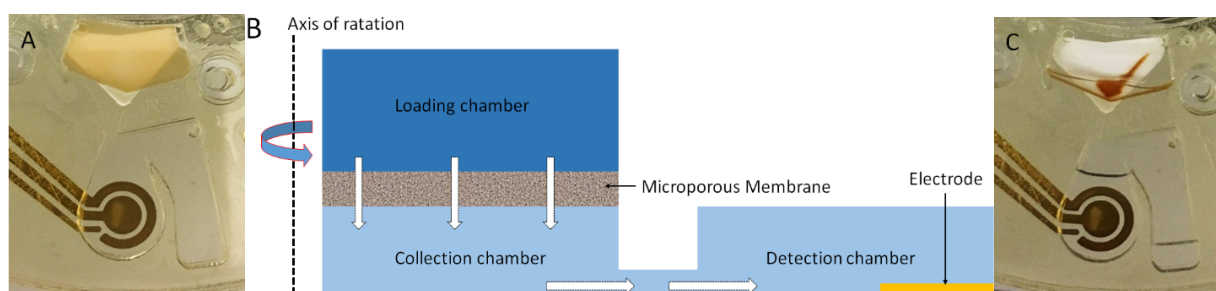

Figure 4. (A) and (C) Photographs demonstrating on-disc filtration of magnetic bead solution before and after filtration respectively. (B) Schematic of the cross section of the microfluidic layout showing flow path through the filtration system (the arrows show the direction of the fluid movement during rotation).

2.2.2 Supported liquid membrane (SLM) extraction

After accomplishing our goal of screening the genetically modified *E. coli* cells based on the determination of the pHCA produced at the end of the bacterial culture (24 hours), we intended to determine pHCA production over time. Time independent detection would help the bioengineers to gain more insight into the kinetics of pHCA production by genetically modified strains. However, the presence of the interfering compound Tyr at different concentrations throughout the cell culture was known to interfere with electrochemical detection. To eliminate the effect of Tyr and to achieve time independent pHCA monitoring, we implemented on-disc SLM extraction, which enabled the extraction of pHCA from the sample. The process was developed and optimized by Ph.D. student Sune Zoega Andreasen.

In analytical chemistry, solid phase extraction (SPE) and liquid/liquid extraction (LLE) are two widely used extraction and purification methods available for sample pre-treatment. In SPE, the samples are adsorbed on solid phase matrix with appropriate chemistry to effect purification or concentration, and they are later released using a stronger eluent. The larger the surface of the solid phase matrix is, the more the samples are adsorbed on matrix. Many SPE based microfluidic devices have been reported that can minimize sample loss and contamination problems as well as reduce the analysis time[90–93]. On the other hand, LLE facilitates the selective removal of one or more components either from a homogeneous liquid mixture or a solution. This is usually achieved by contacting the sample solution with another liquid or solvent, which is partially or wholly immiscible with the sample solution. At the micro scale, the high surface-to-volume ratios and short diffusion distances, combined with laminar flow conditions, offer the possibility of performing chip-based LLE. LLE offers a high versatility and selectivity for the extraction of different types of compounds based on the chemical properties of solvents used in the extraction. However, considering the complexity of fabrication and the difficulty to automate the process, limited work has been done so far to integrate LLE into a microfluidic system[94–96].

Another alternative approach to these two methods is the membrane-based extraction where both porous and non-porous membranes could be used for extraction. In this method, the membrane is

used to separate two liquid phases (donor and acceptor phase) allowing the constituents of the phases to pass through the membrane. In case of porous membranes, the two phases are in direct contact with each other at the interface like in dialysis. Whereas, in case of non-porous membranes where the pores are filled with an organic solvent that is immiscible in both the phases, the two phases are indirectly connected via the organic phase in between. The membrane is used here to support the oil or organic solvent that is needed to separate the acceptor and donor phase to create a simultaneous LLE system at donor-oil and oil-acceptor interfaces[97–99]. This particular extraction approach is called SLM.
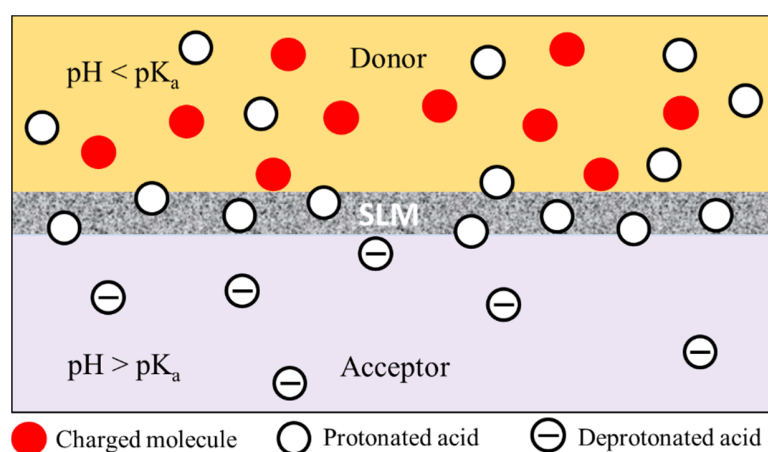

Figure 5. Schematic showing the SLM extraction system where two aqueous phases (donor and acceptor phase) are separated by an organic phase trapped in pores of the hydrophobic membrane by capillary forces. Low pH in donor phase protonates the acid group of the small molecule (protonated acid), hence making it neutral. Neutral molecules diffuse through the organic phase to the acceptor phase, where high pH deprotonates the acid group to develop charge on the molecule (deprotonated acid), thus making it insoluble in the organic phase and retain it in acceptor phase.

The governing principle for SLM is simple and straightforward (Figure 5). By changing the pH in the donor and acceptor solution, it is possible to protonate or deprotonate molecules with acidic (for example carboxylic acid-groups) or basic groups (for example amino-groups), thereby changing the state of the molecule from neutral to an ionized/charged state, and vice versa. Since neutral molecules are much more soluble in an organic phase (given by the partition coefficient, Kp, small), neutral molecules from the donor side can diffuse through the organic phase (trapped in membrane pores separating the donor and acceptor phase) to the acceptor side. By adjusting the pH of the acceptor buffer above the pKa for acidic compounds (below for basic compounds), the

analyte that reaches the membrane-acceptor phase boundary will be deprotonated (protonated for basic compounds) and thus charged. Since the solubility of a charged compound in the organic phase is several orders of magnitude smaller than for the neutral state, the analyte will be effectively trapped in the acceptor phase. As the only analyte in its neutral form can diffuse through the membrane, the concentration gradient driving the extraction is intact (in other words, the concentration of an analyte in a neutral state at the membrane-acceptor boundary is zero), and the analyte will continue to up-concentrate/enrich in the acceptor phase.

pHCA is an organic acid containing the carboxylic group (pKa ~ 4), whereas Tyr contains a basic amino group (pKa ~ 2) (Figure 6). Thus, the above-described SLM extraction principle could be applied for an efficient separation of pHCA from Tyr (from donor phase), and possible enrichment of pHCA (in acceptor phase). To extract pHCA, from a mixture of pHCA and Tyr, in M9 medium (pH 6.8) or cell culture supernatant (pH 5.8), the donor was acidified using sulphuric acid to bring the pH below the pKa value of pHCA i.e., pH < 2. On the contrary, phosphate buffer saline (PBS, pH 7.4) was used as acceptor phase to keep the pH above the pKa value of pHCA. Consequently, the pHCA was neutralized in donor phase (due to protonation at low pH) and transferred to the acceptor phase through the organic phase. The higher pH in acceptor phase further deprotonates the neutral pHCA molecule to a charged molecule, thus leading to its entrapment and enrichment in acceptor phase. Using this procedure, the SLM extraction integrated on LoD device has been successfully used for eliminating the interfering compound Tyr from the *E. coli* cell supernatant to facilitate electrochemical determination of pHCA at different time points during production as described in Paper II.
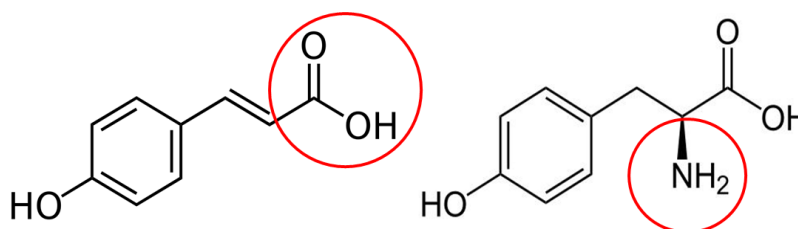

Figure 6. Chemical structure of pHCA and Tyr, containing acidic carboxylic group (left) and basic amino group (right), respectively.

3. Sensor development and applications

In simple words, we can define a sensor as a device for sensing changes or variations in given environment and converting it into an appropriate measurement signal[100]. Based on physical phenomena, the sensors can be classified as optical (absorbance, fluorescence, imaging, etc.), mechanical (displacement, strain, pressure, torque, weight, etc.), thermal (temperature, heat) and electrical (voltage, current, etc.)[101]. Irrespective of the type of sensor, several common parameters have to be considered or given importance in sensor development such as accuracy, precision, resolution, sensitivity, specificity, etc. In addition, in case of certain specific applications (e.g., industrial production or research, integration into microdevices, etc.) some additional factors could also be considered such as fast response time, low-cost, the possibility of multiplexing, user-friendliness, etc.

The ideal sensor is expected to fulfill all the above-mentioned requirements; however, in the majority of cases, this is challenging to achieve. Especially when we consider integrating the sensors with μTAS devices, where the miniaturization of the sensor is imperative along with the other aspects like selectivity, sensitivity, response time, etc. Thanks to the advances in micro- and nanotechnology, numerous μTAS devices have been developed with integrated miniaturized sensors over the past decade. Despite the enormous progress that has been made in the overall field of sensor integration with μTAS devices, to stay within the scope of this thesis, we will focus solely on sensing methods implemented on a sub-section of μTAS, i.e., centrifugal microfluidics or LoD devices. Sensing on LoD devices is indeed a challenging task as the microfluidic disc is spinning while the assays are performed. Still, various sensing methods such as optical, mechanical and electrochemical are successfully implemented on LoD devices to achieve stable read-outs in static (no spinning) and dynamic (while spinning) conditions.

3.1 Optical sensors

Possibly, due to its high sensitivity, specificity and wide array of available sensing techniques, optical detection is one of the most commonly used detection methods for biological assays in general. Moreover, due to the non-contact nature of the read-outs, these detection methods are suitable for implementation and integration with centrifugal microfluidic platforms[13,14]. However,

perfect integration with a spinning disc is somewhat challenging due to the impaired accuracy of optical alignment caused by the wobbling of the spinning disc and the lack of a direct mechanical interface between the rotating disc and the optical detection system. Luckily, several approaches have been already proposed in the literature to limit the wobbling induced read-out errors[64] and to surpass the need of direct optomechanical connection[102–104] that further facilitates reasonable optical sensing on LoD devices. To address several applications in biomedical diagnostics and environmental monitoring, a wide range of label-free approaches such as absorbance,[105–107] scattering,[108,109] total internal reflection[110,111] and label-based methods such as fluorescence[112–115] and luminescence[116] based detection have been successfully implemented on LoD devices. In addition, a lot of importance has also been given to the integration of imaging based[104,117] and optical disc drive (ODD) pick-up based[118,119] methods. Consequently, several LoD devices with integrated optical detection techniques are commercially available and many are on their way to be commercialized soon[12].

3.2 Mechanical sensors

Indeed, sensing and read-out of results using mechanical sensors onto the LoD devices are far more challenging as compared to the optical sensors. Perhaps that is the reason that not much work has been done so far to implement the mechanical sensing techniques on centrifugal microfluidic platforms. However, due to their sensitivity, portability, parallelization, and versatility, micrometer-sized cantilevers are gaining considerable interest for field based applications in point of care diagnostics, homeland security and environmental monitoring[120–122]. Cantilever sensors are primarily used to measure the changes in static deflection, i.e., surface stress. However, the technique can also be used to monitor changes in bulk stress and mass. For the first time, Bosco et al. have demonstrated the integration of cantilever based sensors onto the centrifugal microfluidic platform, where 90 cantilever chips (8 cantilevers per chip) made of silicon or polymer were mounted on a microfluidic disc. The deflection profiles of the cantilevers during rotation were measured using an optical pickup unit (OPU) placed below the disc[123]. The platform was successfully used to demonstrate the detection of an explosive called 2,4-dinitrotoluene (DNT),[124] proteins[125] and a prognostic biomarker (suPAR)[126]. This work shows the potential of using mechanical sensors on a microfluidic disc for easy liquid handling and high throughput screening

of multiple samples. However, the integration and implementation of other mechanical sensors on LoD devices are still challenging.

3.3 Electrochemical sensors

Regarding cost, sensitivity, miniaturization possibility for both sensor (electrode) and instrumentation (potentiostat), portability, and ease of alignment, the electrochemical detection methods are more feasible to implement on LoD devices as compared to other detection techniques. Moreover, the electrochemical detection has faster response time and demands minimal electrical power, is independent of sample turbidity or optical path length. The implementation of electrochemical sensing on disc platforms is governed by simple integration of two (WE and [CE+RE])[127] or three-electrode array (WE, CE and RE)[128–130] onto the microfluidic disc. In the majority of cases, the sample handling is done by spinning the disc followed by the electrochemical measurements in static condition[127,129,131]. However, some reports also demonstrate LoD systems capable of performing electrochemical measurements while spinning the disc with the help of electrical slip ring or mercury-based rotating electrical connector[128,130,132,133]. Although the electrochemical detection in Paper I was performed under static condition, as this was suitable for the assay, the presented electrochemical setup facilitates simultaneous electrochemical measurements in eight different chambers at a rotation speed up to 2500 rpm.

As far as an electrode material is concerned, both metal and carbon electrodes have been integrated into microfluidic discs for various applications, however, in most of the cases, the electrodes are patterned on either Si[129] or glass[128,130,132] substrates, whereas the rest of the fluidic assembly is made in polymers. We have developed an electrode fabrication process to pattern robust and reliable electrodes on non-conductive and low-cost polymer substrates (described in detail in section 5.2) that are commonly used to fabricate the microfluidic disc assemblies. Irrespective of the electrode design and material, various electrochemical detection techniques can be used to detect the target analyte directly (in case of an electroactive analyte like pHCA)[134] or indirectly (in case of a non-electroactive analyte like glucose)[131,135]. Among all the techniques, amperometry is the commonly used technique in conjunction with centrifugal microfluidic platforms. However, reports also confirm the successful implementation of impedance-based detection[127] and other

voltammetry techniques[134]. Overall, a fully automated LoD device integrated with electrochemical sensors has great potential as an analytical tool for applications where ease of handling and minimal sample preparation is required for fast and reliable analysis.

3.3.1 Brief introduction to general Electrochemistry

Electrochemistry is the branch of chemistry that studies the phenomena resulting from combined chemical and electrical effects, i.e., the influence of electric current on chemical reaction or vice-versa. In general, an electrochemical cell consists of two electronic conductors (electrodes) immersed in an ionic conductor (electrolyte solution). A charge transport in the electrodes occur via the motion of electrons or holes, and in the electrolyte via the motion of positive or negative ions. An electrochemical reaction occurs on each electrode, referred to as a half cell reaction for the individual electrodes. Hence, the overall electrochemical reaction of the cell is given by combining the two individual half cell reactions. Depending on the direction of electron transfer from the electrode to the redox species in solution or vice-versa, the half cell reaction can be either oxidation (anode) or reduction (cathode) reaction.

Thermodynamic cell potential

The relation between the free energy change and the maximum electrical work that can be performed, as expressed in terms of electrode potential E of a half cell reaction is,

$$\Delta G = -nFE \tag{3.1}$$

where n is the number of electrons transferred in the reaction (from balanced reaction), F is the Faraday's constant (96485 C/mol). Under standard conditions i.e. pressure of 1 bar, a temperature of 298.15 K, pH = 0 and a concentration of 1.0 M for each product of a reaction, the above equation can be written as,

$$\Delta G^o = -nFE^o \tag{3.2}$$

The Gibbs free energy at standard conditions gives an indication whether the reaction will take place spontaneously or not. That means, when E^o is positive, the reaction is spontaneous and when

E^o is negative, the reaction is non-spontaneous. From thermodynamics, the Gibbs energy change under non-standard conditions can be related to the Gibbs energy change under standard conditions via,
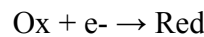
$$\Delta G = \Delta G^o + RT\ lnQ \tag{3.3}$$

where R is the universal gas constant (8.3145 J/mol K), T is the absolute temperature and Q is the reaction quotient of the reaction.

Substituting $\Delta G = -nFE$ and $\Delta G^o = -nFE^o$ in equation 3.3, the electrode potential of a reaction also called Nernst potential can be obtained as,

$$E = E^o - \frac{RT}{nF}\ lnQ \tag{3.4}$$

Considering the reaction,

$$Ox + e\text{-} \rightarrow Red$$

where Ox is the oxidized and Red is the reduced species, respectively. Under standard conditions, the reaction quotient of the reaction can be expressed as,

$$Q = \frac{\alpha_{Red}}{\alpha_{Ox}} \tag{3.5}$$

where α_{Ox} and α_{Red} is the activity of the oxidized and the reduced species, respectively. Substituting $Q = \alpha_{Red}\ /\ \alpha_{Ox}$ in equation 3.4,

$$E = E^o + \frac{RT}{nF}\ ln\frac{\alpha_{Ox}}{\alpha_{Red}} \tag{3.6}$$

In above equation, E is equal to E^o when the activities of all species are unity. However, such standard state conditions are often difficult to achieve in practice, and therefore standard-state potentials are often replaced by the formal potentials, $E^{o\prime}$. The formal potentials are sometimes called conditional potentials to denote that they apply under specified conditions (including pH,

ionic strength, and concentration of complexing agents) rather than under standard conditions[136]. This quantity is the measured potential of the half cell when the ratio of the total concentrations of oxidized and reduced species is unity and other specified substances (e.g. protons) take part in the redox reaction, which is the case for many biological reactions.

At thermodynamic equilibrium, when no current flows through the electrochemical cell in the presence of redox couple in the solution, the concentrations of the oxidized and the reduced species at the electrode surface is equal to the corresponding bulk concentration. Hence, the Nernst equation can be written as,

$$E = E^{o\prime} + \frac{RT}{nF} \ln \frac{C_{Ox}}{C_{Red}} \tag{3.7}$$

where C_{Ox} and C_{Red} are the bulk concentration of the oxidized and the reduced species respectively. This is valid approximation as long as the electrolyte concentration is low, and the pH and ionic strength of the sample matrix is unchanged, which seems reasonable to assume in cases, where electrochemical techniques are used for detection purposes.

Current in electrochemical cells

Two types of processes can conduct currents across an electrode/electrolyte interface in an electrochemical cell. One that involves a direct transfer of electrons via oxidation or reduction reaction at an electrode/electrolyte interface is called a faradaic process. These type of processes are governed by faraday's law, which states that the amount of chemical reaction at the electrode is proportional to the amount of current, the resulting currents are called faradaic currents. On the other hand, when the changes exist in the electrode/electrolyte interface without charge transfer, such processes are called non-faradaic processes. Non-faradaic processes involve the adsorption/desorption of ions and molecules on the electrode surface that can generate transient external currents.

The generation of current in an electrochemical cell can be best explained by looking at the Fermi-level (the highest energy level which an electron can occupy at the absolute zero temperature) of the metal electrode in contact with the electrolyte. The Fermi level can be considered as the sea of

electrons above which no electron exists because of lack of sufficient energy at zero Kelvin. The continuous fermi level of a metal electrode can easily be altered by applying negative or positive potential at the electrode. For example, by applying a negative potential, the Fermi level of an electrode increases above the lowest vacant molecular orbital of the electroactive molecule in the solution, resulting in the transfer of electrons from the electrode to the species in solution (gain of electron). Thus, leading to the reduction of the oxidized species in solution (Figure 7). On the contrary, when a positive potential is applied, the Fermi level drops below the highest occupied molecular orbital of the electroactive molecule, and the transfer of electrons occurs from the species to the electrode (loss of an electron). Consequently, leading to the oxidation of reduced species in solution (Figure 7).
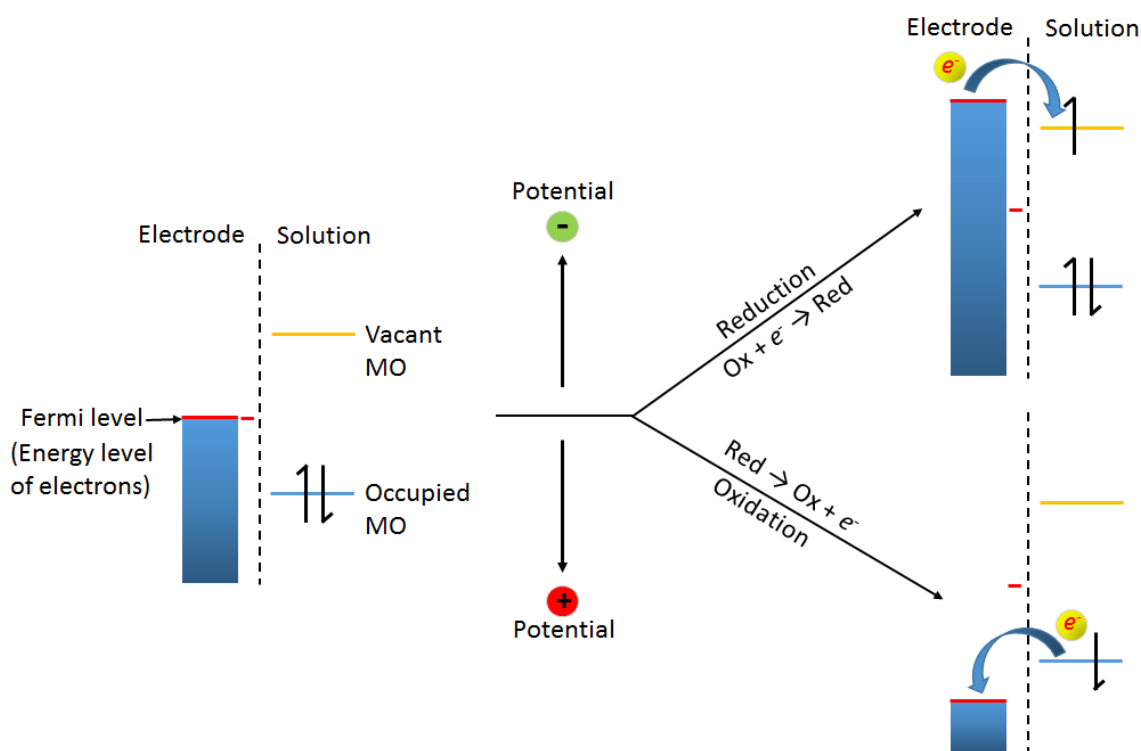

Figure 7. Oxidation and reduction reaction at the electrode/electrolyte interface, caused by applying a positive or negative potential over the equilibrium potential, respectively. Adapted and modified from[137].

The electron transfer between the conductive electrode and the soluble species in the electrolyte generates a current. According to Ohm's law (I = V/R), the amplitude of this current is influenced by the Ohmic resistance of the electrochemical cell and the amplitude of the potential required to

activate the charge-transfer reactions. Therefore, the current response of an electrochemical cell is a nonlinear function of applied potential. This explains why it is possible to probe or quantify a redox active analyte by simply measuring the current(s) generated by the chemical process at a certain applied potential(s). In addition, it is also evident that a positive or negative potential (deviating from formal potential, $E^{o'}$) must be applied for an electrochemical reaction to take place at the electrode/electrolyte interface. This applied potential with respect to the $E^{o'}$ is referred to as overpotential (η) that serves as a driving force to perturb the equilibrium and triggers the electrochemical reaction. In simple words, the overpotential can be defined as the difference between the thermodynamic potential of a reaction and the potential at which it actually occurs. Overpotential is required for several reasons such as electron transfer across the charge double layer, depletion of concentration at electrode surface, chemical reactions that must occur before electron transfer etc.

Resistance in electrochemical cells

There are two types of resistance usually present in an electrochemical cell. The first one is generated due to the electronic current through the electrodes and the external circuit called electronic resistance. Whereas, the other one arises due to the ionic current through the electrolyte called ionic resistance (R). The electronic resistances can be easily minimized by using conducting materials such as metals. However, various ion transport related parameters have to be considered in order to minimize the losses caused by the ionic resistance. The buildup of ionic charge (excess of positive and negative ions at anode and cathode, respectively) has to be released by ion transport where positive ions move from anode to cathode and vice versa. The fractions of current carried by the positive and negative ions are given by their transport numbers t_+ and t_- respectively and the amount carried by each is proportional to its speed. Since,

$$Transport\ number\ of\ ion = \frac{I_{ion}}{I} \tag{3.8}$$

where I_{ion} is the current carried by the ion and I is the total current. Therefore,

$$t_+ = \frac{u_p}{u_p + v_n} \quad \& \quad t_- = \frac{v_n}{u_p + v_n} \tag{3.9}$$

where u_p and v_n represents the speed of migration of the positive and negative ion respectively. The fraction of the total current carried by the ions is directly proportional to their velocities (Hittorf's rule).

$$t_+ + t_- = 1 \tag{3.10}$$

Considering, that more than one type of ion is present in an electrolyte solution, the cumulative transport number of positive and negative ions is given by equation,

$$\Sigma t_i = 1 \tag{3.11}$$

However, the transport number of ions is determined by the conductance (L) of the electrolyte,

$$L = \frac{kA}{l} \tag{3.12}$$

where A is active area of the electrode, l is thickness of the electrolyte matrix and k is an intrinsic property of the electrolyte called conductivity. Conductance has units of Seimens (S), and conductivity of S/cm. The conductivity of the electrolyte has a contribution from every ion in solution and is proportion to the concentration of ion (C), charge of ion (z) and the mobility (property that determines the migration velocity of ion). Mobility is defined as the limiting velocity of the ion in an electric field of unit strength. The force exerted by an electric field of strength E is given by,

$$F = eEz \tag{3.13}$$

where e is the electric charge and z is the charge of ion. However, an opposing force also exists due to frictional drag, which is expressed by the Stokes equation,

$$F_{opp} = 6\pi\vartheta rv \tag{3.14}$$

where ϑ is the viscosity of the electrolyte, r is ionic radius and v is velocity of the ion in the electrolyte. When the forces exactly counterbalance each other, the ion attains a steady state velocity called the terminal velocity. This terminal velocity is termed as mobility (u) when the electric field strength is unity. Hence, from equations 3.13 and 3.14, the equation for mobility is given by,

$$u = \frac{ze}{6\pi r\vartheta} \tag{3.15}$$

As mentioned earlier, the conductivity of the electrolyte has a contribution from every ion in the solution and is proportional to C, z and u. Hence, with the above expression for mobility, we can write the following expression for conductivity,

$$k = F \, \Sigma z_i u_i C_i \tag{3.16}$$

The transport number can be expressed as the ratio of the conductivity by a specific ion to the total conductivity of the solution. Thus,

$$t_i = \frac{z_i u_i C_i}{\Sigma z_i u_i C_i} \tag{3.17}$$

As resistance is reciprocal of conductance, from equation 3.12, we can define resistance as,

$$R = \frac{l}{kA} \tag{3.18}$$

Considering Ohm's law,

$$V = IR \tag{3.19}$$

i.e., resistance will introduce a potential drop, which will increase with current. However, it can be said from equation 3.18 that the ionic resistance can be minimized by minimizing the distance between the electrodes and by increasing the area of contact. Unfortunately, some resistance will always remain, even after considering all the parameters to minimize the ohmic drop. However, it can always be compensated to calculate the actual potential if the value of R is known.

Mass transport in electrochemical cells

Three fundamental modes of mass transport that affect the rate at which the reactants and products move towards or away from the electrode surface in solution are diffusion, migration, and convection. Diffusion arises due to the concentration gradient, i.e. when the concentration of the electroactive species near the electrode surface is different from that of bulk concentration. The region of solution over which diffusion occurs is called diffusion layer (Figure 8A). In the absence of any other modes of mass transport, the thickness of diffusion layer (δ) increases over time as the electroactive species have to diffuse from far distance (Figure 8B) and the diffusion is governed by the Fick's law of diffusion.
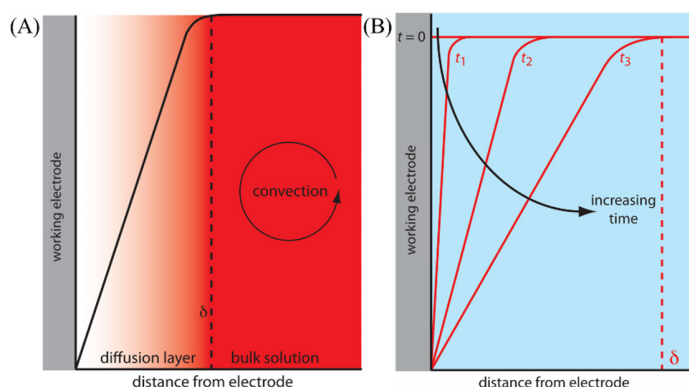

Figure 8. (A) Nernst diffusion layer (δ) separating working electrode from bulk solution, (B) Concentration gradients (red) for electroactive species following the application of a potential that completely reduces it. (Adapted and modified from[138])

Migration is the motion of a charged body (such as an ion) under the influence of an electrical potential gradient. For example, if the electrode surface is positively charged then only anions will be attracted towards the electrode whereas the cations will be repelled towards the bulk solution and vice versa. Migration only affects the charged particles. Therefore, it is possible to eliminate mass transport via migration by adding a high concentration of an inert supporting electrolyte. Convection is a hydrodynamic transport either due to density gradients (natural convection) or due to external means such as stirring (forced convection). Eliminating the natural convection is imperative. However, the forced convection can be easily eliminated simply by not stirring the solution. If diffusion is the only significant form of mass transport, then the current in electrochemical cell is given by

$$i = \frac{nFAD\,(C_{bulk} - C_{x=0})}{\delta} \tag{3.20}$$

where n is the number of electrons in the redox reaction, F is the faraday's constant (96485 C mol-1), D is the diffusion coefficient of the electroactive species (cm^{2}s^{-1}), C_{bulk} and $C_{x=0}$ are the concentration of the electroactive species in bulk and at the electrode surface (mol cm^{-3}), A is the electrode area (cm^2), and δ is the thickness of the diffusion layer.

Three-electrode system

As mentioned earlier, the overall electrochemical reaction consists of two half-reactions that relate to real chemical changes at each electrode. However, often only one of these reactions is favorable. The electrode at which the reaction of interest occurs is conventionally called the working electrode (WE). To concentrate on the reaction of interest, the other half-cell needs to be consistent. For that purpose, an electrode with a fixed potential and constant defined composition is used, conventionally referred to as reference electrode (RE). Thus, any change in the cell is due to the WE. To close the circuit, a third electrode named counter electrode (CE) is used. In fact, the excitation potential is applied to the WE and is adjusted with respect to RE, whereas the current flows between CE and WE through the electrolyte. For avoiding the interference of CE reactions with the WE reactions, usually an inert material with fast electron transfer kinetics is used for CE. Figure 9 illustrates the schematic of a three-electrode system (designed, fabricated and employed in Paper III).
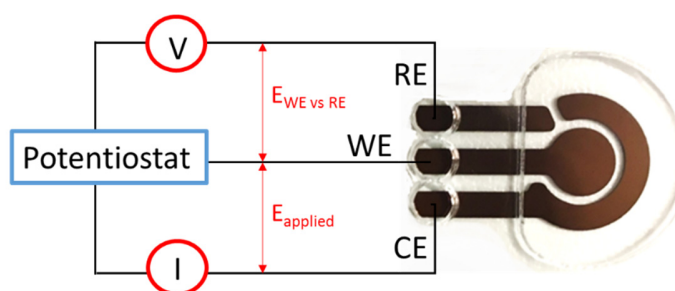

Figure 9. Three-electrode system demonstrating counter (CE), working (WE) and reference (RE) electrode. The excitation potential is applied to the WE and is adjusted with respect to the RE. The current response of the system is measured between WE and CE.

Working electrode

The WE acts as a source or sink of electrons for exchange with electroactive molecules at the electrode/electrolyte interface. For the success of an experiment, several important factors must be considered to select a proper material to fabricate the WE. It should be chemically inert and exhibit favorable redox behavior with the analyte, i.e., fast and reproducible electron transfer kinetics without electrode fouling. The potential window over which the electrode performs in a given electrolyte solution should be as wide as possible to allow the greatest degree of analyte characterization. It should have low background current over the potential range required for the analysis along with high signal-to-noise ratio. Additional considerations include surface reproducibility, availability, regeneration capability following a measurement, cost, mechanical properties, and toxicity. The most commonly used WE materials are platinum, Au, carbon (glassy carbon, graphite, carbon paste, pyrolytic carbon, etc.) and mercury. They can be used directly or can be modified in different ways as per the requirement of the experiment. Moreover, semiconductors can also be used as WE. However, the electron transfer kinetics would be much slower here as compared to the metals due to the low density of electrons. The performance of WE is also size dependent, where decreasing the size of the electrode to micro dimensions (microelectrode) reduces the ohmic drop at the electrode, reduces the electrode capacitance and at the electrode surface changes the diffusion from linear to radial[136,139].

Counter/Auxiliary electrode

The CE is made of an inert conducting metal that balances the electrochemical reaction occurring at the surface of WE without limiting and interfering it. To support the current generated at the WE, i.e., to receive all the electrons transferred from the working electrode, the surface area of the auxiliary electrode must be equal to, or larger than, that of WE. Moreover, the material of the CE should possess similar or faster electron transfer kinetics as compared to the WE. Platinum (Pt) is one such metal that possesses all these characteristics, and it is often used in electrochemical experiments. However, in this study, we have used Au as the material to fabricate the CE, where the area of CE is more than twice as that of WE.

Reference electrode

An ideal reference electrode is one that maintains a constant potential irrespective of the amount of current passed through it. It should not react with sample under investigation, should be non-polarizable (charge can move in and out without changing its potential), and should have stable and well-defined electrochemical potential. Standard hydrogen electrode (SHE) is a primary reference electrode whose potential is considered to be zero and used to determine the standard electrochemical potentials under standard conditions. It consists of a Pt electrode immersed in a solution with 1 M hydrogen ion concentration, which is bubbled through with hydrogen gas, at 1 atm pressure. SHE is not widely used, as it is hard to obtain a solution of 1 M activity and to keep hydrogen gas at 1 atm pressure during all electrochemical measurements. Instead, secondary reference electrodes such as saturated calomel electrode (SCE) and silver/silver chloride electrode (Ag/AgCl) are much more commonly used reference electrodes. In SCE, a calomel (Hg_2Cl_2) coated mercury electrode is immersed in a solution of potassium chloride and saturated calomel. Whereas, in Ag/AgCl electrode, the silver chloride coated silver electrode is immersed in saturated potassium chloride solution. Although, these electrodes are more stable and reliable, given the size constraints and the cumbersome fabrication process, pseudo-reference electrodes (pseudo-RE) are more popular in microfluidic systems[140].

In this work, we have recorded the electrochemical signals against Au pseudo-RE, as it was easy to fabricate it along with CE and WE by simply depositing the Au through the same shadowmask. Moreover, to run short-term electrochemical experiments, it was acceptable to use Au pseudo-RE for reproducible measurements. In addition, we have also tried chlorinated silver wire as a Ag/AgCl pseudo-RE in batch assembly setup designed to work with nano-structured Au coated Si substrates as WE (batch assembly setup is described in section 5.4).

3.4 Dual functionality sensors

In this thesis, more emphasis has been given to the electrochemical sensing due to several advantages associated with the technique. However, the capability of optical sensors such as SERS cannot be omitted providing low detection limits down to single molecular levels[141]. There are reports available where researchers have developed sensors suitable for both detection techniques

such as dual functionality sensor[15–20] or exploited electrochemistry to enhance the SERS signal such as EC-SERS[21–27]. However, in the majority of cases, the dual or bi-functionality sensor comprises of substrate capable of performing SERS and acts as WE requiring external CE and RE for electrochemical measurements. These set-ups are comparatively big and require sample volumes in milliliter range for the analysis, for example dipping the WE chip in a flask filled with sample/electrolyte along with external CE and RE.

To avoid the operational inconvenience and reduce the sample volume to microliter range, we have designed and developed a miniaturized sensor in the form of three-electrode configuration on fused silica substrate capable of performing SERS as well as electrochemistry. The sensor is fabricated by maskless RIE of fused silica followed by e-beam Au deposition through a shadowmask. Paper III has presented the detailed fabrication, characterization, and applicability (using paracetamol as a model analyte) of the sensor as an efficient dual functionality sensor. In addition, the substrate can be potentially used as EC-SERS by sputtering the Au to pattern the electrode configuration instead of e-beam evaporation. The Au sputtering will cover the entire insulating nanostructures on a glass substrate, making it conductive, thereby potential could be applied to concentrate the target analyte in hot spots suitable for EC-SERS. However, fully conductive nanostructures might influence the SERS activity[142]. Therefore, we fabricated another batch assembly (section 5.4) using Au coated nanostructured Si chips with external CE (Pt wire) and RE (AgCl coated Ag wire). The Si substrate is comparatively cheap to fused silica and does not require sputtering for EC-SERS as potential could be applied in hot spots due to semi conductive nature of Si. Moreover, several batch assemblies (more than 25) could be fabricated from single 4-inch Si wafer leading to high throughput.

The performance of the dual sensor (Au coated nanostructured Si chips) was evaluated for SERS and electrochemistry. CVs showed an improved electrochemical behavior for dopamine on nanostructured electrodes when compared to the 2D electrodes with same geometry (Figure 10A). We observed that nanostructured electrodes provide certain benefits when it comes to electrochemical detection in comparison with planar electrodes. We recorded dopamine oxidation at 350 mV on planar structures, whereas the oxidation potential was lowered by 200 mV for nanostructured electrodes with higher peak currents. For 700 μM dopamine, the oxidation and

reduction peak currents for nanostructured electrodes were 30 µA±3 and 30 µA±3, and for planar electrodes were 12 µA±2 and 7 µA±1, respectively. In addition, the peak potential separation (ΔEp) was reduced remarkably for nanostructured electrodes that lead to improved quasi-reversible behavior of dopamine on these electrodes (ΔEp for nanostructured and planar electrodes were 100 mV and 300 mV, respectively.). The CV was also acquired in 100 mM PBS (pH 7.4) with or without dopamine to confirm that the oxidation and reduction peaks solely belongs to the dopamine (Figure 10B). To confirm the dual functionality of the developed substrate, distinct fingerprint peaks (e.g., the vibrational mode at 1280 cm^{-1}) were obtained for dopamine in PBS using SERS on the same substrate (Figure 10C).
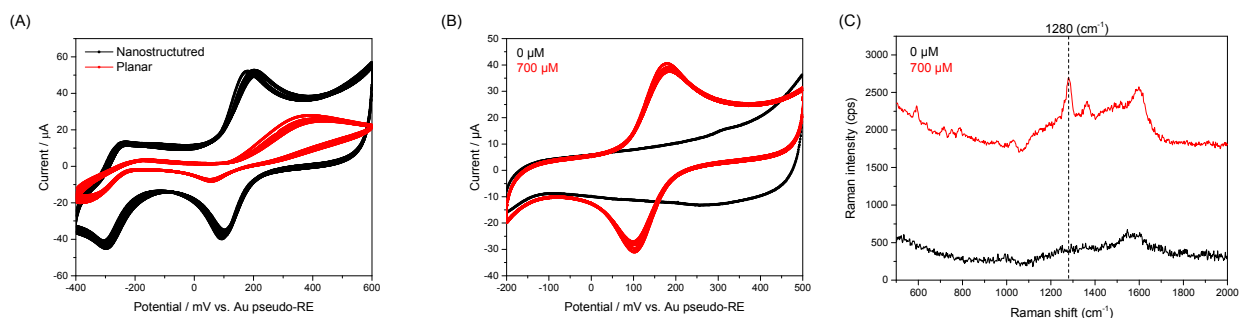

Figure 10. CVs recorded on (A) nanostructured and a planar electrode for 700µM dopamine in PBS (B) nanostructured electrode with or without dopamine in PBS (scan rate 50 mV/s vs. Au pseudo-RE). (C) Raman fingerprints obtained for dopamine in PBS using SERS.

3.5 Smartphone controlled on-disc wireless potentiostat

In the frame of this Ph.D. project, we have successfully demonstrated the use of custom-made PCB with magnetic clamping to interface the multiple on-disc electrodes to the stationary multi-channel potentiostat via an electrical slip ring. This interfacing system shows potential to obtain real time measurements from spinning disc. However, the connection of LoD device to the bulky potentiostat questions its portability and restrain its applicability as a truly miniaturized system. The aim of the truly miniaturized system is to shrink the entire analytical procedure onto the microfluidic platform, which also includes detection and data evaluation unit. Thus, along with microfluidic operations, the miniaturization of the peripheral measuring instrument (for example potentiostat for electrochemical measurements) should also be given equal importance. Thanks to the revolutionary advances in micro and nanotechnology that led to the economic down scaling of electronic

components and devices, for example, computers shrinking from the 1800 square feet ENIAC to a device that can be carried in a pocket. These technological advances also had a great impact in the field of sensing, especially electrochemical detection where both the sensor (electrode) as well as a detection system (potentiostat) can be efficiently miniaturized without losing their analytical performance. Possibly, that is why electrochemical detection is widely used in combination with microfluidics to construct portable, fully automated, miniaturized and inexpensive microfluidic devices.

In addition to commercially available miniaturized battery powered potentiostats (e.g., Dropsens μStat 8000 and PalmSens4 etc.), open-source potentiostats (e.g., CheapStat and DStat) have gained considerable popularity in recent years[143,144]. Surprisingly, these open-source potentiostats can be assembled very cheaply and do not require expert knowledge for their implementation. Access to such resources could lead the development of analytical instrumentation to the next level by providing a decent platform to many researchers for building customized, low-cost and miniaturized potentiostats for various applications. Many recently developed potentiostats can be controlled by single-board microcontrollers and micro-computers such as Arduino, Teensy and Raspberry Pi that can be programmed in various languages such as C, C++, Java or Python. After getting success in miniaturizing potentiostats with improved performance, research is gaining interest on wireless power and data transmission for traditional and paper-based microfluidic platforms[145–147], as well as for LoD platforms[148]. Realizing the need of such portable and user-friendly platforms, we also took a step towards creating a miniaturized smartphone controlled wireless potentiostat, which can be integrated on a rotating platform (Paper IV). The work is going on in collaboration with the group of Assoc. Prof. En-Te Hwu Academia Sinica, Taiwan and the group of Prof. Marco Sampietro Polytechnic University of Milan. The potentiostat, which is under development, will eliminate the need for bulky peripheral instrumentation and slip rings for on-disc electrochemical measurements, thereby making the LoD platforms compact, easy to use, and suitable for on-site applications.
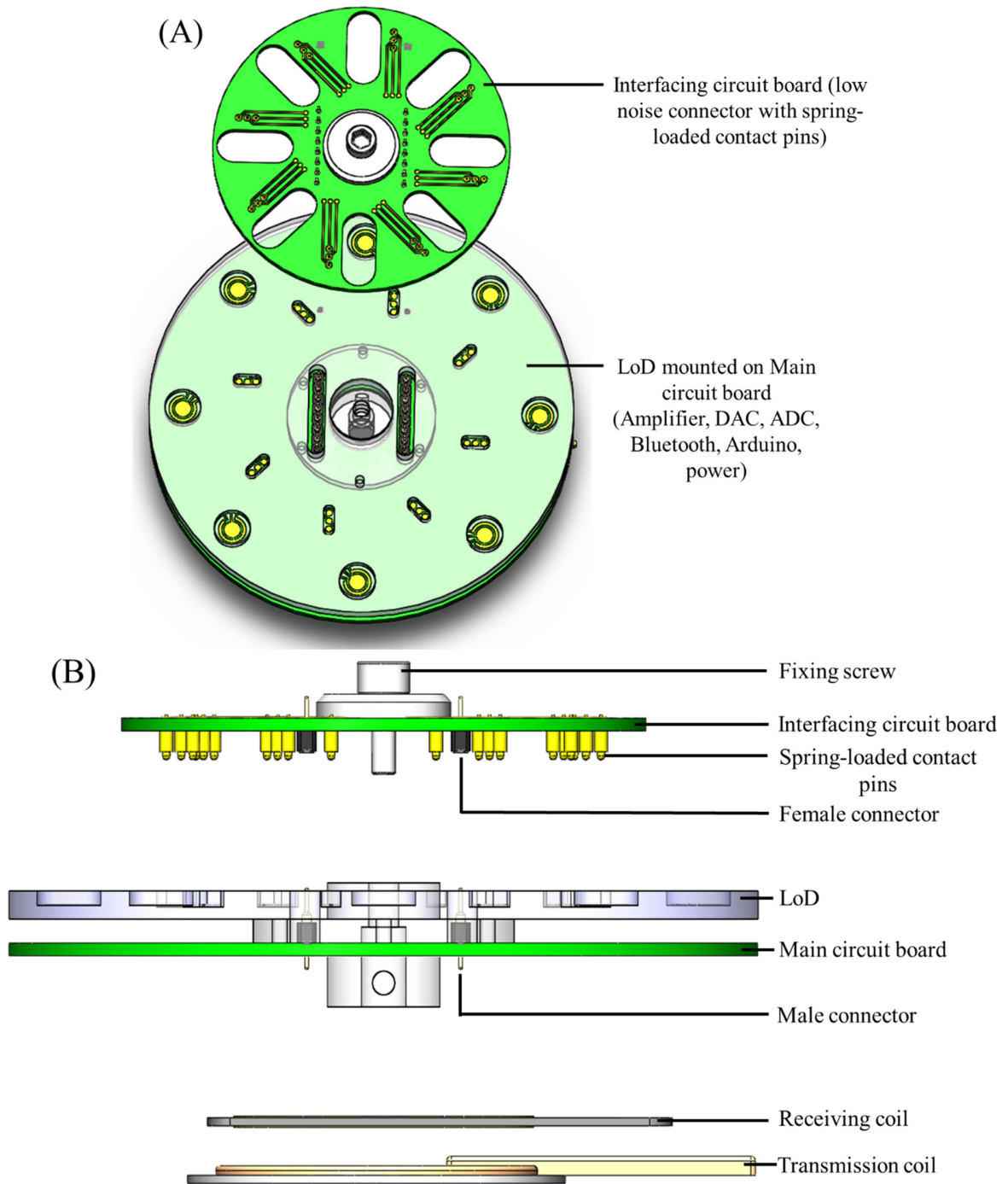
Figure 11. Schematic showing top (left) and side (right) view of smartphone controlled on-disc wireless potentiostat.

The first prototype of an on-disc wireless potentiostat is shown in Figure 11A, B. The main circuit board carries the main components of the wireless potentiostat, and an interfacing circuit board was used to interface the on-disc electrodes with the main circuit board. The main components of the wireless potentiostat are the integrated microcontroller (ATmega2560, Atmel) programmed by an Arduino based firmware, the Bluetooth transmitter, the digital to analog converter (DAC8066, Texas Instruments), the analog to digital converter (ADC7899, Analog Devices), the single channel potentiostat circuit and the power regulator circuit. The digital signal coming from the Android smartphone is converted from the DAC, processed by the potentiostat circuit, filtered (low pass filter RC) and delivered out through the ADC. The potentiostat is powered by a Qi inductive transmission setup and controlled by an Android phone through the Bluetooth wireless communication interface. The Qi inductive power provides 5 V potential which is very noisy and contains 205 kHz and 800mV noise spikes, therefore a CLC - PI filter was used to filter and reduce the high-frequency noise. The circuit design was made with Altium software, and the components were manually welded on the PCB.
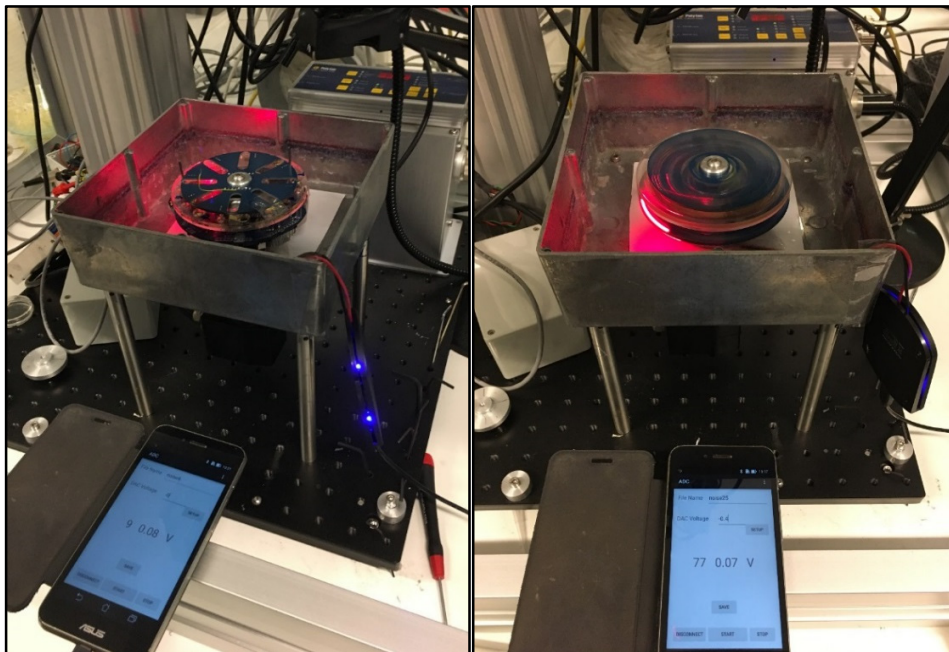

Figure 12. Photographs of smartphone controlled on-disc wireless potentiostat in static (left) and spun (right) mode.

The electrochemical readout from the first prototype of an on-disc wireless potentiostat was compared with the commercial CHI1030A potentiostat (CH Instruments, Inc., Austin, TX, USA) in static condition as well as during rotation. Figure 12 shows the wireless data transmission in case of on-disc potentiostat using an android smartphone in static condition as well as during rotation. To perform the electrochemical measurements in case of a commercial potentiostat, it was connected to the LoD device using a custom-made PCB via a slip-ring (described in Paper I). As can be seen in Figure 13, CVs obtained from the first prototype of an on-disc potentiostat were comparable with commercial potentiostat in a static condition and during rotation at 180 rpm. However, some differences were observed between CHI potentiostat and on-disc wireless potentiostat at higher rotational speeds, which will need further investigation.
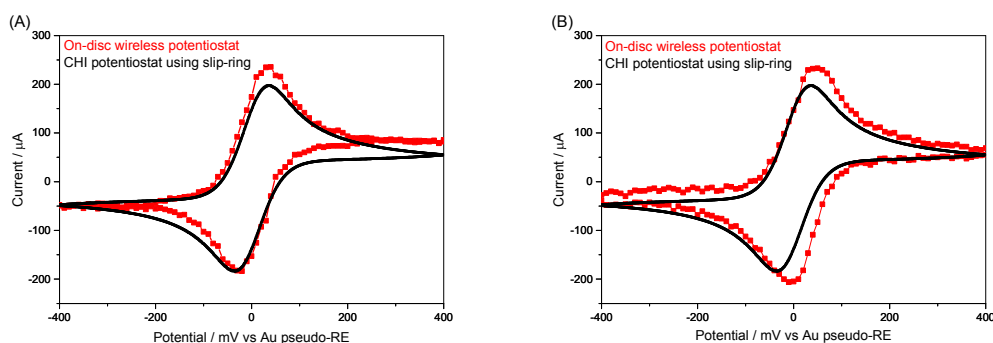

Figure 13. Comparison of CVs between on-disc wireless potentiostat and commercial CHI potentiostat, acquired in 10 mM ferri/ferrocyanide using PBS (pH 7.4) as supporting electrolyte. Static (left) and during rotation at 180 rpm (right).

4. Detection techniques

4.1 Interfacial electrochemical techniques

Based on charge transfer processes at electrode/electrolyte interface, electrochemical techniques can be divided into static and dynamic techniques. In static techniques, current is not allowed to pass through the electrolyte solution, which means no net reaction occurs. Potentiometry is an important quantitative static technique, where the potential of the electrode is measured with respect to the potential of a reference electrode under static conditions. In case of dynamic techniques, current is allowed to flow through the electrolyte solution and a net reaction proceeds. Based on the ability of an electrochemical device to control the excitation (current or potential), the dynamic techniques can be further subdivided into controlled current and controlled potential techniques.
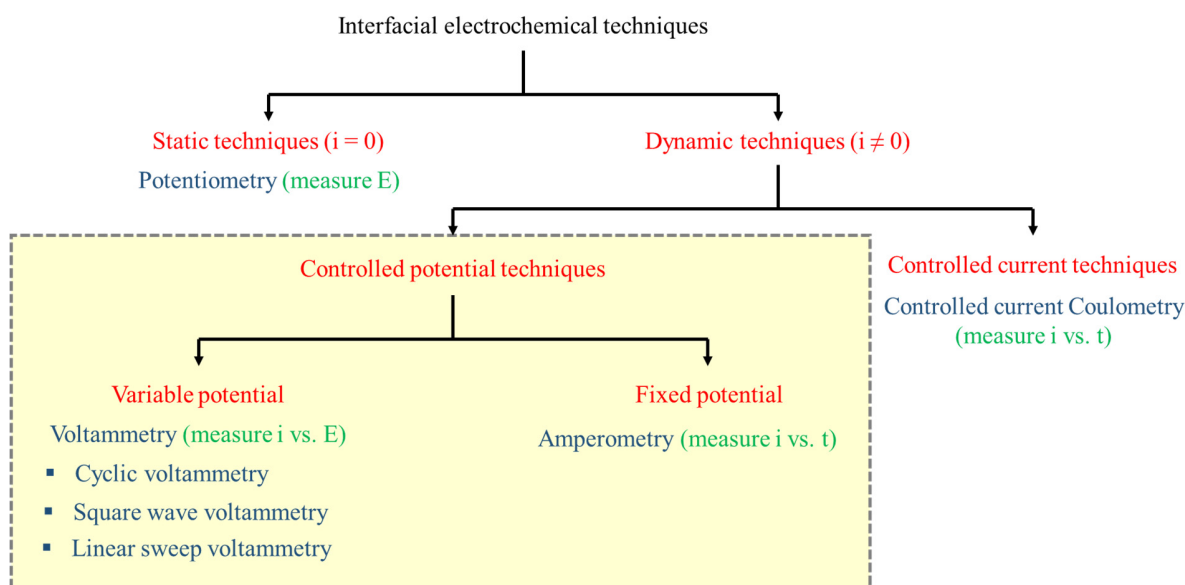

Figure 14. A possible subdivision of interfacial electrochemical techniques. The experimental conditions are shown in red, the specific techniques are shown in blue, and the analytical signals are shown in green. The dashed rectangular box (gray) highlights the techniques used in this work to measure current as a function of a variable or fixed potential.

Most of the interfacial electrochemical techniques are dynamic techniques like coulometry (where the current is measured as a function of time), voltammetry and amperometry (where the current is measured as a function of fixed or variable potential) (Figure 14). In this work, controlled potential

techniques such as amperometry, cyclic voltammetry, square wave voltammetry and linear sweep voltammetry were used for characterization of electrochemical systems and target analyte quantification. Hence, these techniques will be discussed further in detail.

4.1.1 Amperometry

Amperometry is one of the simplest interfacial electroanalytical technique, where a constant oxidizing or reducing potential is applied to the working electrode, and the resulting steady-state anodic or cathodic current is measured as a function of time. Usually, in amperometry, the magnitude of the measured current is proportional to the concentration of the oxidized and reduced analyte (assuming there is no interference). The amperometric methods is highly dependent on the applied potential. However, the electrode material and the composition of the supporting electrolyte can also influence it. In cases, where oxygen in supporting electrolyte interferes with the electrochemical reaction, it may be necessary to remove it by purging the solution using an inert gas like nitrogen or argon.
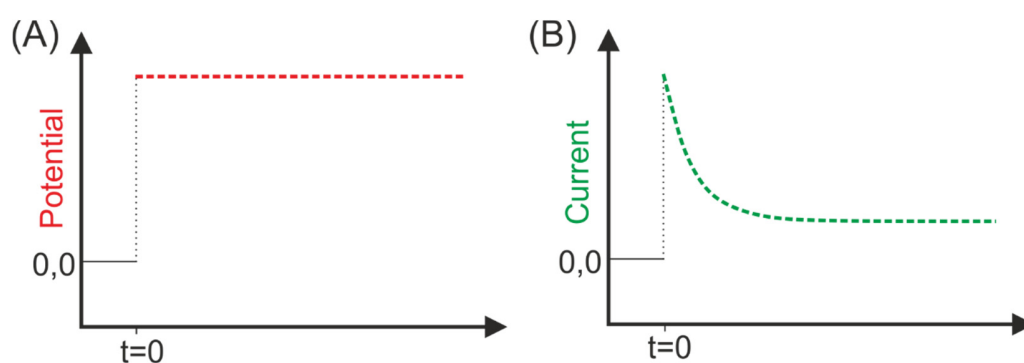

Figure 15. Amperometric detection (A) where the constant positive potential is applied, and (B) subsequent anodic current is recorded.

To perform amperometry, the desired constant potential (specific potential) needed for oxidation or reduction of an analyte on an electrode/electrolyte interface can be determined from anodic and cathodic peak potential values from recorded cyclic voltammogram (discussed in section 4.1.2). The applied overpotential for oxidation or reduction of the target analyte taking place in the vicinity of the electrode must be high enough to ensure the decrease in the concentration of the electroactive species on the electrode surface to zero (Figure 15). For example, in Paper III, anodic peak potential for paracetamol was found at 300 mV using CV recorded against Au pseudo-RE and 450 mV

potential was applied while quantifying the paracetamol using amperometry. However, care must be taken while applying the potential above specific potential, as the application of high nonspecific potential will generate current that maybe contributed by several other electroactive species along with the target analyte.

Assuming a linear diffusion of electroactive species (unstirred solution) on a planar electrode, with fast electrokinetics at the electrode-electrolyte interface, the transient current follows the Cottrell equation as

$$i\,(t) = \frac{nFAD^{1/2}C_b}{(\pi t)^{1/2}} \tag{4.1}$$

where D is the diffusion coefficient of the electroactive species (cm^{2}s^{-1}), C_b is the bulk concentration of the electroactive species (mol cm^{-3}), A is the electrode area (cm^2), F is the faraday's constant (96485 C mol^{-1}), n is the number of electrons involved in the electrode reaction, and t is the electrolysis time (s). According to this equation, the current measured is proportional to the bulk concentration of the electroactive species and decreases toward zero with an increase in electrolysis time, hence, indicates that the concentration of the electroactive species, in the vicinity of the electrode, decreases progressively with time. However, in practice, instead of reaching zero over time, the current reaches a constant value, also called steady state current. This steady state diffusion current is the direct measure of the concentration of the electroactive species in the solution.

4.1.2 Cyclic voltammetry

Cyclic voltammetry is the most widely used potential sweep technique for acquiring qualitative information about fairly complex electrochemical reactions. It was first reported in 1938 and described theoretically by Randles[149]. In cyclic voltammetry, the current is measured against a potential excitation signal applied as the linear potential scan with the triangular waveform (Figure 16).
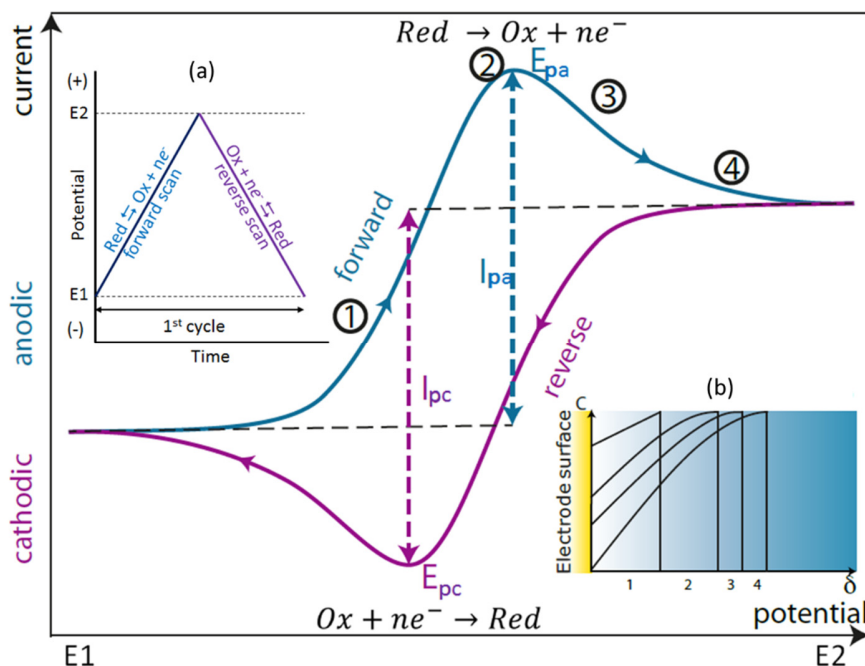
Figure 16. Schematic illustration of a cyclic voltammogram showing the measurement of the peak current and peak potential for a typical reversible redox system. Inset (a) Triangular potential-excitation signal as a function of time showing the initial potential (E1) and the switching potential (E2), (b) The concentration gradients and their corresponding diffusion layer thickness (δ) for different steps during the forward scan.

The triangular potential excitation signal sweeps the electrode potential between two extreme values (switching potentials) at a known scan rate. The CV is usually initiated at a potential where species are not electroactive. During forward scan, a positive potential ramp is applied, i.e., linearly varying potential towards more positive potential (E1 to E2), it results into oxidation process

$$\text{Red} \leftrightarrows \text{Ox} + n e^-$$

where electroactive species (Red) lose an electron at the electrode and give rise to an anodic peak current (i_{pa}) which gives the oxidation peak at a given potential (E_{pa}). However, when the potential reaches a predetermined switching potential (E2), the direction of the applied potential is reversed, i.e., towards more negative potential (E2 to E1). This reverse scan results into a reduction of the electroactive species generated (Ox) during the forward scan back to Red.

$$\text{Ox} + n e^- \leftrightarrows \text{Red}$$

45
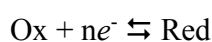
This reduction process results in cathodic peak current (i_{pc}) which gives the reduction peak at a given potential (E_{pc}) (Figure 16).

For cyclic voltammetry carried out in an unstirred solution (the system is diffusion controlled), the Fick's law of diffusion is applicable for both oxidation and reduction. Under these conditions, the peak current (i_p) is given by the Randles-Sevcik equation

$$i_p = (2.687 \times 10^5)n^{3/2}AD^{1/2}v^{1/2}C \tag{4.2}$$

where n is the number of electrons exchanged in the redox reaction, A is the area of the working electrode (cm^2), D is the diffusion coefficient of the electroactive species (cm^2s^{-1}), v is the potential scan rate (Vs^{-1}), and C is the concentration of the electroactive species at the electrode (mol cm^{-3}).

Cyclic voltammogram characteristics for a reversible system at 25 °C:

- The amplitude of peak current should be proportional to the square root of the potential scan rate, $i_p \propto v^{1/2}$.

- $\Delta E_p = E_{pa} - E_{pc} = 59.2$ mV/ n. where n is the number of electrons transferred per redox reaction.

- The amplitude of anodic and cathodic peak currents should be equal, $I_{pa}/I_{pc} = 1$.

- E_p should be independent of the scan rate (v).

Considering the cyclic voltammogram characteristics for a reversible system, newly fabricated electrodes can be characterized simply by running CV's at different scan rates, using a known redox couple, and extracting the information regarding peak current amplitudes (i_p) and potentials (E_p). In Paper I, II and III, the electrodes fabricated on plastic and glass substrates, were characterized by acquiring CV's in 10 mM ferri/ferrocyanide using PBS (pH 7.4) vs. Au pseudo-RE.

4.1.3 Square wave voltammetry

Besides a simple staircase ramp, several other forms of potential modulation have been tried over the years, to increase the speed and sensitivity of an electrochemical technique. Square wave voltammetry is one of those pulse techniques that was first reported by Barker in 1957 and due to advancement in analog, and digital electronics became popular over time for routine quantitative analysis[150,151]. Instead of simple staircase ramp, the SWV consists of a staircase potential ramp modulated with a square wave of potential pulses. That means, the excitation signal consists of a symmetrical square-wave pulse of amplitude E_{sw} superimposed on a staircase waveform of step height E_{step}, where the forward pulse of the square wave (pulse direction same as the scan direction) coincides with the staircase step. The reverse pulse of the square wave occurs half way through the staircase step (Figure 17).

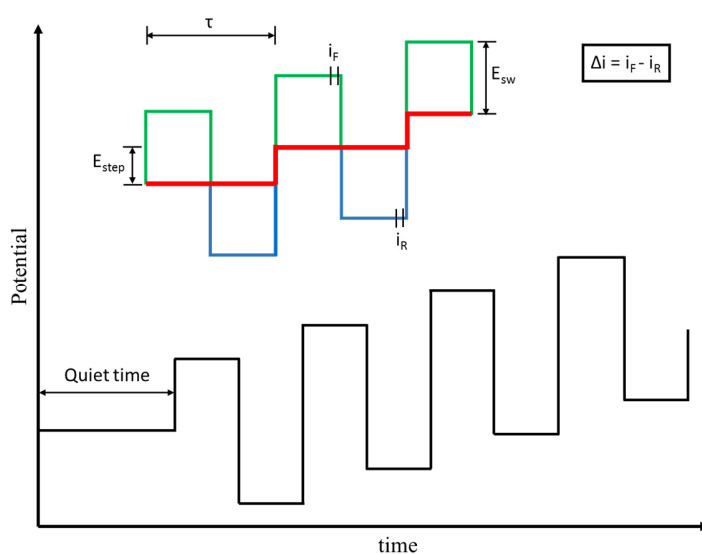**Figure 17**. Input excitation signal in square wave voltammetry showing staircase wave form (red), the forward pulse of the square wave (green), and reverse pulse of the square wave (blue). The signal is sampled at i_F (forward current) and i_R (reverse current).

The scan rate of the SWV can be calculated as:

$$Scan\ rate\left(\frac{mV}{sec}\right) = \frac{E_{step}\ (mV)}{\tau\ (sec)} \tag{4.3}$$

where τ is the time for one square wave cycle or one staircase step and E_{step} is the staircase step size. The τ for SWV is very less (few milliseconds) as compared to other pulse techniques (few seconds)[152]. This allows SWV to employ faster scan rates, which in turn leads to faster determination than other pulse techniques. During each square wave cycle, the current is measured twice, at the end of the forward pulse (forward current = i_F) as well as at the end of the reverse pulse (reverse current = i_R). Finally, the peak height of the net current (Δi) corresponds to the concentration of the molecule under investigation. Moreover, as the forward and reverse currents are measured at the end of the pulses, the SWV can eliminate the contribution from short-lived capacitive currents or charging currents and yield the peaks for faradaic processes alone. SWV was successfully applied in Paper I and II for the detection and quantification of the pHCA. Figure 18 shows the square wave voltammogram recorded for pHCA in paper II. The pHCA was extracted in Tris buffer (50 mM Tris, 150 mM NaCl, pH 7.6) via on-disc SLM extraction from a solution of 750 µM Tyr and 250 µM pHCA dissolved in supernatant from j786 *E. coli* strain.
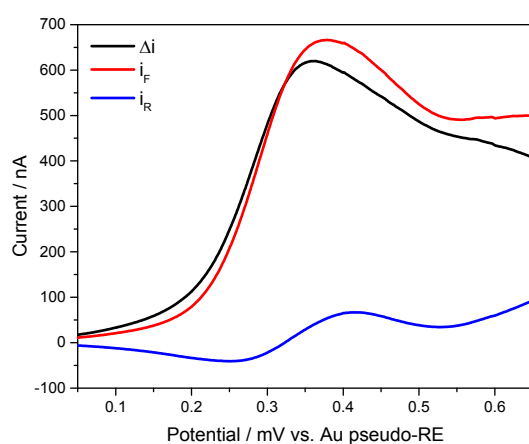
Figure 18. SWVof pHCA in Tris buffer vs. Au pseudo-RE (scan rate 50 mVs^{-1}).

4.2 Surface-enhanced Raman Spectroscopy

When light with a frequency v_0 is scattered by atoms or molecules, a strong Rayleigh scattering light with the same frequency v_0 can be observed. Besides, weak discrete spectral lines whose frequencies are shifted from the excitation frequency v_0 can also be observed. The latter effect is Raman scattering, which is the inelastic scattering of photons. Raman scattering was discovered

by C. V. Raman and K. S. Krishnan in liquids[153] and by G. Landsberg and L. I. Mandelstam in crystals[154]. The amount of frequency shifts for the Raman scattering photon is related to the vibrational frequency of the molecule (v_m). Raman spectroscopy is a spectroscopic technique where Raman scattering effect is used to identify molecules by providing their vibrational fingerprints.
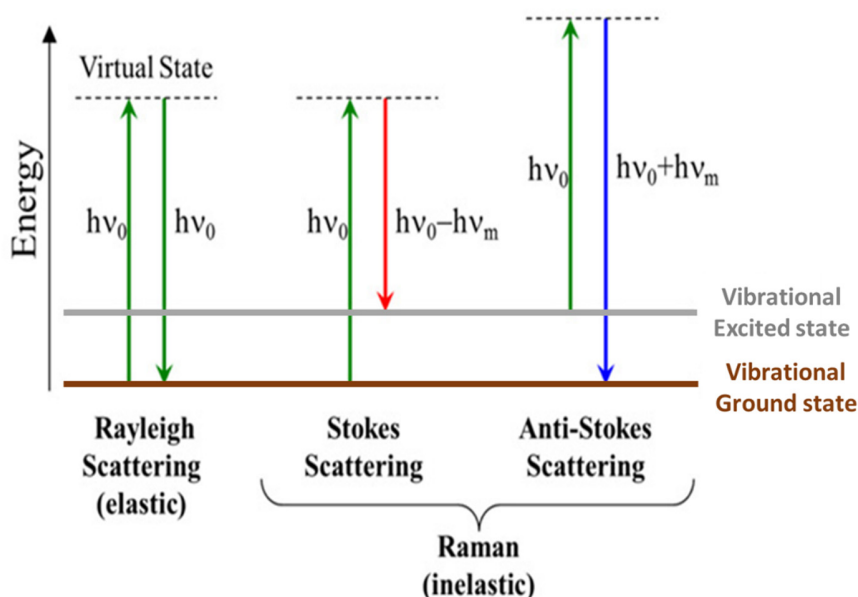

Figure 19. Illustration for the energy transitions involved in Rayleigh scattering and Raman scattering. Raman scattering occurs through the interaction of an incident photon with a molecular vibration mode, gaining (anti-Stokes scattering, blue-shifted) or losing (Stokes scattering, red-shifted) an amount of energy equal to that vibrational mode (Adapted and modified from[155]).

In Raman scattering, photons can appear on either side of the excitation wavelength, depending on whether the incident photon interacts with a molecule in its vibrational ground state or its vibrational excited state (Figure 19). The frequency of the Raman scattering photon can be expressed as either $v_0 - v_m$ or $v_0 + v_m$. In the former case, the incident photon interacts with a molecule in its vibrational ground state. Starting by exciting the molecule to a virtual state, the incident photon transfers the energy of hv_m (h is Planck's constant) to the molecule to stimulate a vibration, and is scattered with a lower frequency ($v_0 - v_m$). Such a process is called Stokes scattering. For the latter case, the incident photon interacts with a molecule in an excited vibrational state. It first excites the molecule to a virtual state, absorbs the energy of hv_m to relax the molecule to the vibrational ground state, and is scattered with a higher frequency ($v_0 + v_m$). This process is

called anti-Stokes scattering. Hence, Stokes scattering describes when the material absorbs more energy, and thus emits a photon with a lower energy than the incident photon, and anti-Stokes scattering describes when the material loses energy, and the emitted photon has a higher energy. The spectrum obtained from Stokes and the anti-Stokes shift is called the Raman spectrum. As the vibrational levels are populated according to the Boltzmann distribution, most molecules are at their ground state at room temperature, and therefore, significantly fewer molecules are available for anti-Stokes scattering. Stokes scattering is thus significantly stronger and therefore most commonly used for detection and identification of molecules.

Although Raman scattering light carries information about the vibrational states of the molecules, it has an extremely low intensity. The reason for this is that the frequency of the Raman excitation light is not in resonance with any molecular transitions. This leads to Raman cross sections for a molecule to be $\sim 10^{-30}$ cm^2/molecule[156]. In comparison, fluorescence processes involve absorption and emission relative to molecular transitions, and the representative value for its cross section is $\sim 10^{-17}$ cm^2/molecule[157]. The extremely low Raman cross sections prevent regular Raman spectroscopy from applications such as sensing trace amounts of molecules. To increase the Raman intensity, resonant Raman spectroscopy can be employed, in which the frequency of the excitation laser matches the electronic transition gap of the target molecule. To further boost the Raman signal, surface-enhanced Raman spectroscopy (SERS) should be used.

Surface-enhanced Raman Spectroscopy (SERS) is the phenomenon that significantly increased Raman scattering signals, probed from molecules attached to or in the very close vicinity of metallic nanostructures. It was recognized in 1977, that enhanced Raman spectra could be obtained from molecules sitting on electrochemically roughened metal surfaces, and the enhancement of the Raman scattered light arises in two ways[158]. First, the excitation field and the Raman scattering field can receive magnifications, near metallic nanostructures that support localized surface plasmon resonance (LSPR)[a]. This is the electromagnetic enhancement of SERS. Second, electronic interactions between the molecule and the metal can affect the Raman scattering process itself, and

---

[a]LSPR is the resonant oscillation and redistribution of charges near the surfaces of metallic nanostructures. The resulting enhanced local optical field is the foundation of plasmon-supported spectroscopies, and is the key for localizing spectroscopic interactions within extremely small volumes.

can consequently increase the Raman cross section of the molecule. Such an effect is the chemical enhancement of SERS. The electromagnetic enhancement explains enhancement factors up to 10^6 - 10^8 for an ensemble of molecules and the chemical effect can provide an additional enhancement factor of 10^1 - 10^3. Due to the strongly increased signals which compensate the extremely low Raman scattering cross sections, SERS transforms Raman spectroscopy from a tool for structural analysis to a nanoscale sensing probe, with lowest detection limits down to single molecular level[141].

In traditional Raman spectroscopy, the total Stokes Raman signal $I_{RS}(v_S)$ is proportional to the Raman cross-section σ^R, the excitation laser intensity $I(v_0)$ and the number of molecules in the probed volume N[159],

$$I_{RS}(v_S) = N \, \sigma^R I(v_0) \tag{4.4}$$

For SERS, the formula is modified, taking into account the EM enhancement as well as the chemical enhancement. The SERS Stokes signal is expressed as follows[160],

$$I_{SERS}(v_S) = N' \, \sigma_{ads} \, |\eta(v_0)|^2 |\eta(v_s)|^2 I(v_0) \tag{4.5}$$

in which $\eta(v_0)$ and $\eta(v_s)$ are the EM enhancement factors for the laser and for the Raman scattered field, σ_{ads} describes the increased Raman cross-section of a molecule adsorbed onto a metal surface, accounting for the chemical enhancement. N' denotes the number of molecules involved in the SERS process, usually those located in the enhanced EM field, and can be significantly lower than [b]N. The SERS enhancement is thus proportional to $|\eta(v_0)|^2|\eta(v_s)|^2$. This term describes the physical process by which the dipole field of a LSPR-supporting structure induced by an external EM field, in turn, induces an oscillating dipole in the molecule. The Stokes radiation emanating from the molecule, although frequency shifted, couples to the LSPR mode of the nanostructure and is further enhanced. The SERS signal I_{SERS} is thus proportional to the electric field enhancement and is greatest when enhanced EM field is at its maximum.

The SERS signal scales with the electric field to the fourth power (E^4) and decays from the surface with $1/r^{12}$, indicating that only molecules that are near the surface give a large SERS signal[161]. While chemical enhancement is a universal method to increase Raman signal, the electromagnetic enhancement using LSPR supporting nanostructures allows for optimization engineering to achieve high enhancement and make trace molecule detection viable by Raman spectroscopy. Typical SERS enhancements for single colloidal or Au spheroids are of the order of 10^6 - 10^7[162–164] but can be greatly increased with sharp features or large curvatures, resulting in a more focused EM field[159]. Additionally, closely spaced metal nanostructures can couple their dipole moments such that the field is further enhanced. For this type of coupling, enhancement factors up to 10^{11} have been reported[165].

Requirement in Plasmonic Systems for Surface-enhanced Raman Spectroscopy

In general, ideal plasmonic systems for reliable and quantitative SERS analyses should fulfill the three requirements below[156,166]:

- The system should exhibit a high and spatially uniform electromagnetic enhancement factor EF_{EM}. To sense analytes of small quantities, a high EF_{EM} is essential to increase the Raman signal, which scales with EF_{EM} to the power of four, as has been mentioned in the previous section. Additionally, a more spatially uniform EF_{EM} would enable quantitative SERS analyses. To quantify a single molecule, molecules should experience the same EF_{EM} despite their locations relative to the LSPR structure. However, in reality, EF_{EM} is dependent on the detailed surface morphologies of the LSPR structures and can vary by several orders among different regions. Nevertheless, one should strive to achieve a more spatially uniform EF_{EM} to improve SERS uniformity and reproducibility, as application-wise it is not always necessary to reach a quantification level down to single molecules [157]. Due to the non-uniform nature of the local optical fields, in practical use, the average total enhancement factor EF_{AVG} is measured experimentally to assess the performance of a SERS system. EF_{AVG} can be described by:

$$EF_{AVG} = \frac{[I_{SERS}/N_{Surf}]}{[I_{RS}/N_{Vol}]} \qquad (4.6)$$

where I_{SERS} is the measured SERS intensity, N_{Surf} is the number of molecules bound to the enhancing SERS-active structure, I_{RS} is the measured Raman intensity without enhancement, and N_{Vol} is the number of molecules in the excitation volume for measuring I_{RS}[167,168]. To characterize the uniformity of EF_{EM}, SERS scans/mappings over certain distances/areas are usually performed on the SERS-active structure, with different quantities of analytes bound to its surface. The relative standard deviations of pronounced SERS peaks then reflect the spatial uniformity of EF_{EM} for such a structure.

- The system should exhibit widely tunable LSPR wavelengths. This is mainly because resonant surface-enhanced Raman scattering (SERRS) takes place when the excitation wavelength is in resonance with the absorption wavelength of the analyte. SERRS can provide additional Raman signal enhancement of $\sim 10^2$ [169].

- The system should be easy to fabricate in a reproducible manner. This requirement has been achieved extensively thanks to the rapid development of nanofabrication techniques[159]. In terms of nanofabrication, the majority of produced SERS systems are either (i) metallic nanoparticles in colloidal suspensions, or (ii) nanostructured solid substrates.

In this study, SERS was used to detect the molecular fingerprints of paracetamol (Paper III) and dopamine (batch assembly set-up integrated with Au coated nanostructured Si chip), followed by their quantification using electrochemistry.

5. Fabrication

Since the introduction of the Lab-on-a-chip devices, the number of applications associated with microfluidic devices has increased tremendously. Based on the application, the microfluidic device may demand various prerequisites like chemical resistance, heat resistance, transparency, gas permeability, flexibility, biocompatibility, etc. In order to fulfill these prerequisites, the substrate material to fabricate a microfluidic system needs to be chosen very carefully. The proper selection of material is highly dependent on the material properties and the fabrication process. Initially, most of the microfluidic devices consisted of Si or glass, however, as the field advanced new materials were introduced for cost efficient production of microfluidic devices on a large scale such as paper and polymers. Besides low-cost production, polymers also offer several other advantages over Si and glass, such as good optical transparency, biocompatibility, fast prototyping and friendly system integration. The most popular polymers used to fabricate the microfluidic devices are poly(methyl methacrylate) (PMMA), poly(carbonate) (PC), poly(styrene) (PS), cyclic olefin copolymer (COC), poly(ethylene terephthalate glycol) (PETG) and poly(dimethylsiloxane) (PDMS). Due to their inherent material properties, different polymers are compatible with different fabrication techniques (Table 2).

Table 2. Comparison of polymer properties and fabrication techniques used for fabrication of microfluidic device (adapted from[4])

Polymer	Main characteristics	Fabrication techniques
PMMA	Thermoplastic. Transparent. UV resistance. Low water absorption. Good abrasion resistance.	Injection molding. Hot embossing. Laser photoablation. X-ray lithography.
COC	Thermoplastic with high transparency. High heat resistance. Low water absorption. High stiffness and strength.	Injection molding. Hot embossing.
PS	Thermoplastic. Excellent electrical properties. Resistant to a wide variety of chemicals.	Injection molding. Hot embossing. Laser photoablation.

PC	Transparent thermoplastic. High heat resistance. High stiffness and strength.	Injection molding. Hot embossing. Laser photoablation.
PTEG	Transparent thermoplastic. Good impact and chemical resistance.	Hot embossing. Laser photoablation.
PDMS	Transparent elastomeric polymer. Biocompatibility. High flexibility. High gas permeability. UV resistance. Chemically inert. Thermally stable.	Soft-lithography. Direct laser plotting.

In addition, concerning factors like fabrication time, cost, resolution, precision, material compatibility, etc., the fabrication techniques differ from each other in many ways (Table 3). Although, there are several polymers and fabrication techniques available to fabricate the microfluidic device, the final selection of material and fabrication technique generally depends on the specific purpose and application. The purpose could be either industrial scale production where production cost and time plays an important role or the laboratory based research where rapid prototyping with low fabrication cost is the main concern to quickly test the new ideas and improve. Indeed, most often the prototypes developed in research labs are also suitable for industrial scale production. Considering the application (detection of pHCA from *E. coli* supernatant) presented in this work where no organic solvents were involved as such, PMMA was chosen as a material for rapid prototyping of the microfluidic devices using laser ablation. Moreover, it was also taken into account that, after the development of the final microfluidic device, it can be easily injection molded using PMMA or other solvent resistant polymers like PC or PS. In this chapter, the fabrication of electrochemical sensor integrated microfluidic set-ups, designed and developed during the Ph.D. project is presented and discussed.

Table 3. Advantages and disadvantages of fabrication techniques used to fabricate polymer based microfluidic devices (adapted from[4])

Methods	Advantages	Disadvantages
Hot embossing	Precise and rapid in the replication of microstructures. Mass production.	Restricted to thermoplastics. Time-consuming. Complex 3D structures are difficult to be fabricated.

Injection moulding	Mass production. Fine features. Low cycle time. Highly automated.	Restricted to thermoplastics. High cost mold. Micro size precision is limited.
Laser photoablation	Rapid. Large format production.	Limited materials. Multiple treatment session. Difficulties for mass production. Micro size precision is limited.
Soft-lithography	High-resolution and 3D geometries. Cost-effective. Excellent micro size precision.	Pattern deformation and vulnerability to defects. Difficult to fabricate circular geometries.
X-ray lithography	High-resolution. Straight and smooth walls.	Complex and difficult master fabrication. Time-consuming and high-cost process.
Xurography	Low-cost and rapid technique.	Complex 3D structures are difficult to be fabricated. Micro size precision is limited.
Direct laser plotting	Low-cost and rapid technique. Free-mask technique.	Complex 3D structures are difficult to be fabricated. Micro size precision is limited. Reproducibility of the microdevices.
3D-printing	Low-cost and rapid technique.	Multiple treatment session. Difficulties for mass production. Micro size precision is limited.

5.1 Polymer microfabrication: PMMA, PSA and membrane cutting

PMMA is a biocompatible and optically clear high-grade polymer used for the fabrication of microfluidic devices for a wide range of applications[170]. In this Ph.D. project, PMMA was used for fast prototyping because of its low cost and ease of fabrication. A tabletop $CO2$ laser-cutter (Epilog Mini 18, 30 W from Epilog, USA) has been used to cut chambers and engrave the desired microstructures/microchannels in PMMA substrates for microfluidic disc/chip fabrication. The frequency, power, number of iterations and the speed of the laser was optimized based on the thickness of the PMMA substrate and the requirement of cutting through or engraving the substrate. While cutting the polymer with higher power and low speed, it was observed that the process was faster, but the polymer was melting more at the top giving rise to inclined cut instead of the straight

cut. To avoid this, and to accomplish high resolution and precise cut of the PMMA substrate, low power, high speed, and several iterations were chosen. For instance for cutting through a 0.5-mm thick PMMA, the power was set to 50 % and the speed to 40 % with 5 iterations, whereas for cutting through a 1.5-mm thick PMMA these parameters were adjusted to 70 % power and 25 % speed with 10 iterations.

Usually, the microfluidic system is composed of multiple subunits made up of similar or different materials. Bonding or sealing of these subunits is one of the critical steps to obtain a functional microfluidic device. As discussed at the beginning of this chapter, due to their diverse material properties, polymers are very attractive substrate material for developing microfluidic systems. Thanks to the same material properties, various polymer bonding options are available. In case of thermoplastic polymers like PMMA, the bonding can be achieved either indirectly by using adhesives like pressure sensitive adhesives, or it can be done directly by exploiting the material properties of the polymer like thermal bonding[171]. In thermal bonding, substrates are heated up to a temperature near or above glass transition temperature (Tg) of one or both the substrate materials, while applying pressure to increase mating contact forces. Thermal bonding was used to bond the microfluidic device in Paper II as described later in this chapter. However, double sided pressure sensitive adhesive (PSA) was used in Paper I for bonding as well as to define the microfluidic channels. PSA (ARcare_90106, Adhesives Research Ireland Ltd.) is transparent, thin and flexible polyester film coated on both sides with a MA-69 acrylic hybrid medical grade adhesive. The double-sided PSA is protected from both sides with two release liners that can be easily removed while using the tape for microfluidic assembly. Computer controlled tabletop vinyl cutter (Silhouette V3, Silhouette ApS, USA) was used to cut PSA. To safely cut the PSA throughout, one layer of blue tape was fixed on one side of the PSA. The same side of PSA with blue tape was placed on a sticky cutting mat that was loaded finally into the vinyl cutter. Based on the features to be patterned on the PSA the speed and depth of the vinyl cutter blade were adjusted. Once the desired pattern is transferred to the PSA, the excess material was removed from the patterned structures with the help of a sharp scalpel.
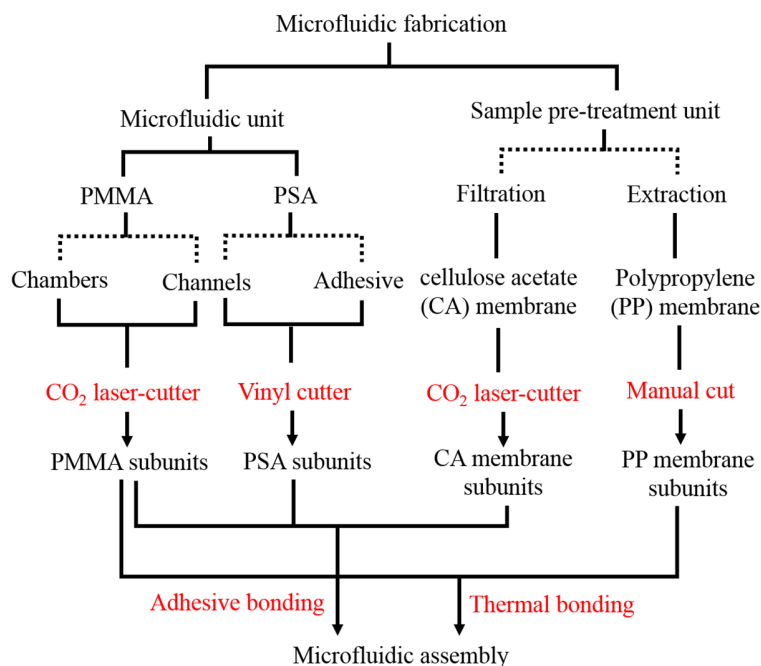
Figure 20. Schematic showing steps involved in microfluidic assembly fabrication. Dotted lines (…..) shows the possibility of choosing one or multiple options.

To detect and quantify pHCA from *E. coli* supernatant, two different sample pre-treatment approaches were used in Paper I and II, respectively. In Paper I, the aim was to filter out all the *E. coli* cells from the cell culture supernatant to facilitate the cell-free electrochemical detection of pHCA, whereas selective extraction and pre-concentration of pHCA was the ultimate goal in Paper II. Based on the purpose, two different kinds of membranes were used. Microporous Cellulose acetate membranes (Tisch Scientific, North Bend, OH, USA) with 0.22 μm pore size were used for the filtration enabled microfluidic assembly, whereas 25 μm thick nanoporous polypropylene (PP) membranes (Celgard 2500, Celgard Inc., USA) with 64 nm pore size and 55 % porosity were selected for SLM extraction based microfluidic setup. Both membranes were delicate to handle and susceptible to tear, so it was difficult to cut them manually in desired shape and size. To overcome this problem, a CO_2 laser-cut based process was developed to cut the small membrane sheets into pieces with defined geometry. For this, a circular cellulose acetate membrane sheet (25mm diameter) was mounted over a flat PMMA sheet after fixing it between two sticky notes. Finally, the pattern designed to obtain membranes with specific geometry was transferred to the fixed membrane sheet through single pass laser ablation with 60 % power and 35 % speed. The procedure

worked well to cut through the cellulose acetate membranes but seemed to be inappropriate for polymer based polypropylene membrane used for SLM extraction experiment. The conclusion was made as the procedure mentioned above resulted in shrunk PP membrane pieces with wavy edges instead of pieces with defined shape and size. The reason could be that the thin layer of polypropylene is unable to withstand the laser beam temperature, which is above the melting temperature of the PP (160 °C). The process was not only affecting the morphology of the small pieces of the PP membranes (4 mm x 6 mm), but the melting of the polymer could also lead to the blockage of the nanopores in the membrane. Therefore, we had to make a compromise in case of PP membrane and use the CO_2 laser-cutter based process partially to mark the sticky note with the desired pattern. Finally, the membrane was kept between the patterned sticky note and the untreated sticky note mounted over the PMMA sheet followed by cutting the pattern manually using a sharp scalpel.

5.2 Electrode fabrication

Thanks to microfabrication techniques, miniaturized electrodes, which can be integrated with microfluidic devices can be realized. The performance of these electrodes can be influenced by various factors like the electrode design, fabrication process, the substrate material on which the electrode is fabricated and the material composition of the electrode itself. The electrodes can be made of several materials like metals, carbon and semiconductor materials. However, metal electrodes are often preferred as they offer very favorable electron transfer kinetics. There are several reports where metal electrodes were fabricated on Si or glass substrates using cumbersome lithography processes for microfluidic applications[128–130,132]. However, few reports are also available to show the possibility of patterning metal electrodes on plastic substrates in a cost-efficient way using screen printing[172] or shadowmasking[173]. In this Ph.D. thesis, 2D (planar) and 3D (nanostructured) Au electrodes were designed and fabricated using the lithography-free technique (e-beam metal evaporation via shadowmask) on different substrates like PMMA, glass, and Si (Figure 21).
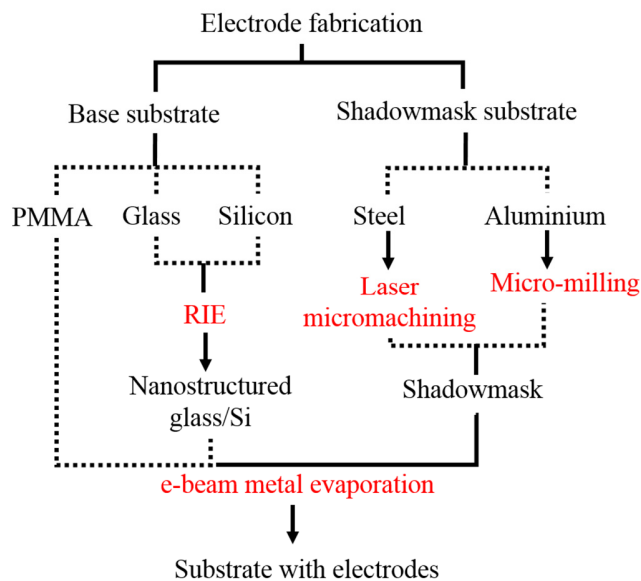
Figure 21. Schematic showing steps involved in electrode fabrication. Dotted lines (…..) shows the possibility of choosing one or multiple options.

5.2.1 Shadow mask/stencil fabrication

Photolithography and screen-printing are currently the most widely used techniques for the fabrication of metal electrodes for microfluidic applications. Although photolithography is a powerful method to realize precise and high-quality structures, the processes involved are time-consuming and labor intensive. Furthermore, lithography is not convenient to fabricate the electrodes on polymer substrates that are cheaply available and optimal for fast prototyping of microfluidic devices. Therefore, electrode patterning through shadowmasking was chosen as a fast and cheap alternative to lithography techniques. Shadow mask refers to a stencil made of thin metal sheets, where a cut pattern is used to transfer the design on the below substrate via metal deposition.

Laser micromachining

Laser micromachining tool (3D-Micromac AG, D-09126 Chemnitz, Germany) was used to obtain a shadowmask containing the electrode pattern in 100, 150 and 200 µm thick steel foil using 50W Time-Bandwidth picosecond laser with wavelength 532 nm and focal length 255 mm (visible green optics). The laser beam has an intensity distribution across the beam in the form of a Gaussian

intensity profile (Figure 22 A) with intensity peak value in the center of the beam. As we look further away from the beam's central axis, the beam is less focused, and the intensity smoothly decreases in the radial direction from the center (Figure 22 B). For an intensity equal to $1/e^2$ of the maximum intensity of the Gaussian beam, the cross-sectional diameter of the beam (spot diameter) is about~40 µm. This means that the beam will not only target the material along one hairline but will rather cover a width of the same size as its spot diameter. The material that is not hit by the focused beam will undergo a smaller ablation rate.
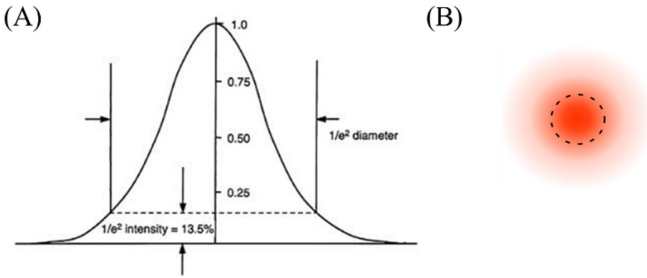

Figure 22. (A) Intensity distribution profile for laser beam (B) Laser spot (laser beam intensity more focused at the center) Adapter from[174]

To obtain a shadow mask with the required dimensions, the electrode pattern was designed in SolidWorks as an offset of 70 µm towards the interior side of the actual design. Five parallel lines were then added to the exterior side of the offset pattern keeping 10 µm gap between each successive line (Figure 23). The design was finally imported as a DXF file since the laser micromachining tool can read only the DXF file format. Depending on the dimensions of the electrode pattern various parameters were optimized for cutting through the steel (Table 4).

Table 4. Parameters optimized to cut through steel sheets with different thicknesses.

Thickness (µm)	Frequency (kHz)	Intensity	Power measured @10% (W)	Writing speed (mm/s)	No. of bursts	No. of iterations	No. of parallel lines	Gap between lines (µm)
100	200	20%	2.4	500	1	95	5	10
150	200	25%	2.4	500	1	120	5	10
200	200	25%	2.4	500	1	155	5	10

The laser was programmed to start cutting from inside of the pattern towards the outer edges. A high number of iterations and small gap (10 µm) between the lines ensure that the laser ablation

removes all the material as it repeats the same path. Moreover, as the laser proceeds from inside towards the edges of the pattern, the debris would have less chance to be deposited on the edges. Finally, the beam is set to pass twice over the outermost line. This step would result in smoother edges as the laser ablation removes the excess material from the edges. However, to avoid the beam from infringing the desired actual margins, a safety distance equal to half the spot diameter (20 μm) was considered in the calculation of offset distance (Figure 23).
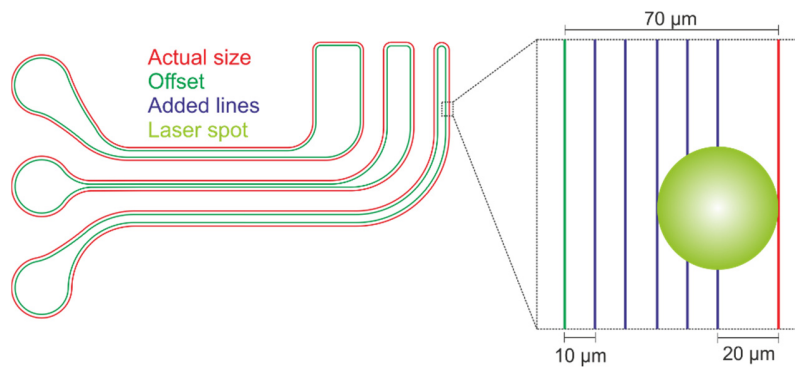

Figure 23. Design optimization for laser cut (photograph of laser cut shadow mask can also be added)

To remove any leftover debris after the laser treatment, the shadow masks were given a ultra-sonic bath in water for about 15 minutes followed by cleaning with absolute ethanol. In the end, the 150 μm thick shadow mask was used to pattern electrodes on the PMMA substrate, as 100 μm thick mask seemed to be bit fragile while aligning it over the substrate using screws, whereas the 200 μm thick mask seemed to have the structures bit smaller than expected due to inclined laser cut.

Micro-milling

A laser-micromachine tool is an appropriate choice to prepare shadow mask with flat metal sheets, where the flat shadow mask has to be placed in direct contact with the substrate and aligned by using alignment holes present in both shadow mask and the substrate prior to metal evaporation. It is difficult to make alignment holes in the substrate if the substrate is brittle such as glass or Si. Moreover, if the substrate contains some 3D structures, the direct contact of the flat shadow mask with the substrate will lead to the destruction of the 3D structures. To develop dual functionality sensor (Paper III), the metal had to be evaporated on a nanostructured fused silica substrate. To avoid the direct contact of the shadow mask with the nanostructures and to obtain perfect alignment

with a shadow mask, 5mm thick aluminum (Al) sheet was micro-milled to create the holder for the used metal evaporator (Wordentec). This metal evaporator can carry micro-milled holder with an inbuilt shadowmask that is capable of holding the nanostructured substrate 100 μm from the shadow mask (Figure 24). Two different holders for Al and Au evaporation were designed using SolidWorks, followed by defining micro-milling parameters and simulating the process in the form of g-code using Cimatron12. The majority of the Al was scrapped using 3mm endmill tool, whereas the final structures were milled with 100 μm end-mill tool. The Al substrate was fully immersed in oil during the milling process to prevent the overheating of the milling tool and keeping the tool safe from damage.

Figure 24. Schematic showing micro-milled holder with inbuilt shadow mask and room for holding 4-inch wafer with nanostructures.

5.2.2 Reactive ion etching (RIE) process

The nanostructures over an entire 4-inch Si wafer were produced via a mask-less Si reactive ion etching (RIE) process developed by Schmidt et al.[175]. For this, 4-inch p-type single-side polished wafer was used. Etching was conducted in an Advanced Silicon Etcher (Surface Technology Systems MESC Multiplex ICP) at an $SF_6:O_2$ flow ratio of 1.12, platen power of 120 W and a chamber pressure of 36 mTorr. Subsequently, an oxygen plasma process of 1 minute was applied to remove Si RIE byproducts from the Si surface. Here, an Advanced Silicon Etcher was used at an O_2 flow of 45 sccm, a platen power of 20 W, a coil power of 800 W and a chamber pressure of 10 mTorr.

Though nanostructured Si is a good SERS substrate, still it is not suitable for patterning on-substrate 3-electrode array for electrochemistry due to its n- or p-type doped semiconductive nature. In contrast, fused silica is an insulator with exceptional optical transmission property suitable for Raman scattering measurement from the front and backside of the substrate, as well as the possibility of patterning on-substrate 3-electrode configuration for electrochemistry. To produce glass nanostructures, the RIE process was adapted from previously described Si nanostructure fabrication. Usually, local nanoscale masks are produced on the glass substrate by using layers of either polymer[176] or metal[177] as a sacrificial thin film. It is convenient to use the polymer as a sacrificial mask because, under certain etching conditions, the RIE tool itself is capable of creating polymer layers using fluorocarbon gases. However, considering the complications in controlling the polymer thickness[178], metal is still the preferred source for producing local nano masks. In this work, Al was chosen as the source of local nano masks for nanostructuring glass. Anil Thilsted, during his Ph.D., had optimized all the etching parameters and developed the process for producing glass nanostructures across wafer-scale areas. Using previously described shadow mask, 600nm thick non-sacrificial Al layer was deposited on certain areas of a fused silica wafer, which is utilized by RIE tool (Advanced Oxide Etcher, STS MESC Multiplex ICP) for electrostatic clamping of the wafer. The advanced etcher was used at an O_2 flow of 70 sccm, an SF_6 flow of 170 sccm, a platen power of 110 W, a coil power of 450 W, chuck temperature 5 °C and a chamber pressure of 75 mTorr. During the etching process, less-volatile AlF_3[179] was produced and thus induced local nanoscale regions with a lower etch rate, leading to nanostructures.

In this work, the initial shadow mask used to deposit Al as an outer ring alone resulted into a significant inhomogeneity in nanostructures density, with much lower density near the center of the wafer, and a much higher density near the Al ring (Figure 25). This could be explained by the fact that the uniformity of the glass nanostructuring is dependent on the distance to the non-sacrificial Al layers[178,180]. This is in turn attributed to the electric field concentrations generated by the plasma electric field near the mask areas, affecting the ion flux and the angle of incidence during the plasma etch process. In addition to this effect, the redeposition of Al is also distance dependent. Thus, the combination of the electric-field distribution and the concentration of metallic

64

impurities affects the morphology and in particular the density of the nanopillars. Therefore, to solve the problem of inhomogeneity in nanostructure density, Al cross was added at the center of the wafer, thus reducing the distance to Al patterned areas. SEM imaging confirmed a homogeneous morphology across wafer-scale areas (Figure 25).
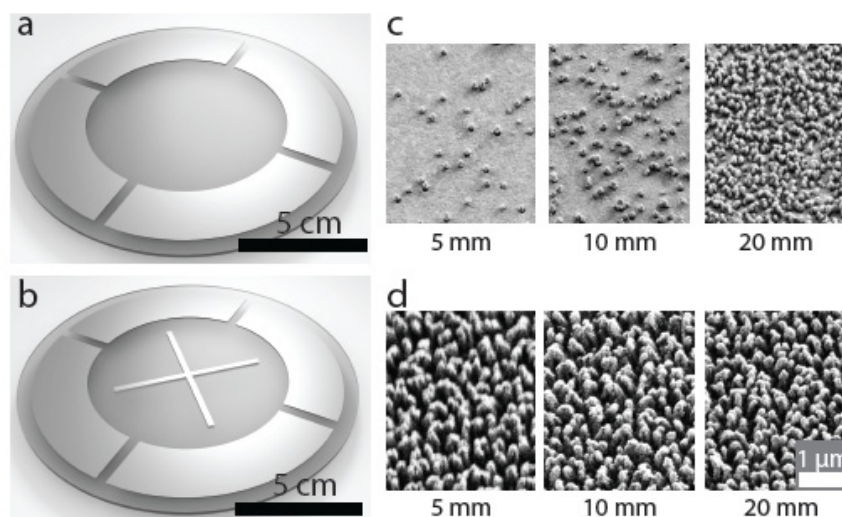

Figure 25. Illustrations of the 4-inch fused silica wafers with the Al pattern (a) without and (b) with the center cross. (c) SEM images of Au covered nanopillars taken at 5, 10 and 20 mm from the center of the wafer, showing increasing density and (d) constant density for the wafer with the Al cross. (Images were taken by Ph.D. student Anil Thilsted)

5.2.3 Thin-film metal deposition

Wordentec QCL 800 was used to deposit metals like Au, Cr or Al through a shadow mask on different substrates such as PMMA, fused silica or Si via electron beam evaporation. In the case of fused silica, the micro-milled holder with inbuilt shadow mask was used directly to load the silica substrate into the metal deposition chamber. Whereas, for PMMA substrate, laser machined shadow mask was first fixed onto the substrate with small screws (2 mm diameter) using the alignment holes present in both shadow mask as well as in the PMMA substrate. Thenceforth, substrate-mask assembly was placed on a 4-inch wafer holder followed by loading it into the metal deposition chamber. Prior to the metal deposition, the deposition chamber was brought to the high vacuum ($< 4 \times 10^{-9}$ bar) followed by activating an electron gun that shoots high-energy electrons towards the metal crystal. After being hit by the high-energy electrons, the atoms in the crystal absorbs the energy from the electrons and evaporates from the solid source. The metallic vapor is

further directed towards the substrate by an electric field and is deposited as a thin film on the substrate through the hollow patterns in the shadow mask.

To mediate the adhesion of Au on PMMA substrate, a thin layer of chromium/titanium (20nM) was deposited on PMMA prior to 200 nm Au deposition. The rate of deposition was 5 Å/s and 10 Å/s for Cr/Ti and Au respectively. For maskless reactive ion etching, 600 nm Al was directly deposited onto the silica substrate with 10 Å/s deposition rate. Once the nanostructures were developed on the fused silica, electrodes were patterned by depositing 170 nm Au with 10 Å/s rate of deposition in restricted areas via a shadow mask. Surprisingly, nanostructures on the substrate provided good adhesion to the Au, and we surpassed the use of additional adhesion layer that would have otherwise led to lower SERS performance. 200 nm Au with 10 Å/s deposition rate was also deposited on an entire 4-inch Si wafer with nanostructures. To be used as an electrode, the Au-deposited Si wafer was diced into small chips (9 mm x 13 mm) using laser micromachining tool and the chips were further integrated into small batch systems described in section 5.4.

5.3 Multi-channel PCB with magnetic clamping

For reliable electrochemical measurements, it is very important to have a good connection between the electrodes and the electrochemical measuring device. However, it is cumbersome to connect on-disc electrodes to the potentiostat to measure the electrochemical signal while spinning the disc. Although lots of work has been done already on electrochemical sensing based centrifugal microfluidic devices, still very few were able to achieve efficient connection of on-disc electrodes to the potentiostat[128,130,132,133]. For example, Andreasen et al. have shown the use of single channel low-noise electrical slip-ring to achieve continuous online monitoring of electrochemical experiments while the disc is spinning at high velocities[132].

In this work, it has been given great importance to design and fabricate a printed circuit board (PCB) that can be easily mounted onto the centrifugal microfluidic device and capable of connecting eight on-disc electrodes simultaneously to the eight-channel CHI1030A potentiostat (CH Instruments, Inc., Austin, TX, USA). The g-code file for milling PCB was prepared in a similar way as other micro-milling files mentioned in section 5.2.1. The multi-channel PCB has eight similar units connected in such a way that it allows convenient sample handling on the microfluidic

disc and do not interfere with the visibility of the fluid movement. For each unit, four parallel trenches were micro-milled on single sided PCB leads to the formation of three conductive copper islands. On each conductive island, a small hole was milled through the board, and the Au-coated spring-loaded contact pins (Mill-Max Mfg. Corp., Oyster Bay, NY, USA) were soldered through these holes. To retain the possibility of taking the real-time electrochemical measurements while spinning the disc (up to 2500 rpm), the PCB was connected to the potentiostat via a high speed eight-channel electrical slip ring (Model: SRS110073, Penlink, Sweden). The potentiostat was connected to the stationary part of the slip ring, whereas the moving part was coupled to the PCB. The slip ring was held in place by a 3D printed (Printer: MakerBot Industries, LLC, Brooklyn, NY, USA) holder made of poly-lactic acid (Reprap Aps, Copenhagen, Denmark), which was fixed on top of the disc mounted on the spin-stand using Ø 2-mm screws. In the initial design, the custom-made PCB interface was clamped onto the disc by using screws and nuts (Figure 26A), which is later on improvised and accustomed with magnetic clamping to facilitate quick, reliable and hassle free coupling of the PCB to the microfluidic disc (Figure 26B). The magnetic clamping was obtained by incorporating rod-shaped magnets of Ø 4 mm and 3 mm height (Webcraft GmbH, Gottmadingen, Germany) in the PMMA layer (1 mm) glued to the PCB and in an additional PMMA layer (2 mm) placed below the LoD (described in Paper I).
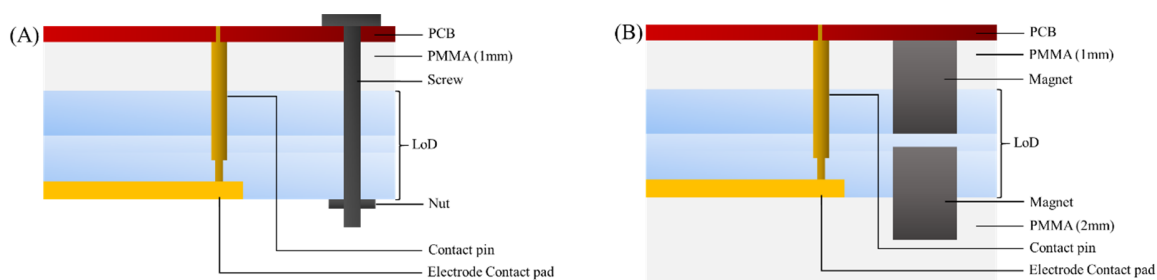

Figure 26. Cross-sectional schematic of PCB (A) with screws and (B) with magnetic clamping.

5.4 System Integration

To obtain optimum assay performance on centrifugal microfluidic platforms, the microfluidic set-ups require well-defined and easy to use functionality integration strategies. However, with the increasing complexity of the microfluidic devices, assembling individual components into one functional unit can be a challenge. Concerning this fact, we have tried to minimize this challenge

either by fabricating less complex microfluidic and sensor units (as explained in earlier sections) or by adapting to simple system integration strategies.

Membrane integration

As mentioned earlier in section 5.1, two different membranes were chosen for two different applications. The integration of microporous cellulose acetate (CA) membranes into the microfluidic system were rather simple and straightforward as compared to the integration of nanoporous polypropylene (PP) membranes. Being strong adhesive, biocompatible and easy to pattern (using a tabletop vinyl cutter), PSA was suitable to integrate the CA membrane in a microfluidic assembly designed for cell filtration. The integration was attained by placing the CA membrane directly onto the PSA adhered to the periphery of the collection chamber (Figure 27A). On the contrary, when the PSA was availed to integrate the PP membrane in a similar manner, PSA was found to foul and block the membrane during impregnating the membrane with oil (Di-hexyl ether) for SLM extraction. Possibly, the PSA is not compatible with the oil used for membrane impregnation. Thus, the oil is partially dissolving the PSA and clogging the nanopores in the membrane.
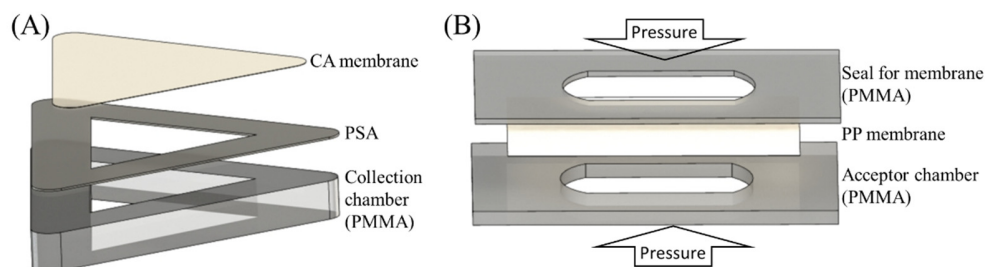
Figure 27. Schematic showing (A) cellulose acetate membrane integration using PSA (B) Polypropylene membrane integration using thermal bonding.

To solve the above-mentioned problem and avert the use of PSA for membrane integration, it was decided to incorporate the PP membrane between two PMMA layers using thermal bonding. During thermal bonding, the membrane itself did not contribute to the bonding. Instead, it was held in place by pressing it between two PMMA layers bonded at high pressure (20-25 bars) and temperature (85-95 °C) (Figure 27B). The use of high pressure and temperature for thermal bonding deformed the PMMA layers slightly that in turn pushed the PP membrane marginally into

the extraction chamber. As a result, the membrane could not stay flat and deflected a bit in and out of either the acceptor or donor chamber, making either chamber slightly bigger or smaller than intended. However, this effect was minimized by using a careful approach for handling the assembly during extraction experiments (i.e., filling and sealing the donor and acceptor channels in the same order every time).

Microfluidic assembly integration

In centrifugal microfluidics, the flow is regulated by the rotational speed of the microfluidic device, which in turn depends on the fluidic design, fabrication procedure as well as the precise alignment of the multiple subunits. This supports the fact that perfect fluidic design and fabrication procedure may also lead to irreproducible or unreliable flow dynamics if the various subunits of microfluidic assembly are not aligned properly. Therefore, in this work, apart from optimizing fabrication procedure for various components of the microfluidic assembly, equal importance was also given to precise alignment of the multiple components. All the layers that constitute the fluidic part of the cell filtration and the SLM extraction based microfluidic systems are described in Paper I and II respectively. Each subunit of the microfluidic systems was designed to have holes (diameter = 4mm) for magnetic clamping; the same holes were exploited to align all the subunits into the complete microfluidic assembly using custom-made alignment holder (Figure 28).
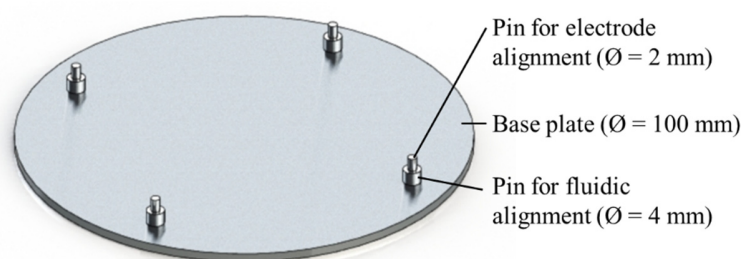

Figure 28. Schematic of custom-made alignment holder for aligning entire cell filtration assembly and SLM assembly.

For nanostructured glass and Si substrates, the assembly was designed and fabricated to carry out static batch experiments. The batch assembly for nanostructured glass is described in Paper III. However, due to semiconductive nature of Si substrate, it was not possible to pattern counter and reference electrodes along with the working electrode on the substrate itself. Still, the use of Si

chips seemed to be a blessing in disguise, as more than 25 Si chips (9 mm x 13 mm) could be obtained from single 4-inch Si wafer. That would ultimately lead to a possibility of running several experiments from the same batch of fabrication. Moreover, due to semiconductive nature of the Si, the same substrate also has potential as a perfect candidate for electrochemical SERS (EC-SERS). Consequently, we considered using Si chip as a WE and developed a different approach to prepare a batch assembly that incorporated Au-coated nanostructured Si chips. Primarily, a Lego type unit was cast in PDMS that contains external counter and reference electrodes. Here, Pt wire was used as CE, and chlorinated silver wire formed the Ag/AgCl pseudo-RE. In order to chlorinate the silver wire, 300 cycles of CVs were run in concentrated potassium chloride solution. This PDMS Lego type assembly was designed in such a way that it interlocks with rest of the batch assembly in a leak proof manner (Figure 29).
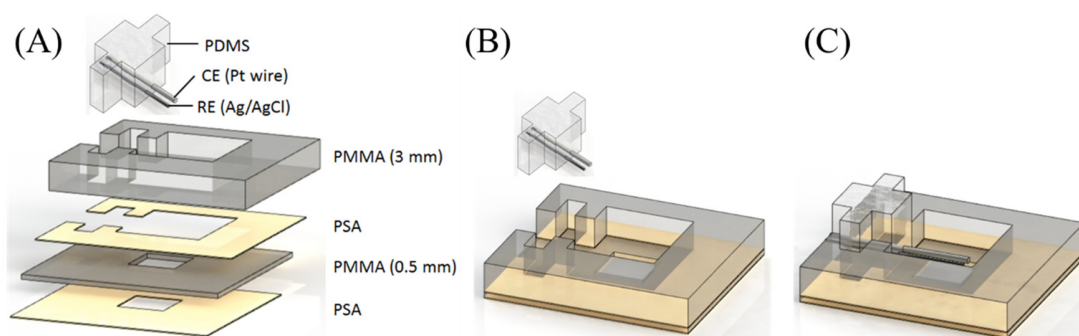

Figure 29. Schematic showing batch assembly for integrating Au-coated nanostructured Si chip as the working electrode (A) exploded view, (B) and (C) progressive integration view.

Sensor integration

In this study, all the substrates with electrodes were bonded to the rest of the assembly with PSA. PMMA substrates carrying electrodes were aligned with rest of the microfluidic assembly using custom-made alignment holder through the holes that were used earlier for shadow mask alignment. As it was not possible to make any alignment holes in the brittle fused silica substrate, a special alignment holder was micro-milled that could accommodate electrode carrying glass substrate at a fixed position using the primary flat of the substrate. The same holder has incorporated three more pins (diameter = 2mm) to align layers of PSA and PMMA onto the glass substrate.
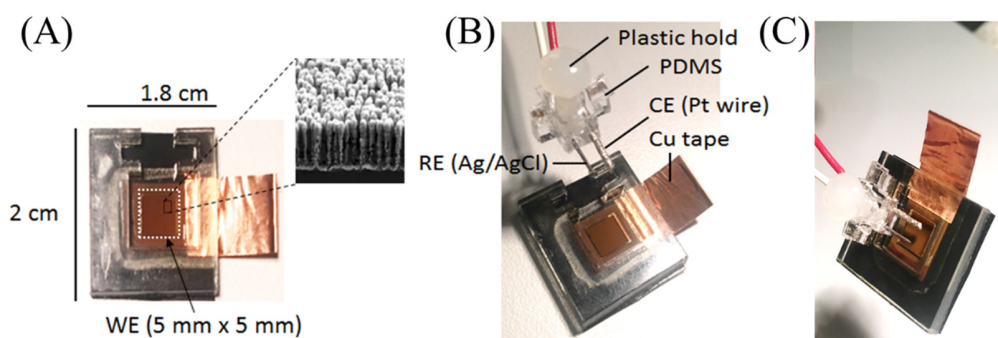
Figure 30. Photograph of (A) batch assembly set-up integrated with Au coated nanostructured Si chip as working electrode (inset: SEM image of nanostructured Si coated with Au), (B) PDMS cast Lego unit carrying counter and a reference electrode on top of batch assembly integrated with working electrode, (C) Fully integrated nanostructured Si batch assembly.

In the case of the Si substrate, the alignment was done by naked eye as the chips were big enough (9 mm x 13 mm) and the passivation layer of PSA and PMMA unit defined the working area (5 mm x 5 mm) of the electrode. The Si chip was bonded to the bottom PSA of batch assembly keeping the conductive copper tape in between (away from electrode working area) for robust connection to the potentiostat (Figure 30).

6. Conclusion and future perspective

During this Ph.D. project, the metal electrodes, which were integrated into the custom-designed polymeric LoD systems, were patterned on polymer substrates using a simple yet robust, lithography-free, stencil-based process. Several electrode designs were evaluated, during the development and optimization process to find the best electrode configuration suitable for the specific electrochemical application. All electrodes were well characterized for their performance and reproducibility prior to integration into the LoD systems. Two different sample pre-treatment methods such as filtration and SLM extraction were adapted onto the LoD platforms to eliminate the factors that could possibly affect the electrochemical measurements of target analyte. The factors considered in this study were high cell density at the end of the cell culture (24 hours) and the presence of interfering molecules at different time points during the cell culture. Finally, the applicability of developed LoD systems integrated with sample-pretreatment and electrochemical detection units was verified by addressing one of the most common problems in bioprocess monitoring, i.e., quantification of the produced metabolite for which the microorganism is genetically engineered. The influence of high cell density at the end of cell culture was successfully excluded using on-disc cell filtration, facilitating cell-free electrochemical quantification of pHCA from the supernatant of genetically modified *E. coli* cells. On the other hand, the on-disc SLM extraction simplified the pHCA quantification at different time points during the cell culture by eliminating an interfering compound Tyr and enriching pHCA from the original sample matrix of *E. coli* supernatant.

The developed LoD platforms proved to possess the potential of being used as an at-line bioprocess monitoring tools for the detection of the bacterial metabolite. However, there is still room for further improvement and optimization for other applications in bioprocess monitoring. In addition, these platforms could be adapted, redesigned and optimized for various other applications in medical diagnostics as well in food and environmental analysis. To be able to make the presented LoD device even more usable for application in the field of bioprocess monitoring it would be wise to combine both sample pre-treatment techniques, i.e., filtration and SLM extraction on the same platform. To boost the applicability, sensing capacity and commercial value of the LoD system , it would be beneficial to increase the number of sensing units as well as to enable other sensing

approaches such as optical detection. To accommodate more than eight sensing units on presented LoD device, further miniaturization of electrochemical sensors and microfluidics could be done. The miniaturization of electrochemical sensors will also enhance the sensitivity and limit of detection (LOD) by reducing the capacitive current and, thereby increasing the signal-to-noise ratio. Combination of the integrated electrochemical sensors with optical detection or using so called dual functionality sensors would widen the range of detectable analyte and in some cases could improve sensitivity (e.g., electrochemical enhancement of SERS detection).

Although the majority of work in this thesis is focused on electrochemical sensing, yet we cannot underestimate the potential of optical sensing. Considering the equal dominance of both the sensing techniques and the possibility of complementing each other, many researchers have already integrated them into a common sensor. We have added one more sensor to the same list in the form of Au coated fused silica nanostructures, capable of SERS-based sensing as well as electrochemical measurements. We are looking forward to incorporating them into the LoD device to achieve more advanced on-disc sensing through miniaturized electrochemical and SERS device (developed by Ph.D. student Onur Durucan during his Ph.D. project) integrated onto the rotating platform. In addition, one more miniaturized batch assembly set-up was developed containing Au coated nanostructured Si chip as WE, with external CE and RE. In future, the set up will be used as EC-SERS to exploit the applied electrochemical potential to increase the SERS signal.

However, the fact cannot be neglected that the commercial value of any device is highly dependent on fast and low-cost production on a large scale. This will further demand an investigation of alternative materials and fabrication procedures. For example, the developed platforms were fabricated using PMMA through rapid prototyping techniques easily accessible in research laboratories and which might not be suitable when considering commercialization of the product. Hence, based on the applications requirement, solvent resistant polymers can be considered for fabrication, along with the alternative manufacturing approach such as injection molding. Due to very precise channels and chambers, the use of injection molding will also improve the reproducibility and robustness of the flow actuation in LoD platforms.

To improve the way we interface electrodes with the instrumentation (potentiostat), we developed a magnetic clamping system, which enabled the connection of multiple on-disc electrodes to a stationary multichannel potentiostat simply and easily. The interfacing system (PCB with incorporated magnets and electrical slip ring) shows potential for real time measurements during spinning, however, the use of bulky potentiostat restrain its applicability in on-site and resource limited settings. To develop a more user-friendly electrochemical detection on a LoD platform, we have been working on the development of a miniaturized smartphone controlled wireless potentiostat, which can be integrated on a rotating platform, thereby eliminating the need for bulky peripheral instrumentation and slip rings for on-disc electrochemical measurements.

References

1. Terry, S. C., Herman, J. H. & Angell, J. B. A gas chromatographic air analyzer fabricated on a silicon wafer. *IEEE Trans. Electron Devices* **26,** 1880–1886 (1979).

2. Manz, A., Graber, N. & Widmer, H. áM. Miniaturized total chemical analysis systems: a novel concept for chemical sensing. *Sensors actuators B Chem.* **1,** 244–248 (1990).

3. Geschke, O., Klank, H. & Tellemann, P. *Microsystem Engineering of Lab-on-a-Chip Devices. Weinheim: Wiley-VCH* **258,** (2004).

4. Rodrigues, R. O., Lima, R., Gomes, H. T. & Silva, A. M. T. Polymer microfluidic devices: an overview of fabrication methods. *U.Porto J. Eng.* **1,** 67–79 (2015).

5. Nge, P. N., Rogers, C. I. & Woolley, A. T. Advances in Microfluidic Materials, Functions, Integration and Applications. *NIH Public Access* **113,** 2550–2583 (2013).

6. Gorkin, R. *et al.* Centrifugal microfluidics for biomedical applications. *Lab Chip* **10,** 1758–1773 (2010).

7. Michael, I. J., Kim, T. H., Sunkara, V. & Cho, Y. K. Challenges and opportunities of centrifugal microfluidics for extreme point-of-care testing. *Micromachines* **7,** 1–14 (2016).

8. Gilmore, J., Islam, M. & Martinez-Duarte, R. Challenges in the use of compact disc-based centrifugal microfluidics for healthcare diagnostics at the extreme point of care. *Micromachines* **7,** 1–26 (2016).

9. Czugala, M. *et al.* Portable lab-on-a-disc system integrating photo-switchable micro-valves for in-situ aquatic environmental monitoring. *Proc. 16th Int. Conf. Miniaturized Syst. Chem. Life Sci. MicroTAS 2012* 269–271 (2012).

10. Duford, D. A., Xi, Y. & Salin, E. D. Enzyme inhibition-based determination of pesticide residues in vegetable and soil in centrifugal microfluidic devices. *Anal. Chem.* **85,** 7834–7841 (2013).

11. Kim, T.-H., Park, J., Kim, C.-J. & Cho, Y.-K. Fully integrated lab-on-a-disc for nucleic acid analysis of food-borne pathogens. *Anal. Chem.* **86,** 3841–8 (2014).

12. Strohmeier, O. *et al.* Centrifugal microfluidic platforms: advanced unit operations and applications. *Chem. Soc. Rev.* **44,** 6187–6229 (2015).

13. King, D., O'Sullivan, M. & Ducrée, J. Optical detection strategies for centrifugal microfluidic platforms. *J. Mod. Opt.* **61,** 85–101 (2014).

14. Burger, R., Amato, L. & Boisen, A. Detection methods for centrifugal microfluidic platforms. *Biosens. Bioelectron.* **76,** 54–67 (2016).

15. Chen, Y., Hsu, J., Lin, Y. & Hsu, Y. Silver nanowires on coffee filter as dual-sensing functionality for efficient and low-cost SERS substrate and electrochemical detection. *Sensors Actuators B. Chem.* **245,** 189–195 (2017).

16. Ilkhani, H., Hughes, T., Li, J., Zhong, C. J. & Hepel, M. Nanostructured SERS-electrochemical biosensors for testing of anticancer drug interactions with DNA. *Biosens. Bioelectron.* **80,** 257–264 (2016).

17. Bailey, M. R., Martin, R. S. & Schultz, Z. D. Role of Surface Adsorption in the Surface-Enhanced Raman Scattering and Electrochemical Detection of Neurotransmitters. *J. Phys. Chem. C* **120,** 20624–20633 (2016).

18. Zong, X., Zhu, R. & Guo, X. Nanostructured gold microelectrodes for SERS and EIS measurements by incorporating ZnO nanorod growth with electroplating. *Sci. Rep.* **5,** 16454 (2015).

19. Convertino, A., Mussi, V. & Maiolo, L. Disordered array of Au covered Silicon nanowires for SERS biosensing combined with electrochemical detection. *Sci. Rep.* **6,** 25099 (2016).

20. El-Said, W. A., Kim, S. U. & Choi, J.-W. Monitoring in vitro neural stem cell differentiation based on surface-enhanced Raman spectroscopy using a gold nanostar array. *J. Mater. Chem. C* **3,** 3848–3859 (2015).

21. Storey, J. M. E., Shelton, R. D., Barber, T. E. & Wachter, E. A. Electrochemical SERS detection of chlorinated hydrocarbons in aqueous solutions. *Appl. Spectrosc.* **48,** 1265–1271 (1994).

22. Abdelsalam, M. E. *et al.* Electrochemical SERS at a structured gold surface. *Electrochem. commun.* **7,** 740–744 (2005).

23. Harroun, S. G. *et al.* Electrochemical surface-enhanced Raman spectroscopy (E-SERS) of novel biodegradable ionic liquids. *Phys. Chem. Chem. Phys.* **15,** 19205–12 (2013).

24. Wu, D.-Y., Li, J.-F., Ren, B. & Tian, Z.-Q. Electrochemical surface-enhanced Raman spectroscopy of nanostructures. *Chem. Soc. Rev.* **37,** 1025–1041 (2008).

25. Karaballi, R. A., Nel, A., Krishnan, S., Blackburn, J. & Brosseau, C. L. Development of an electrochemical surface-enhanced Raman spectroscopy (EC-SERS) aptasensor for direct detection of DNA hybridization. *Phys. Chem. Chem. Phys.* **17,** 21356–21363 (2015).

26. Goodall, B. L., Robinson, A. M. & Brosseau, C. L. Electrochemical-surface enhanced Raman spectroscopy method for early preeclampsia detection. *Phys. Chem. Chem. Phys.* **15,** 1382–1388 (2013).

27. Zaleski, S. *et al.* Identification and Quantification of Intravenous Therapy Drugs Using Normal Raman Spectroscopy and Electrochemical Surface-Enhanced Raman Spectroscopy. *Anal. Chem.* **89,** 2497–2504 (2017).

28. Dos Santos, D. P., Andrade, G. F. S., Temperini, M. L. A. & Brolo, A. G. Electrochemical control of the time-dependent intensity fluctuations in surface-enhanced Raman scattering (SERS). *J. Phys. Chem. C* **113,** 17737–17744 (2009).

29. Tian, Z. & Ren, B. Adsorption and reaction at electrochemical interfaces as probed by surface-enhanced Raman spectroscopy. *Annu. Rev. Phys. Chem.* **55,** 197–229 (2004).

30.   Etchegoin, P. G., Ru, E. C. Le, Fainstein, A., Vela, E. & Salvarezza, R. C. Electrochemical Modulation for Signal Discrimination in Surface Enhanced Raman Scattering (SERS). *Anal. Chem.* **82,** 6919–6925 (2010).

31.   Wittem-sterzel, R. Diagnosis: the doctor and the urine glass. *Lancet* 354 (2000).

32.   Kouba, E., Wallen, E. M. & Pruthi, R. S. Uroscopy by Hippocrates and Theophilus: Prognosis Versus Diagnosis. *J. Urol.* **177,** 50–52 (2007).

33.   Bassous, E., Taub, H. H. & Kuhn, L. Ink jet printing nozzle arrays etched in silicon. *Appl. Phys. Lett.* **31,** 135–137 (1977).

34.   Churski, K., Michalski, J. & Garstecki, P. Droplet on demand system utilizing a computer controlled microvalve integrated into a stiff polymeric microfluidic device. *Lab Chip* **10,** 512–518 (2010).

35.   Kaigala, G. V, Hoang, V. N. & Backhouse, C. J. Electrically controlled microvalves to integrate microchip polymerase chain reaction and capillary electrophoresis. *Lab Chip* **8,** 1071–1078 (2008).

36.   Kim, J., Chen, D. & Bau, H. H. An automated, pre-programmed, multiplexed, hydraulic microvalve. *Lab Chip* **9,** 3594–3598 (2009).

37.   Blanco-Gomez, G., Glidle, A., Flendrig, L. M. & Cooper, J. M. Integration of low-power microfluidic pumps with biosensors within a laboratory-on-a-chip device. *Anal. Chem.* **81,** 1365–1370 (2009).

38.   Chang, S. T., Beaumont, E., Petsev, D. N. & Velev, O. D. Remotely powered distributed microfluidic pumps and mixers based on miniature diodes. *Lab Chip* **8,** 117–124 (2008).

39.   Munyan, J. W., Fuentes, H. V, Draper, M., Kelly, R. T. & Woolley, A. T. Electrically actuated, pressure-driven microfluidic pumps. *Lab Chip* **3,** 217–220 (2003).

40.   Sweet, E. C., Mehta, R. R., Lin, R. & Lin, L. Finger-powred, 3D printed microfluidic pumps. *Transducers 2017* 1766–1769 (2017).

41.   Haeberle, S., Schmitt, N., Zengerle, R. & Ducrée, J. Centrifugo-magnetic pump for gas-to-liquid sampling. *Sensors Actuators, A Phys.* **135,** 28–33 (2007).

42.   Mair, D. a, Schwei, T. R., Dinio, T. S., Svec, F. & Fréchet, J. M. J. Use of photopatterned porous polymer monoliths as passive micromixers to enhance mixing efficiency for on-chip labeling reactions. *Lab Chip* **9,** 877–883 (2009).

43.   Rosenfeld, C., Serra, C., Brochon, C. & Hadziioannou, G. Influence of micromixer characteristics on polydispersity index of block copolymers synthesized in continuous flow microreactors. *Lab Chip* **8,** 1682–1687 (2008).

44.   Zhang, C., Xing, D. & Li, Y. Micropumps, microvalves, and micromixers within PCR microfluidic chips: Advances and trends. *Biotechnol. Adv.* **25,** 483–514 (2007).

45.   Gao, J. *et al.* Hybrid electrokinetic manipulation in high-conductivity media. *Lab Chip* **11,**

1770–1775 (2011).

46. Wang, L. & Dandy, D. S. A microfluidic concentrator for cyanobacteria harvesting. *Algal Res.* (2016). doi:10.1016/j.algal.2017.03.018

47. Nghe, P. *et al.* Microfluidics and complex fluids. *Lab Chip* **11,** 788–794 (2011).

48. Squires, T. M. & Quake, S. R. *Microfluidics: Fluid physics at the nanoliter scale. The American Physical Society* **77,** (2005).

49. Mark, D., Haeberle, S., Roth, G., Stetten, F. von & Zengerle, R. Microfluidic lab-on-a-chip platforms: requirements, characteristics and applications. *Chem. Soc. Rev.* **39,** 1153–1182 (2010).

50. Haeberle, S., Mark, D., Von Stetten, F. & Zengerle, R. Microfluidic platforms for lab-on-a-chip applications. *Microsystems Nanotechnol.* **7,** 1094–1110 (2012).

51. Dittrich, P. S., Tachikawa, K. & Manz, A. Micro Total Analysis Systems. Latest Advancements and Trends. *Anal. Chem.* **78,** 3887–3908 (2006).

52. Volpatti, L. R. & Yetisen, A. K. Commercialization of microfluidic devices. *Trends Biotechnol.* **32,** 347–350 (2014).

53. Chin, C. D., Linder, V. & Sia, S. K. Commercialization of microfluidic point-of-care diagnostic devices. *Lab Chip* **12,** 2118–2134 (2012).

54. Duffy, D. C., Gillis, H. L., Lin, J., Sheppard, N. F. & Kellogg, G. J. Microfabricated centrifugal microfluidic systems: Characterization and multiple enzymatic assays. *Anal. Chem.* **71,** 4669–4678 (1999).

55. Schwemmer, F. *Advanced Centrifugal Microfluidics : Timing , Aliquoting and Volume Reduction. Ph.D. Thesis, IMTEK - Institut für Mikrosystemtechnik* (2016).

56. Bruus, H. *Theoretical Microfluids. Oxford University Press* (2008). doi:10.1017/CBO9781107415324.004

57. Beebe, D. J., Mensing, G. a & Walker, G. M. Physics and applications of microfluidics in biology. *Annu. Rev. Biomed. Eng.* **4,** 261–286 (2002).

58. Cho, H., Kim, H. Y., Kang, J. Y. & Kim, T. S. How the capillary burst microvalve works. *J. Colloid Interface Sci.* **306,** 379–385 (2007).

59. Ekstrand, G. *et al.* in *Micro Total Analysis Systems* 311–314 (2000). doi:10.1007/978-94-017-2264-3_71

60. Wu, M.-H., Huang, S.-B. & Lee, G.-B. Microfluidic cell culture systems for drug research. *Lab Chip* **10,** 939--956 (2010).

61. Brenner, T., Glatzel, T., Zengerle, R. & Ducrée, J. Frequency-dependent transversal flow control in centrifugal microfluidics. *Lab Chip* **5,** 146–150 (2005).

62. Grumann, M., Geipel, a, Riegger, L., Zengerle, R. & Ducrée, J. Batch-mode mixing on

centrifugal microfluidic platforms. *Lab Chip* **5,** 560–565 (2005).

63. Ducrée, J. *et al.* The centrifugal microfluidic Bio-Disk platform. *J. Micromechanics Microengineering* **17,** S103–S115 (2007).

64. Nolte, D. D. Invited review article: Review of centrifugal microfluidic and bio-optical disks. *Rev. Sci. Instrum.* **80,** 101101(1-22) (2009).

65. Madou, M. J. & Kellogg, G. J. The LabCDTM: A Centrifuge-Based microfluidic platform for diagnostics. *Proc. SPIE* **3259,** 80–93 (2017).

66. Chen, J. M., Huang, P.-C. & Lin, M.-G. Analysis and experiment of capillary valves for microfluidics on a rotating disk. *Microfluid. Nanofluidics* **4,** 427–437 (2008).

67. Martinez-Duarte, R., Gorkin, R., Abi-Samra, K. & Madou, M. J. The integration of 3D carbon-electrode dielectrophoresis on a CD-like centrifugal microfluidic platform. *Lab Chip* **10,** 1030–1043 (2010).

68. Kim, J., Kido, H., Rangel, R. H. & Madou, M. J. Passive flow switching valves on a centrifugal microfluidic platform. *Sensors Actuators, B Chem.* **128,** 613–621 (2008).

69. Al-Faqheri, W. *et al.* Development of a passive liquid valve (PLV) utilizing a pressure equilibrium phenomenon on the centrifugal microfluidic platform. *Sensors (Switzerland)* **15,** 4658–4676 (2015).

70. Andersson, P., Jesson, G., Kylberg, G., Ekstrand, G. & Thorsén, G. Parallel nanoliter microfluidic analysis system. *Anal. Chem.* **79,** 4022–4030 (2007).

71. Park, J.-M., Cho, Y.-K., Lee, B.-S., Lee, J.-G. & Ko, C. Multifunctional microvalves control by optical illumination on nanoheaters and its application in centrifugal microfluidic devices. *Lab Chip* **7,** 557–564 (2007).

72. Whitesides, G. Solving problems. *Lab Chip* **10,** 2317–2318 (2010).

73. Sin, M. L., Gao, J., Liao, J. C. & Wong, P. System Integration - A Major Step toward Lab on a Chip. *J. Biol. Eng.* **5,** 1–21 (2011).

74. Mohammed, M. I., Haswell, S. & Gibson, I. Lab-on-a-chip or Chip-in-a-lab: Challenges of Commercialization Lost in Translation. *Procedia Technol.* **20,** 54–59 (2015).

75. Chen, X. & Cui, D. F. Microfluidic devices for sample pretreatment and applications. *Microsyst. Technol.* **15,** 667–676 (2009).

76. Lichtenberg, J., Se Rooij, N. F. & Verpoorte, E. Sample pretreatment on microfabricated devices. *Talanta* **56,** 233–266 (2002).

77. Park, M. *et al.* Combination of a Sample Pretreatment Microfluidic Device with a Photoluminescent Graphene Oxide Quantum Dot Sensor for Trace Lead Detection. *Anal. Chem.* **87,** 10969–10975 (2015).

78. Rios, A. & Zougagh, M. Sample preparation for micro total analytical systems (μ-TASs).

TrAC - Trends Anal. Chem. **43,** 174–188 (2013).

79.   Jendresen, C. B. *et al.* Highly active and specific tyrosine ammonia-lyases from diverse origins enable enhanced production of aromatic compounds in bacteria and Saccharomyces cerevisiae. *Appl. Environ. Microbiol.* **81,** 4458–4476 (2015).

80.   Karle, M., Wohrle, J., Von Stetten, F., Zengerle, R. & Mark, D. Axial centrifugal filtration A novel approach for rapid bacterial concentration from a large volume. *Conf. proceedings, Transducers* 1235–1238 (2013).

81.   Templeton, E. J. & Salin, E. D. A novel filtration method integrated on centrifugal microfluidic devices. *Microfluid. Nanofluidics* **17,** 245–251 (2014).

82.   Lee, A. *et al.* All-in-One Centrifugal Micro fl uidic Device for Size-Selective Circulating Tumor Cell Isolation with High Purity. *Anal. Chem.* **86,** 11349−11356 (2014).

83.   Czugala, M. *et al.* Optical sensing system based on wireless paired emitter detector diode device and ionogels for lab-on-a-disc water quality analysis. *Lab Chip* **12,** 5069–5078 (2012).

84.   Boettcher, M. *et al.* Lab-on-Chip-Based Cell Separation By Combining Dielectrophoresis and Centrifugation. *Biophys. Rev. Lett.* **1,** 443–451 (2006).

85.   LaCroix-Fralish, A., Templeton, E. J., Salin, E. D. & Skinner, C. D. A rapid prototyping technique for valves and filters in centrifugal microfluidic devices. *Lab Chip* **9,** 3151–3154 (2009).

86.   Steigert, J. *et al.* Integrated sample preparation, reaction, and detection on a high-frequency centrifugal microfluidic platform. *JALA - J. Assoc. Lab. Autom.* **10,** 331–341 (2005).

87.   Steigert, J. *et al.* Integrated siphon-based metering and sedimentation of whole blood on a hydrophilic lab-on-a-disk. *Biomed. Microdevices* **9,** 675–679 (2007).

88.   Xi, Y., Duford, D. A. & Salin, E. D. Automated liquid-solid extraction of pyrene from soil on centrifugal microfluidic devices. *Talanta* **82,** 1072–1076 (2010).

89.   Xi, Y., Templeton, E. J. & Salin, E. D. Rapid simultaneous determination of nitrate and nitrite on a centrifugal microfluidic device. *Talanta* **82,** 1612–1615 (2010).

90.   Kutter, J. P., Jacobson, S. C. & Ramsey, J. M. Solid phase extraction on microfluidic devices. *J. Microcolumn Sep.* **12,** 93–97 (2000).

91.   Yu, C., Davey, M. H., Svec, F. & Fréchet, J. M. J. Monolithic porous polymer for on-chip solid-phase extraction and preconcentration prepared by photoinitiated in situ polymerization within a microfluidic device. *Anal. Chem.* **73,** 5088–5096 (2001).

92.   Lee, E. Z. *et al.* Removal of bovine serum albumin using solid-phase extraction with in-situ polymerized stationary phase in a microfluidic device. *J. Chromatogr. A* **1187,** 11–17 (2008).

93. Chen, X., Cui, D. F., Liu, C. C. & Li, H. Fabrication of DNA purification microchip integrated with mesoporous matrix based on MEMS technology. *Microsyst. Technol.* **14,** 51–57 (2008).

94. Tokeshi, M., Minagawa, T. & Kitamori, T. Integration of a microextraction system on a glass chip: Ion-pair solvent extraction of Fe(II) with 4,7-diphenyl-1,10-phenanthrolinedisulfonic acid and tri-n-octylmethylammonium chloride. *Anal. Chem.* **72,** 1711–1714 (2000).

95. Hisamoto, H. *et al.* On-chip integration of sequential ion-sensing system based on intermittent reagent pumping and formation of two-layer flow. *Anal. Chem.* **73,** 5551–5556 (2001).

96. Reddy, V. & Zahn, J. D. Interfacial stabilization of organic-aqueous two-phase microflows for a miniaturized DNA extraction module. *J. Colloid Interface Sci.* **286,** 158–165 (2005).

97. Jönsson, J. Å. & Mathiasson, L. Memrane extraction in analytical chemistry. *J. Sep. Sci.* **24,** 495–507 (2001).

98. Jönsson, J. Å., Lövkvist, P., Audunsson, G. & Nilvé, G. Mass transfer kinetics for analytical enrichment and sample preparation using supported liquid membranes in a flow system with stagnant acceptor liquid. *Anal. Chim. Acta* **277,** 9–24 (1993).

99. Jönsson, J. Å. & Mathiasson, L. Liquid membrane extraction in analytical sample preparation. II. Applications. *TrAC - Trends Anal. Chem.* **18,** 325–334 (1999).

100. McGrath, M. & Ni Scanaill, C. in *Sensing and Sensor Fundamentals* 15–50 (2013). doi:10.1007/978-1-4302-6014-1_2

101. Ripka, P. & Tipek, A. *Modern Sensors Handbook. ISTE Ltd* (2007). doi:10.1002/9780470612231

102. Puckett, L. G. *et al.* Investigation into the applicability of the centrifugal microfluidics platform for the development of protein-ligand binding assays incorporating enhanced green fluorescent protein as a fluorescent reporter. *Anal. Chem.* **76,** 7263–7268 (2004).

103. Nagai, H., Narita, Y., Ohtaki, M., Saito, K. & Wakida, S.-I. A single-bead analysis on a disk-shaped microfluidic device using an antigen-immobilized bead. *Anal. Sci.* **23,** 975–979 (2007).

104. Riegger, L. *et al.* Read-out concepts for multiplexed bead-based fluorescence immunoassays on centrifugal microfluidic platforms. *Sensors Actuators, A Phys.* **126,** 455–462 (2006).

105. Czugala, M. *et al.* CMAS: fully integrated portable centrifugal microfluidic analysis system for on-site colorimetric analysis. *RSC Adv.* **3,** 15928–15938 (2013).

106. Hwang, H. *et al.* Lab-on-a-disc for simultaneous determination of nutrients in water. *Anal. Chem.* **85,** 2954–2960 (2013).

107. Nwankire, C. E. *et al.* A portable centrifugal analyser for liver function screening. *Biosens. Bioelectron.* **56,** 352–358 (2014).

108. Kim, J., Liu, G. & Lee, L. Lens-scanning Raman microspectroscopy system using compact disc optical pickup technology. *Opt. Express* **13,** 4780–4785 (2005).

109. Choi, D., Kang, T., Cho, H., Choi, Y. & Lee, L. P. Additional amplifications of SERS via an optofluidic CD-based platform. *Lab Chip* **9,** 239–243 (2009).

110. Grumann, M. *et al.* Sensitivity enhancement for colorimetric glucose assays on whole blood by on-chip beam-guidance. *Biomed. Microdevices* **8,** 209–214 (2006).

111. Steigert, J. *et al.* Direct hemoglobin measurement on a centrifugal microfluidic platform for point-of-care diagnostics. *Sensors Actuators, A Phys.* **130,** 228–233 (2006).

112. Lai, S. *et al.* Design of a Compact Disk-like Microfluidic Platform for Enzyme-Linked Immunosorbent Assay. *Anal. Chem.* **76,** 1832–1837 (2004).

113. He, H. *et al.* Design and testing of a microfluidic biochip for cytokine enzyme-linked immunosorbent assay. *Biomicrofluidics* **3,** 022401(1-17) (2009).

114. Koh, C. Y. *et al.* Centrifugal microfluidic platform for ultrasensitive detection of botulinum toxin. *Anal. Chem.* **87,** 922–928 (2015).

115. Walsh Iii, D. I. *et al.* A centrifugal fluidic immunoassay for ocular diagnostics with an enzymatically hydrolyzed fluorogenic substrate. *Lab Chip* **14,** 2673–80 (2014).

116. Kubo, I., Kanamatsu, T. & Furutani, S. Microfluidic Device for Enzyme-Linked Immunosorbent Assay (ELISA) and Its Application to Bisphenol A Sensing. **26,** 615–621 (2014).

117. Burger, R. *et al.* An integrated centrifugo-opto-microfluidic platform for arraying, analysis, identification and manipulation of individual cells. *Lab Chip* **15,** 378–381 (2015).

118. La Clair, J. J. & Burkart, M. D. Molecular screening on a compact disc. *Org. & Biomol. Chem.* **1,** 3244–3249 (2003).

119. Zhang, L., Li, X., Li, Y., Shi, X. & Yu, H.-Z. Indirect Competitive Assays on DVD for Direct Multiplex Detection of Drugs of Abuse in Oral Fluids. *Anal. Chem.* **87,** 1896–1902 (2015).

120. Boisen, A., Dohn, S., Keller, S. S., Schmid, S. & Tenje, M. Cantilever-like micromechanical sensors. *Reports Prog. Phys.* **74,** 036101(1-30) (2011).

121. Tamayo, J., Kosaka, P. M., Ruz, J. J., San Paulo, Á. & Calleja, M. Biosensors based on nanomechanical systems. *Chem. Soc. Rev.* **42,** 1287–311 (2013).

122. Waggoner, P. S. & Craighead, H. G. Micro- and nanomechanical sensors for environmental, chemical, and biological detection. *Lab Chip* **7,** 1238–1255 (2007).

123. Bosco, F. G. *et al.* High throughput label-free platform for statistical bio-molecular

sensing. *Lab Chip* **11,** 2411–6 (2011).

124.   Bosco, F. G. *et al.* Statistical analysis of DNT detection using chemically functionalized microcantilever arrays. *Sensors Actuators, B Chem.* **171,** 1054–1059 (2012).

125.   Bosco, F. G. *et al.* Micromechanical PDGF recognition via lab-on-a-disc aptasensor arrays. *Sensors Actuators, A Phys.* **195,** 154–159 (2013).

126.   Bache, M. *et al.* Nanomechanical recognition of prognostic biomarker suPAR with DVD-ROM optical technology. *Nanotechnology* **24,** 444011(1-7) (2013).

127.   Nwankire, C. E. *et al.* Label-free impedance detection of cancer cells from whole blood on an integrated centrifugal micro fl uidic platform. *Biosens. Bioelectron.* **68,** 382–389 (2015).

128.   Kim, T.-H. *et al.* Flow-enhanced electrochemical immunosensors on centrifugal microfluidic platforms. *Lab Chip* **13,** 3747–3754 (2013).

129.   Li, T., Fan, Y., Cheng, Y. & Yang, J. An electrochemical Lab-on-a-CD system for parallel whole blood analysis. *Lab Chip* **13,** 2634–40 (2013).

130.   Abi-Samra, K. *et al.* Electrochemical velocimetry on centrifugal microfluidic platforms. *Lab Chip* **13,** 3253–3260 (2013).

131.   Rattanarat, P. *et al.* An Electrochemical Compact Disk-type Microfluidics Platform for Use as an Enzymatic Biosensor. *Electroanalysis* **27,** 703–712 (2015).

132.   Andreasen, S. Z. *et al.* Integrating electrochemical detection with centrifugal micro fl uidics for real-time and fully automated sample testing. *RSC Adv.* **5,** 17187–17193 (2015).

133.   Noroozi, Z., Kido, H. & Madou, M. J. Electrolysis-Induced Pneumatic Pressure for Control of Liquids in a Centrifugal System. *J. Electrochem. Soc.* **158,** P130–P135 (2011).

134.   Sanger, K. *et al.* Lab-on-a-disc platform for screening of genetically modified E. coli cells via cell-free electrochemical detection of p-coumaric acid. *Sensors Actuators B Chem.* **253,** 999–1005 (2017).

135.   Cho, H. K., Lee, Y. H., Couch, R. A., Jagadeesh, J. M. & Olson, C. L. Development of a multichannel electrochemical centrifugal analyzer. *Clin. Chem.* **28,** 1956–1961 (1982).

136.   Scholz, F. *Electroanalytical Methods*. (2010).

137.   Cao, G. & Liu, D. Template-based synthesis of nanorod, nanowire, and nanotube arrays. *Adv. Colloid Interface Sci.* **136,** 45–64 (2008).

138.   Harvey, D. Analytical Chemistry 2.0-an open-access digital textbook-Chapter 11. *Anal. Bioanal. Chem.* **399,** 149–152 (2010).

139.   Heinze, J. Ultramicroelectrodes in Electrochemistry. *Angew. Chemie Int. Ed. English* **32,** 1268–1288 (1993).

140.   Waleed Shinwari, M. *et al.* Microfabricated reference electrodes and their biosensing

applications. *Sensors* **10,** 1679–1715 (2010).

141. Kneipp, K., Wang, Y., Kneipp, H., Perelman, L. T. & Itzkan, I. Single molecule detection using surface-enhanced Raman scattering (SERS). *Phys. Rev. Lett.* **78,** 1667–1670 (1997).

142. Li, T. *et al.* Wafer-Scale Nanopillars Derived from Block Copolymer Lithography for Surface-Enhanced Raman Spectroscopy. *ACS Appl. Mater. Interfaces* **8,** 15668–15675 (2016).

143. Rowe, A. A. *et al.* Cheapstat: An open-source, 'do-it-yourself' potentiostat for analytical and educational applications. *PLoS One* **6,** e23783(1-7) (2011).

144. Dryden, M. D. M. & Wheeler, A. R. DStat: A versatile, open-source potentiostat for electroanalysis and integration. *PLoS One* **10,** 0140349(1-17) (2015).

145. Cruz, A. F. D., Norena, N., Kaushik, A. & Bhansali, S. A low-cost miniaturized potentiostat for point-of-care diagnosis. *Biosens. Bioelectron.* **62,** 249–254 (2014).

146. Lazarus, N., Meyer, C. D. & Turner, W. J. A microfluidic wireless power system. *RSC Adv.* **5,** 78695–78700 (2015).

147. Ruecha, N. *et al.* Paper-Based Digital Microfluidic Chip for Multiple Electrochemical Assay Operated by a Wireless Portable Control System. *Adv. Mater. Technol.* **2,** 1600267(1-8) (2017).

148. Höfflin, J., Torres Delgado, S. M., Suárez Sandoval, F., Korvink, J. G. & Mager, D. Electrifying the disk: a modular rotating platform for wireless power and data transmission for Lab on a disk application. *Lab Chip* **15,** 2584–2587 (2015).

149. Randles, J. E. B. A cathode ray polarograph. Part II.-The current-voltage curves. *Trans. Faraday Soc.* **44,** 327–338 (1948).

150. Barker, G. C. Square wave polarography and some related techniques. *Anal. Chim. Acta* **18,** 118–131 (1958).

151. Mirceski, V. *et al.* Square-Wave Voltammetry: A Review on the Recent Progress. *Electroanalysis* **25,** 2411–2422 (2013).

152. Princeton. Square wave voltammetry Application Note S-7. *Princet. Appl. Res.* 1–5 (1957). doi:10.1021/ac00279a004

153. Käll, M., Xu, H. & Johansson, P. Field enhancement and molecular response in surface-enhanced Raman scattering and fluorescence spectroscopy. *J. Raman Spectrosc.* **36,** 510–514 (2005).

154. Kneipp, K. Surface-enhanced raman scattering. *Phys. Today* **60,** 40–46 (2007).

155. Moura, C. C., Tare, R. S., Oreffo, R. O. C. & Mahajan, S. Raman spectroscopy and coherent anti- Stokes Raman scattering imaging : prospective tools for monitoring skeletal cells and skeletal regeneration. *J. R. Soc. Interface* **13,** 9–11 (2016).

156. Le Ru, E. C. & Etchegoin, P. G. Single-Molecule Surface-Enhanced Raman Spectroscopy. *Annu. Rev. Phys. Chem.* **63,** 65–87 (2012).

157. Schlücker, S. Surface-enhanced raman spectroscopy: Concepts and chemical applications. *Angew. Chemie - Int. Ed.* **53,** 4756–4795 (2014).

158. Chen, H. Y., Lin, M. H., Wang, C. Y., Chang, Y. M. & Gwo, S. Large-Scale Hot Spot Engineering for Quantitative SERS at the Single-Molecule Scale. *J. Am. Chem. Soc.* **137,** 13698–13705 (2015).

159. Kneipp, K., Kneipp, H., Itzkan, I., Dasari, R. R. & Feld, M. S. Surface-Enhanced Raman Scattering and Biophysics. *J. Phys. Condens. Matter Matter* **14,** R597–R624 (2002).

160. Stiles, P. L., Dieringer, J. A., Shah, N. C. & Van Duyne, R. P. Surface-Enhanced Raman Spectroscopy. *Annu. Rev. Anal. Chem.* **1,** 601–626 (2008).

161. Schatz, G. C., Young, M. A. & Van Duyne, R. P. Electromagnetic mechanism of SERS. *Top. Appl. Phys.* **103,** 19–46 (2006).

162. Kerker, M., Siiman, O., Bumm, L. A. & Wang, D. S. Surface enhanced Raman scattering (SERS) of citrate ion adsorbed on colloidal silver. *Appl. opt.* **19,** 4137–4137 (1980).

163. Wang, D. S. & Kerker, M. Enhanced Raman scattering by molecules adsorbed at the surface of colloidal spheroids. *Phys. Rev. B* **24,** 1777–1790 (1981).

164. Zeman, E. J. & Schatz, G. C. An accurate electromagnetic theory study of surface enhancement factors for silver, gold, copper, lithium, sodium, aluminum, gallium, indium, zinc, and cadmium. *J. Phys. Chem.* **91,** 634–643 (1987).

165. Xu, H., Aizpurua, J., Käll, M. & Apell, P. Electromagnetic contributions to single-molecule sensitivity in surface-enhanced Raman scattering. *Phys. Rev. E - Stat. Physics, Plasmas, Fluids, Relat. Interdiscip. Top.* **62,** 4318–4324 (2000).

166. Tong, L., Xu, H. & Käll, M. Nanogaps for SERS applications. *MRS Bull.* **39,** 163–168 (2014).

167. Li, J. F. *et al.* Shell-isolated nanoparticle-enhanced Raman spectroscopy. *Nature* **464,** 392–395 (2010).

168. Samal, A. K. *et al.* Size tunable Au@Ag core-shell nanoparticles: Synthesis and surface-enhanced raman scattering properties. *Langmuir* **29,** 15076–15082 (2013).

169. López-Puente, V., Abalde-Cela, S., Angelomé, P. C., Alvarez-Puebla, R. A. & Liz-Marzán, L. M. Plasmonic mesoporous composites as molecular sieves for SERS detection. *J. Phys. Chem. Lett.* **4,** 2715–2720 (2013).

170. Alrifaiy, A., Lindahl, O. A. & Ramser, K. Polymer-based microfluidic devices for pharmacy, biology and tissue engineering. *Polymers (Basel).* **4,** 1349–1398 (2012).

171. Tsao, C. W. & DeVoe, D. L. Bonding of thermoplastic polymer microfluidics. *Microfluid. Nanofluidics* **6,** 1–16 (2009).

172. Metters, J. P., Kadara, R. O. & Banks, C. E. New directions in screen printed electroanalytical sensors: an overview of recent developments. *Analyst* **136,** 1067–1076 (2011).

173. Xu, Y., Huang, L.-B., Yung, K.-L., Xie, Y.-C. & Lee, T. M.-H. Low cost fabrication of microelectrodes on plastic substrate. *Microsyst. Technol.* **17,** 361–366 (2011).

174. Fischer, R. & Tadic-Galeb, B. in *Optical system design* (2000).

175. Schmidt, M. S., Hübner, J. & Boisen, A. Large Area Fabrication of Leaning Silicon Nanopillars for Surface Enhanced Raman Spectroscopy. *Adv. Opt. Mater.* **24,** 11–18 (2012).

176. Ye, X. *et al.* Formation of broadband antireflective and superhydrophilic subwavelength structures on fused silica using one-step self-masking reactive ion etching. *Sci. Rep.* **5,** 13023(1-10) (2015).

177. Zeze, D. A., Cox, D. C., Weiss, B. L. & Silva, S. R. P. Lithography-free high aspect ratio submicron quartz columns by reactive ion etching. *Appl. Phys. Lett.* **84,** 1362–1364 (2004).

178. Bellouard, Y., Said, A., Dugan, M. & Bado, P. Monolithic Three-Dimensional Integration of Micro-Fluidic Channels and Optical Waveguides in Fused Silica. *Mater. Res. Soc. Symp. - Proc.* **782,** 63–68 (2003).

179. Metwalli, E. & Pantano, C. G. Reactive ion etching of glasses: Composition dependence. *Nucl. Instruments Methods Phys. Res. Sect. B Beam Interact. with Mater. Atoms* **207,** 21–27 (2003).

180. Hein, E., Fox, D. & Fouckhardt, H. Lithography-free glass surface modification by self-masking during dry etching. *J. Nanophotonics* **5,** 051703(1-13) (2011).

Paper I

Lab-on-a-disc platform for screening of genetically modified *E. coli* cells via cell-free electrochemical detection of *p*-Coumaric acid

Paper II

Combining electrochemical detection with supported liquid membrane extraction for selective detection of bacterial metabolites on a centrifugal microfluidic platform

Lab-on-a-chip, under review

Paper III

Large-scale, Lithography-free Production of Transparent Nanostructured Surface for Dual-functional Electrochemical and SERS Sensing

Paper IV

Wireless, smartphone controlled potentiostat integrated with Lab-on-a-disc platform

Proceedings of the 21st International Conference on Miniaturized Systems for Chemistry and Life Sciences, October 22-26, 2017, Georgia, USA.

WIRELESS, SMARTPHONE CONTROLLED POTENTIOSTAT INTEGRATED WITH LAB-ON-DISC PLATFORM

Chung-Hsiang Cheng[1,3], Kinga Zor[2], Jen-Hung Wang[1,3], Kuldeep Sanger[2], Wei-Min Wang[1,3], Alessandro M. Capria[2], Anja Boisen[2], Kuang-Yuh Huang[1], En-Te Hwu[3]

[1]*National Taiwan University, Taiwan,*
[2]*Technical University of Denmark, Denmark,*
[3]*Academia Sinica, Taiwan*

ABSTRACT

A smartphone controlled wireless data transmitting and inductive powering Power Lab-on-disc (PLoD) platform is developed based on 2.4 GHz Bluetooth and 205 kHz Qi techniques, respectively. A potentiostat is integrated on the PLoD platform, and amperometric measurements are performed. The wireless potentiostat can provide -3~3 V with 14-bit resolution for amperometry in a range of -300~300 μA with a readout noise floor of 1.2 μA (p-p) in a static condition. A 0~3000 rpm spinning test shows that a phosphate buffer saline (400 mV potential) baseline noise is proportional to spinning acceleration and deceleration.

KEYWORDS: Wireless, Smartphone, Potentiostat, Bluetooth, Qi, Android, Arduino

INTRODUCTION

It is beneficial to integrate miniature microfluidics-based instruments on centrifugal microfluidic platforms or so called lab-on-disc (LoD) systems. Combining Arduino based microcontroller, inductive wireless power and Bluetooth data transmission, wireless rotating platform has even more potential applications. Since the inductive wireless power has been standardized as "Qi" for powering mobile devices, it is easy to find the Qi power transmitter and receiving coils in shops.

We developed a smartphone controlled Power Lab-on-disc (PLoD) platform prototype based on 2.4 GHz Bluetooth and
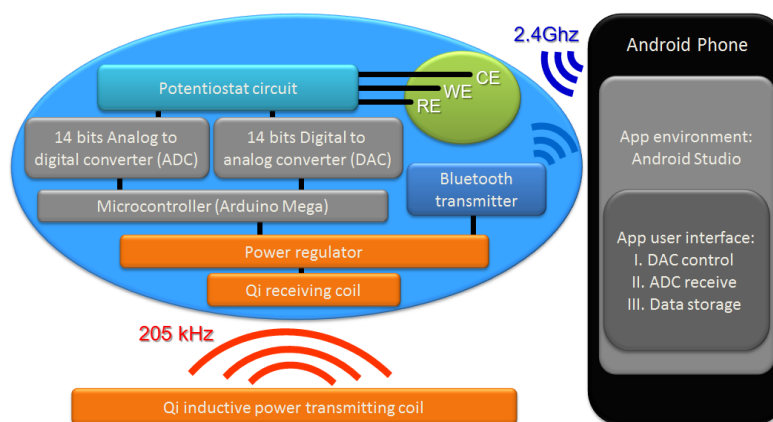

Figure 1: Block diagram of the wireless potentiostat integrated into PLoD platform.

205 kHz Qi techniques, respectively. A block diagram of the PLoD is shown in Figure 1. The platform integrates a microcontroller, a Bluetooth transmitter, a 14-bit resolution digital to analog converter (DAC) and a 14-bit resolution analog to digital converter (ADC), single channel potentiostat circuit and a power regulator.

Figure 2 shows a photo of the PLoD platform prototype which has a diameter and height of 100 mm and 53 mm, respectively. A microfluidic disc with 24 sets of potentiostat electrodes was placed between a top and a main circuit discs. Gold coated spring contact electrodes on the top circuit disc provided mechanical clamping and electrical contact to the microfluidic disc. A Qi coil was fixed at the bottom of the platform for receiving
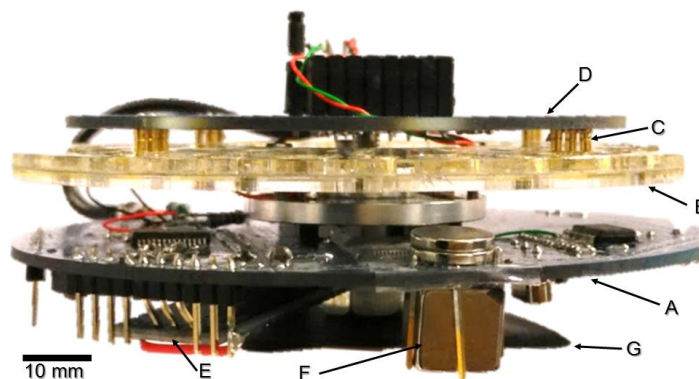

Figure 2: Photo of the wireless potentiostat integrated with the PLoD platform. A: Main circuit disc. B: Microfluidic disc. C: Gold electrodes contacted with spring loaded pins. D: Top circuit board. E: Bluetooth transmission module. F: Counterweight. G: Qi receiving coil.

power from a Qi transmitting coil (not shown). The platform was carefully balanced by a counterweight to achieve high spinning speed and low vibration.

EXPERIMENTAL

The Qi inductive power provides 5V and can transmit 5~10 Watt within 5 mm distance. However, the Qi power is very noisy and contains 205 kHz and 800mV noise spikes. A specialized filter is crucial for filtering the high-frequency noise, the filtered noise level is reduced to 80mV. The ADC and DAC are controlled by digital I/O pins of the microcontroller for higher resolution analog input and output. The potentiostat circuit can provide -3~3 V for amperometry and measure current in a range of -300~300 µA with a readout noise floor of 1.2 µA (p-p) in static condition.

Figure 3: The platform spun at 3000 rpm.
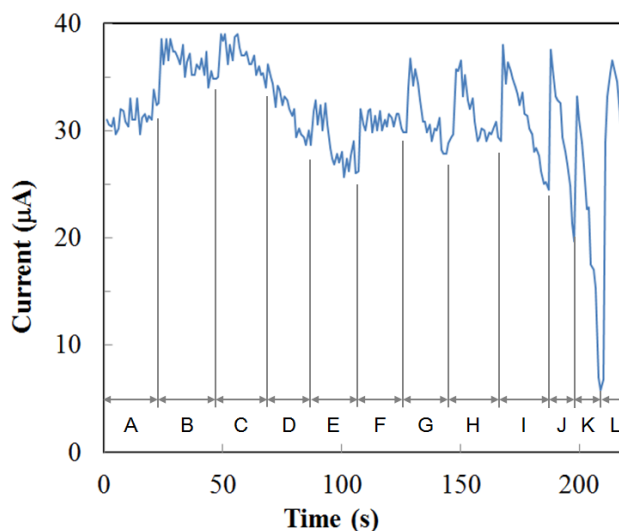
Figure 4: Baseline noise vs. spinning seed. A: 0 rpm. B: 300 rpm. C: 600 rpm. D: 900 rpm. E: 1200 rpm. F: 1500 rpm. G: 1800 rpm. H: 2100 rpm. I: 2400 rpm. J: 2700 rpm. K: 3000 rpm. L: 0 rpm.

RESULTS AND DISCUSSION

The PLoD can spin stably up to 3000 rpm, as shown in Figure 3. A 0~3000 rpm spinning test with a phosphate buffer saline (PBS) baseline noise (400 mV potential) is proportional to spinning acceleration and deceleration. The wireless potentiostat PBS baseline noise versus the spinning speed is shown in Figure 4. The noise peaked at the spinning acceleration and deceleration. When the platform was spinning at a constant speed, the noise dropped to a range of 3 µA (p-p). We believe the noise is proportional to the vibration while spinning as well.

CONCLUSION

The goal of this work is to develop high resolution and multi-channel PLoD for various transducers combined with centrifugal microfluidics as a portable analysis platform for bioprocess, diagnostics, food safety and environmental monitoring.

CONTACT

* En-Te Hwu; phone: +886-920-560-784; whoand@gmail.com

Paper V

A Lab-on-a-disc platform for trapping of cells, monitoring of cell behavior and evaluation of redox metabolism

A LAB-ON-A-DISC PLATFORM FOR TRAPPING OF CELLS, MONITORING OF CELL BEHAVIOUR AND EVALUATION OF REDOX METABOLISM

Letizia Amato, Kuldeep Sanger, Sheida Esmail Tehrani, Robert Burger, Claudia Caviglia, Sune Zoega Andreasen, Arto Heiskanen, Jenny Emnéus, Anja Boisen
Technical University of Denmark, Kgs. Lyngby, Denmark

ABSTRACT

In this work, we demonstrate an integrated electrochemical system on a centrifugal microfluidic platform for cell studies by combining electrochemical impedance spectroscopy and amperometry, and comparison of different cleaning protocols for gold electrodes on plastic substrate.

KEYWORDS: Electrochemical detection, lab on a disc platform, electrochemical impedance spectroscopy, amperometry, yeast metabolism.

INTRODUCTION

For centrifugal microfluidic platforms, electrochemical-based detection may show some benefits compared to the widely applied optical detection [1] in terms of ease of alignment, cost, and portability. Electrochemical sensing has been already integrated with rotating microfluidic platforms, e.g. to identify cancer cells [2], to detect a biomarker for cardiovascular disease[3], and to analyse whole blood [4].

Here, we present the fabrication of a microfluidic system for capture of yeast population (a model organism for drug discovery [5]) on a lab-on-a-disc platform. The cell trap is integrated with electrochemical detection for evaluation of behaviour and redox metabolism of yeast population with electrochemical impedance spectroscopy (EIS) and amperometry respectively.

In electrochemical experiments, the quality of the electrode surface will affect the measurement and the cleaning protocols developed for gold electrodes on silicon substrates[6] cannot directly be transferred to electrodes on plastic substrates. Here, three different cleaning protocols (potassium hydroxide – hydrogen peroxide; oxygen plasma treatment; potential sweep with potassium hydroxide) were tested on the electrodes and their effect was evaluated with cyclic voltammetry (CV) and EIS.

EXPERIMENTAL

CO_2 laser ablation and rapid prototyping were used for fabrication of the microfluidic disc. The gold electrodes were patterned on the poly(methylmethacrylate) (PMMA) bottom disc via electron beam evaporation (20 nm Cr adhesion layer/200 nm Au) through a shadow mask, fabricated with a laser micromachining tool (Fig. 1A). The microfluidic disc consists of 2 layers of pressure sensitive adhesives (PSA - 140μm) sandwiched between 3 layers of PMMA substrates (1.5 mm). Overall, the microfluidic disc design comprises: i) an electrode chip, ii) a loading and a collection chamber (PMMA layer), iii) and a circular chamber (for cell capture) connected to a microfluidic channel (PSA layer) placed on top of the electrode and connecting the loading chamber to the collection chamber. Interconnections between the electrode chip and the potentiostat were obtained using a tailor-made portable circuit board (Fig. 1B).
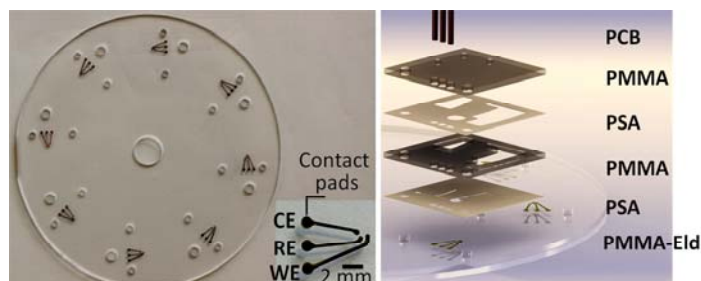

Figure 1: A) Image of 8 gold electrodes patterned through a shadow mask onto 1.5 mm PMMA layer. Inset: detail of the three electrode system with pseudo-reference gold electrode (RE), counter (CE) and working electrode (WE). B) Exploded view of a microfluidic disc with embedded electrodes on the bottom PMMA disc (PMMA-Eld). Pressure sensitive adhesive layers (PSA) are interspersed between 3 PMMA layers. A portable circuit board (PCB) with gold plated spring loaded pins connect the electrode chip and an external potentiostat.

For cleaning of electrodes on plastic substrates, three different cleaning procedures were applied and their effect was then evaluated with CV and EIS in presence of 10 mM of the potassium hexacyanoferrate (II/III) redox probe using PBS as supporting electrolyte.

50 mM potassium hydroxide (KOH) and 5% hydrogen peroxide (H_2O_2) (abbreviated ''KOH + H_2O_2'' in the results) – a similar method has been used by Heiskanen et al. as an intermediate step in a gold cleaning protocol [7]. Samples spent 5 or 10 min in a solution of 50mM KOH and 5% H_2O_2 before rinsing with Milli-Q water.

Oxygen plasma treatment (abbreviated 'O_2'in the results) – this method was applied using a 13.56 MHz RF generator-equipped Atto Plasma System (Diener Electronic GmbH, Ebhausen, Germany). The chamber was evacuated initially to a pressure below 15 Pa, after which O_2 was introduced (pressure stabilization at 30 Pa) and the plasma was ignited (power 50 W, duration 1 min). Immediately after plasma-treatment, the gold electrodes were used for characterization or for cell studies.

Potassium hydroxide potential sweep (abbreviated 'KOH sweep' in the results) - this is the second part of the cleaning protocol used by Heiskanen et al. [7]. After the treatment described above samples were placed in 50mM KOH and connected to a potentiostat. The electrode potential was swept from -200 to -1200 mV (vs. Ag/AgCl) once, at 50 mV s^{-1} scan rate, and then rinsed in Milli-Q water.

RESULTS AND DISCUSSION

The peak currents in CV and the frequency response during EIS will be dependent on the surface composition of the gold electrode surface. A low peak-current potential-difference and charge transfer resistance (R_{CT}) indicates a cleaner surface. The O_2 and the KOH+H_2O_2 treatment are found to leave comparable cleanliness, while the KOH sweep is not beneficial (Fig. 2).
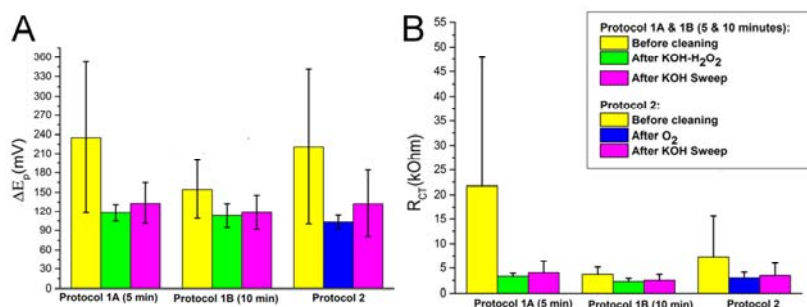

Figure 2: Tests of three different cleaning protocols of gold electrodes on plastic substrates: potassium hydroxide – hydrogen peroxide (KOH-H_2O_2) applied for 5 (protocol 1A) or 10 min (protocol 1B); oxygen plasma treatment (O_2); KOH potential sweep (KOH sweep). The bars indicate the average values for peak-current potential difference (ΔEp) (A) and charge transfer resistance (R_{CT}) (B) (average ± st. dev., n= 9) derived from CV and EIS measurements, respectively.

Thanks to the specially designed cell capture unit fast analyte diffusion to the electrode surface was facilitated and the yeast cells were successfully kept in close proximity of the electrodes to allow impedance monitoring and amperometric detection (Fig. 3). EIS measurements, performed before and after cell loading (Fig. 3D), confirmed sedimentation of cell population on the electrode surface. Upon adhesion of the yeast cells to the electrode surface, the electrode area is not accessible to the electroactive probe anymore due to the presence of cells, hence an increase in R_{CT} is observed. Additionally, R_{CT} increases with increasing amount of sedimented cells (3E4 and 3E6 cells per vial), which is in accordance with the fact that additional cells will cause a further barrier for $[Fe(CN)_6]^{3-/4-}$ to access the electrode surface.

After medium exchange, it was possible to follow the changes in the amperometric signal recorded from yeast redox metabolism with the menadione/ferricyanite double mediator system (Fig. 3E). Before starting the amperometric measurements, the cell capture/culture/detection unit was filled with yeast cell suspension (20 mg/ml) in 2mM ferricyanide (F) (PBS was the supporting electrolyte). The working electrode was biased at +400mV with respect to the on-chip gold pseudo-reference electrode. Then, 100µM menadione (M) and 10mM glucose (G) was sequentially added by spinning the disc to allow bursting of the loading chamber. The initial current level in presence of yeast cells only is due to the reduction of F to

ferrocyanide and is rather small since F is not able to diffuse inside the cell membrane (Fig. 3F). When a stable baseline is obtained the M is then added to the detection unit (F+M). Since M can diffuse through the cell wall the redox metabolism of the yeast cell is measured resulting in increased current response. Finally, the amperometric signal increases further upon addition of G to the chamber. This is due to the acceleration in the redox metabolism of the yeast cell population, compared with the redox activity measured in the absence of glucose (arrow labeled (M))
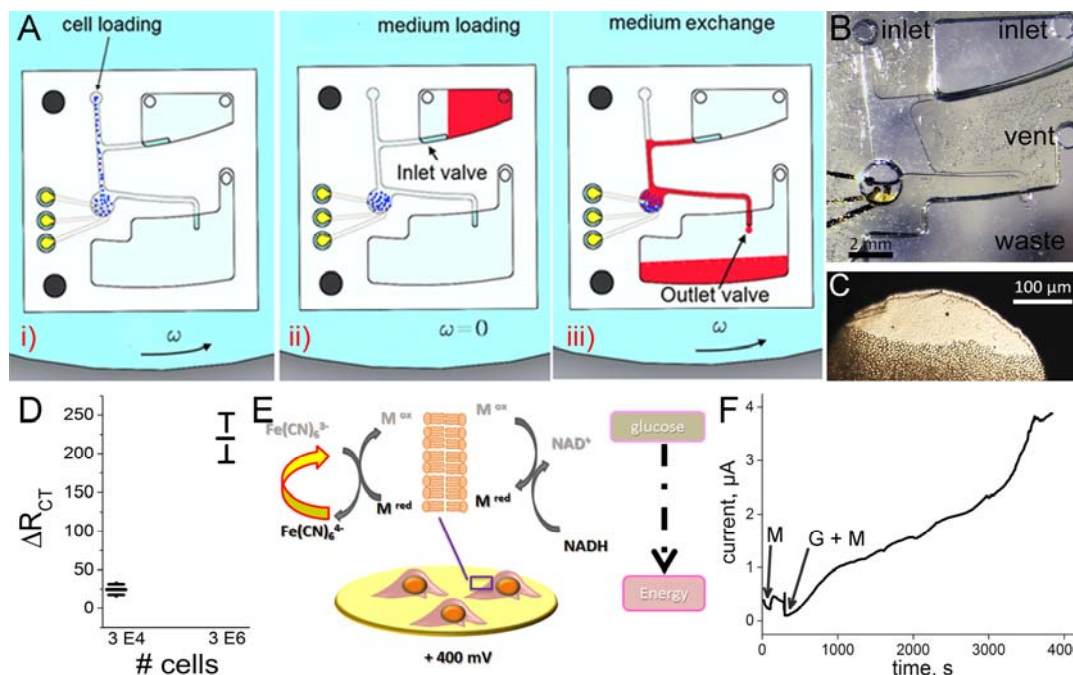

Figure 3: A) Schematic representation of the cell loading and medium exchange. (i) The yeast suspension is loaded in the inlet and is driven to the capture unit by spinning the disc at 1000 RPM. (ii) In stationary conditions ($\omega=0$) fresh medium/or buffer solution is loaded in the chamber with a pipette. (iii) Upon disc spinning, the fluid reaches the cells in the capture unit and the excess liquid is collected in the waste chamber via the outlet. B) Stroboscopic image of the assembled microfluidic disc design with cell capture unit integrated with miniaturized gold electrodes for electrochemical detection. C) Optical microscope image of yeast population trapped on the gold working electrode. D) Differential R_{CT} values (ΔR_{CT}) for two amount of sedimented yeast cells (3E4 and 3E6 cells per vial) with respect to the initial R_{CT} values without cells (average ± st. dev., n = 3). E) Putative mechanism of menadione reaction cycle. Menadione (M^{ox}) diffuses inside a cell, where it is reduced to menadiol (M^{red}). The latter diffuses to the outside the cell and reacts with ferrycianide $Fe(CN)_6^{3-}$, recovering M^{ox} to complete the cycle. Oxidation of the formed $Fe(CN)_6^{4-}$ is measured amperometrically at +400 mV. Addition of glucose results in the formation of NADH and NADPH in glycolysis and pentose phosphate pathway. F) Representative amperometric current-time trace response of yeast population in presence of potassium ferricyanide and menadione. The arrows mark the injection of menadione (M) and glucose (G) in the chamber.

CONCLUSION

Due to the excellent performances of the cell capture/detection unit in trapping cell population and monitoring the amperometric signal recorded from yeast redox metabolism, the developed platform has the potential to be a high-throughput monitoring device e.g. in drug screening and toxicity tests.

REFERENCES

[1]   King D, O'Sullivan M, Ducrée J. Optical detection strategies for centrifugal microfluidic platforms. J Mod Opt 2014;61:85–101.
[2]   Nwankire CE, Venkatanarayanan A, Forster RJ, Ducrée J. Electrochemical detection of cancer cells on a centrifugal microfluidic platform. Proceeding µTAS 2012:1510–2.
[3]   Kim T-H, Abi-Samra K, Sunkara V, Park D-K, Amasia M, Kim N, et al. Flow-enhanced electrochemical immunosensors on centrifugal microfluidic platforms. Lab Chip 2013;13:3747–54.
[4]   Li T, Fan Y, Cheng Y, Yang J. An electrochemical Lab-on-a-CD system for parallel whole blood analysis. Lab Chip 2013;13:2634–40. .
[5]   Hughes TR. Yeast and drug discovery. Funct Integr Genomics 2002;2:199–211. .
[6]   Fischer LM, Tenje M, Heiskanen AR, Masuda N, Castillo J, Bentien A, et al. Gold cleaning methods for electrochemical detection applications. Microelectron Eng 2009;86:1282–5.
[7]   Heiskanen AR, Spégel CF, Kostesha N, Ruzgas T, Emnéus J. Monitoring of saccharomyces cerevisiae cell proliferation on thiol-modified planar gold microelectrodes using impedance spectroscopy. Langmuir 2008;24:9066–73.

DTU Nanotech
Department of Micro- and Nanotechnology